DYNAMICS OF FUSION-FISSION REACTIONS NEAR COULOMB BARRIER

By

ABHIRUP CHAUDHURI
Enrolment No. : PHYS04201104005
Variable Energy Cyclotron Centre, Kolkata, India

A thesis submitted to the
Board of Studies in **Physical Sciences**
In partial fulfillment of requirements
For the Degree of

DOCTOR OF PHILOSOPHY

of

HOMI BHABHA NATIONAL INSTITUTE

August, 2018

Homi Bhabha National Institute[1]

Recommendations of the Viva Voce Committee

As members of the Viva Voce Committee, we certify that we have read the dissertation prepared by ABHIRUP CHAUDHURI entitled "DYNAMICS OF FUSION FISSION REACTIONS NEAR COULOMB BARRIER" and recommend that it may be accepted as fulfilling the thesis requirement for the award of Degree of Doctor of Philosophy.

Chairman - Dr. Chandana Bhattacharya	C. Bhattacharya	**Date:** 12.4.2019
Guide / Convener - Dr. Tilak Kumar Ghosh	T. Ghosh	**Date:** 12/04/2019
Co-guide - <Name> (if any) None		**Date:**
Examiner - Prof. Bivash Ranjan Behera	B. R. Behera	**Date:** 12/04/2019
Member 1- Dr. Gopal Mukherjee	Gopal Mukherjee	**Date:** 12/04/2019
Member 2- Prof. Satyajit Saha	S Saha.	**Date:** 12/04/19

Final approval and acceptance of this thesis is contingent upon the candidate's submission of the final copies of the thesis to HBNI.

I/We hereby certify that I/we have read this thesis prepared under my/our direction and recommend that it may be accepted as fulfilling the thesis requirement.

Date: 12/04/2019

Place: Saltlake, Kolkata

T. Ghosh

<Signature>

Guide: Dr. Tilak Kumar Ghosh

[1] This page is to be included only for final submission after successful completion of viva voce.

STATEMENT BY AUTHOR

This dissertation has been submitted in partial fulfillment of requirements for an advanced degree at Homi Bhabha National Institute (HBNI) and is deposited in the Library to be made available to borrowers under rules of the HBNI.

Brief quotations from this dissertation are allowable without special permission, provided that accurate acknowledgement of source is made. Requests for permission for extended quotation from or reproduction of this manuscript in whole or in part may be granted by the Competent Authority of HBNI when in his or her judgment the proposed use of the material is in the interests of scholarship. In all other instances, however, permission must be obtained from the author.

Abhirup Chaudhuri

ABHIRUP CHAUDHURI

DECLARATION

I, hereby declare that the investigation presented in the thesis has been carried out by me. The work is original and has not been submitted earlier as a whole or in part for a degree / diploma at this or any other Institution / University.

Abhirup Chaudhuri

ABHIRUP CHAUDHURI

List of Publications

A. In Peer Reviewed Journal

*1. "Direct evidence of washing out of nuclear shell effects", **A. Chaudhuri**, T. K. Ghosh, K. Banerjee, S. Bhattacharya, Jhilam Sadhukhan, C. Bhattacharya, S. Kundu, J. K. Meena, G. Mukherjee, R. Pandey, T. K. Rana, P. Roy, T. Roy, V. Srivastava, and P. Bhattacharya, *Phys. Rev. C* 91, 044620-1-6 **(2015)**.

*2. "No influence of $N = 126$ Neutron Shell Closure in Fission Fragment Mass Distributions", **A. Chaudhuri**, T. K. Ghosh, K. Banerjee, S. Bhattacharya, Jhilam Sadhukhan, S. Kundu, C. Bhattacharya, J. K. Meena, G. Mukherjee, A. K. Saha, Md. A. Asgar, A. Dey, S. Manna, R. Pandey, T. K. Rana, P. Roy, T. Roy, V. Srivastava, P. Bhattacharya, D. C. Biswas, B. N. Joshi, K. Mahata, A. Shrivastava, R. P. Vind, S. Pal, B. R. Behera, Varinderjit Singh, *Phys. Rev. C* 92, 041601-1-5(R) **(2015)**.

*3. "Fusion fission dynamics studies using mass distribution as a probe", T. K. Ghosh, **A. Chaudhuri**, K. Banerjee, S. Bhattacharya, C. Bhattacharya, S Kundu, G Mukherjee, R.Pandey, T. K.Rana, P. Roy, T. Roy, V Srivastava, P Bhattacharya, *Pramana* 85, 291-301 **(2015)**.

*4. "Fission fragment mass distributions in reactions populating ^{200}Pb", **A. Chaudhuri**, A. Sen, T. K. Ghosh, K. Banerjee, Jhilam Sadhukhan, S. Bhattacharya, P. Roy, T. Roy, C. Bhattacharya, Md. A. Asgar, A. Dey, S. Kundu, S. Manna, J. K. Meena, G. Mukherjee, R. Pandey, T. K. Rana, V. Srivastava, R. Dubey, Gurpreet Kaur, N. Saneesh, P. Sugathan, and P. Bhattacharya, *Phys. Rev. C* 94, 024617-1-5 **(2016)**.

B. In Conference & Symposia

*__1.__ "Fusion fission dynamics for the pre-actinides and actinides near the coulomb barrier energies", **Abhirup Chaudhuri**, *Applications of radio-tracers and energetic beams in sciences*, Vol 5, 311-312 **(2018)**.

*__2.__ "Fusion fission dynamics: fragment mass distribution studies", S. Bhattacharya, **A. Chaudhuri**, T. K. Ghosh, K. Banerjee, C. Bhattacharya, S. Kundu, G. Mukherjee, T. K. Rana, P. Roy, R. Pandey and P. Bhattacharya, *EPJ Web of Conferences* 86, 00004-1-6 **(2015)**.

*__3.__ "Shell effects in fission fragment mass distributions", **A. Chaudhuri**, T. K. Ghosh, K Banerjee, S. Bhattacharya, C. Bhattacharya, S. Kundu, J. K. Meena, R. Mondal Saha,G. Mukherjee, R. Pandey, T. K. Rana, P. Roy, T. Roy, A. K. Saha, J. K. Sahoo, V. Srivastava, P. Bhattacharya, *Proceedings of the DAE Symp. on Nucl. Phys.* 59, 478-479 **(2014)**.

*__4.__ "Study of fusion − fission dynamics of ^{200}Pb through fission fragment mass distribution", **A. Chaudhuri**, T. K. Ghosh, K. Banerjee, S. Bhattacharya, P. Roy, T. Roy,C. Bhattacharya, S. Kundu, J. K.Meena, G. Mukherjee, Md. A. Asgar, A. Dey, S. Manna, R. Pandey, T. K. Rana, A. Sen, M. Sinha, V. Srivastava, P. Bhattacharya, R. Dubey, N. Saneesh, P. Sugathan, Gurpreet Kaur, *Proceedings of the DAE Symp. on Nucl. Phys.* 60, 506-507 **(2015)**.

*__5.__ "Effect of neutron shell closure in fission fragment mass distributions of $^{206,210}Po$", **A. Chaudhuri**, T. K. Ghosh, K. Banerjee, S. Bhattacharya, Jhilam Sadhukhan, S. Kundu, C. Bhattacharya, J. K. Meena, G. Mukherjee, A. K. Saha, Md. A. Asgar, A. Dey, S. Manna, R. Pandey, T. K. Rana, T. Roy, P. Roy, V. Srivastava, P. Bhattacharya, D. C. Biswas, B. N Joshi,

K. Mahata, A. Shrivastava, R. P. Vind, S. Pal, B. R. Behera, Varinderjit Singh, *Proceedings of the DAE Symp.on Nucl. Phys.* 60, 360-361 **(2015)**.

(*) indicates papers on which this thesis is based.

C. Other publications

1. "The effect of clusters on fragment emission mechanism", S. Manna, T. K. Rana, C. Bhattacharya, S. Bhattacharya, S. Kundu, K. Banerjee, P. Roy, R. Pandey, V. Srivastava, **A. Chaudhuri**, T. Roy, T. K. Ghosh, G. Mukherjee, J. K. Meena, S. K. Pandit, K. Mahata, A. Shrivastava and V. Nanal, *J. Phys.: Conf. Ser.* 863 012064 **(2017)**.

2. "Fragment emission mechanism in the $^{32}S+^{12}C$ reaction", Ratnesh Pandey, S. Kundu, C. Bhattacharya, K. Banerjee, T. K. Rana, S. Manna, G. Mukherjee, J. K. Meena, **A. Chaudhuri**, T. Roy, Pratap Roy, Md. A. Asgar, V. Srivastava, A. Dey, M. Sinha, T. K. Ghosh, S. Bhattacharya, S. K. Pandit, K. Mahata, P. Patle, S. Pal, A. Shrivastava, and V. Nanal, *Phys. Rev. C* 95, 064603 **(2017)**.

3. "Survival of cluster correlation in dissipative binary breakup of $^{24,25}Mg$", S. Manna, T. K. Rana, C. Bhattacharya, S. Bhattacharya, S. Kundu, K. Banerjee, Pratap Roy, R. Pandey, Vishal Srivastava, **A. Chaudhuri**, T. Roy, T. K. Ghosh, G. Mukherjee, J. K. Meena, S. K. Pandit, K. Mahata, A. Shrivastava, and V. Nanal, *Phys. Rev. C* 94, 051601(R) **(2016)**.

4. "Experimental investigation of T = 1 analog states of ^{26}Al and ^{26}Mg", Vishal Srivastava, C. Bhattacharya, T. K. Rana, S. Manna, S. Kundu, S. Bhattacharya, K. Banerjee, P. Roy, R. Pandey, G. Mukherjee, T. K. Ghosh, J. K. Meena, T. Roy, **A. Chaudhuri**, M. Sinha, A. K. Saha, Md.

A. Asgar, A. Dey, Subinit Roy, and Md. M. Shaikh, *Phys. Rev. C* 93, 044601 **(2016)**.

5. "Fission dynamics study in ^{243}Am and ^{254}Fm", K. Banerjee, T. K. Ghosh, P. Roy, S. Bhattacharya, **A. Chaudhuri**, C. Bhattacharya, R. Pandey, S. Kundu, G. Mukherjee, T. K. Rana, J. K. Meena, G. Mohanto, R. Dubey, N. Saneesh, P. Sugathan, R. Guin, S. Das, and P. Bhattacharya, *Phys. Rev. C* 93, 064602 **(2016)**.

6. "Experimental study of ^{26}Al through the 1n pick-up reaction $^{27}Al(d,t)$", Vishal Srivastava, C. Bhattacharya, T. K. Rana, S. Manna, S. Kundu, S. Bhattacharya, K. Banerjee, P. Roy, R. Pandey, G. Mukherjee, T. K. Ghosh, J. K. Meena, T. Roy, **A. Chaudhuri**, M. Sinha, A. Saha, Md. A. Asgar, A. Dey, Subinit Roy, Md. M. Shaikh, *Phys. Rev. C* 91, 054611 **(2015)**.

7. "Structure of ^{26}Al studied by one - nucleon transfer reaction $^{27}Al(d,t)$", Vishal Srivastava, C. Bhattacharya, T. K. Rana, S. Manna, S. Kundu, S. Bhattacharya, K. Banerjee, P. Roy, R. Pandey, G. Mukherjee, T. K. Ghosh, J. K. Meena, T. Roy, **A. Chaudhuri**, M. Sinha, A. Saha, A. Dey, Md. A. Asgar, Subinit Roy, Md. M. Shaikh, *EPJ Web of Conferences* 86, 00055 **(2015)**.

8. "Fragment emission studies in low energy light heavy-ion reactions", T. K. Rana, C. Bhattacharya, S. Manna, V. Srivastava, K. Banerjee, S. Kundu, P. Roy, R. Pandey, **A. Chaudhuri**, T. Roy, T. K. Ghosh, G. Mukherjee, S. Bhattacharya, J. K. Meena, S. K. Pandit, K. Mahata, P. Patale, A. Shrivastava, V. Nanal, *EPJ Web of Conferences* 86, 00036 **(2015)**.

9. "Fission fragment anisotropy for breakup/transfer induced reactions", A. Parihari, S. Santra, A. Pal, D. Chattopadhyay, T. K. Ghosh, **A. Chaud-**

huri, K. Banerjee, S. Kundu, A. Shrivastava, K. Mahata, R. Tripathi, K. Ramachandran, S. Pandit, V. V. Parkar, J. K. Meena, N. L. Singh, S. Kailas, *Proceedings of the DAE Symp.on Nucl. Phys.* 59, 374 **(2014)**.

10. "Study of one neutron pick-up reaction $^{27}Al(d,t)$", Vishal Srivastava, C. Bhattacharya, T. K.Rana, S. Manna, S. Kundu, S. Bhattacharya, K. Banerjee, P. Roy, R Pandey, G. Mukherjee, T.K.Ghosh, J. K Meena, T Roy, **A. Chaudhuri**, M. Sinha, A.Saha, Md. A. Asgar, A Dey, Subinit Roy, Md. Moin Shaikh, *Proceedings of the DAE Symp.on Nuci. Phys.* 59, 358**(2014)**.

11. "Characterization of a segmented clover detector", Md. Ali Asgar, Tanmoy Roy, G. Mukherjee, Soumik Bhattacharya, **A. Chaudhuri**, Vishal Srivastava, S. Bhattacharyya, Sailajananda Bhattacharya, Chandana Bhattacharya, Tilak Kumar Ghosh, Kaushik Banerjee, Samir Kundu, Ratnesh Pandey, Tapan Kumar Rana, Pratap Roy, Santu Manna, Jayanta Kumar Sahoo, Jaikiran Meena, Amiya Kumar Saha, Ruchismita Mondal Saha, Pulak Mukhopadhyay, Anindita Choudhury, Imran Shaik, *Proceedings of the DAE Symp.on Nucl. Phys.* 59, 882 **(2014)**.

12. "Fragment emission mechanism in $^{12,13}C +^{12} C$ reactions", S. Manna, C. Bhattacharya, T. K. Rana,V. Srivastava, K. Banerjee,S. Kundu, P. Roy, R. Pandey, **A. Chaudhuri**, T. Roy, T. K. Ghosh, G. Mukherjee, S. Bhattacharya,J. K. Meena, S.K. Pandit, K. Mahata, P. Patale, A. Shrivastava, V. Nanal, S. Pal, *Proceedings of the DAE Symp.on Nucl. Phys.* 59, 560 **(2014)**.

13. "Study of fragment emission in $^{32}S +^{12} C$ reaction ", R. Pandey, C. Bhattacharya, S. Kundu, K Banerjee, S Manna, T. K. Rana, J. K. Meena, T Roy, **A. Chaudhuri**, Md. A. Asgar, V. Srivastava, A. Dey, M. Sinha,

G. Mukherjee, P. Roy, T. K. Ghosh, S. Bhattacharya, A. Srivastava, K. Mahata, S. K. Pandit, P. Patle, S. Pal, V Nanal, *Proceedings of the DAE Symp.on Nucl. Phys.* 59, 614 **(2014)**.

14. "Measurement of efficiency and time resolution of PPAC", R. Pandey, T. K. Ghosh, K. Banerjee, P. Roy, C. Bhattacharya, **A. Chaudhuri**, S.Kundu, T.K.Rana, G. Mukherjee, J. K. Meena, V. Srivastava, A. K Saha, J. K Sahoo, S Bhattacharya, *Proceedings of the DAE Symp.on Nuci. Phys.* 58, 982 **(2013)**.

15. "Isotopic effects in fragment emission studies in low energy light ion reactions ", C. Bhattacharya, T. K. Rana, Santu Manna, V.Srivastava, K. Banerjee, S. Kundu, P. Roy, R. Pandey, A. Chaudhuri, T. Roy, **T. K. Ghosh**, G. Mukherjee, S. Bhattacharya, J. K. Meena, S. K. Pandit, K. Mahata, P. Patale , A. Shrivastava, V. Nanal, *Proceedings of the DAE Symp.on Nuci. Phys.* 58, 530 **(2013)**.

Abhirup Chaudhuri
ABHIRUP CHAUDHURI

DEDICATIONS

Dedicated to my father and mother

Mr. Siladitya Chaudhuri and Mrs. Sumita Chaudhury

ACKNOWLEDGEMENTS

Over the years, the work pertaining to this thesis have received inspiration and support of several people, directly and indirectly. Firstly, I would like to express my sincerest gratitude and respect to my supervisor, Prof. Tilak Kumar Ghosh, who has introduced me to the field of experimental nuclear physics and guided me through the rigors of past several years. I have learnt immensely from him and have received his valuable advise and encouragement in all the stages of this work. His experimental skills are unparalleled. It was a pleasure that I was given an opportunity to work under him. He was actively involved in all stages of the work right from the inception to the end.

I am deeply grateful Dr. Sailajananda Bhattacharya whose deep insights and years of experience have enhanced this work severalfold. I would like to thank Dr. Chandana Bhattacharya for pursuing me to join the wonderful field of low energy nuclear physics and the constant encouragement and suggestions that I have received throughout the tenure. I would also like to thank my collaborators Dr. Gopal Mukherjee, Dr. Samir Kundu, Dr. Kaushik Banerjee, Dr. Tapan Rana, Dr. Pratap Roy, Ratnesh Pandey, Santu Manna and J. K Meena for their encouragement and active participation in all the experiments and giving their valuable inputs. All the experiments in this thesis wouldn't have been complete without their dedicated participation and supervision. Dr Jhilam Sadhukhan deserves a special mention for the help in the theoretical aspects of the work. Without him, most of the theoretical calculations would not have been complete. I would like to thank Dr P. Bhattacharya for actively participating in every experiment and sharing his vast experience with us.

I would like to thank Soumik Bhattacharya, Arindam Sikdar, Dr. Vishal Srivastava, Dr. Balaram Dey, Debasish Atta and Asif Reja for the lively dis-

cussions we had, both academic and non academic. Thanks to the Cyclotron operators at VECC and Pelletron operators at IUAC, Delhi and BARC-TIFR, Mumbai for ensuring smooth running of the accelerator without any hiccups in all the experiments. I would like to warmly thank my colleagues cum friends Somnath Kar, Tanmoy Roy and Debojit Sarkar for their constant support and friendly banter. I would like to thank my senior colleagues Mandira di, Aparajita di, Purnendu da, Hari da, Trambak da, Surasree di, Younus da, Sudipan da, Subhash da, Nihar da, Somnath da, Manish da, Arnab da, Nasim da, Sukanya di, Amal da, Maitreyee di, Rihan da, Sumit da, Balaram da and Subikash da for their support and guidance.

I would also like to thank my junior colleagues Rana, Rajendra, Sarwar, Arunabha, Arghya, Noor, Asgar, Utsav and Shabnam for their support and lively discussions. I would like to thank Dr D. N. Basu for being always ready to help whenever I got struck with any aspect of theoretical nuclear physics. His theoretical acumen has always impressed me. I would like to thank Dr D. K Srivastava (former Director, VECC Kolkata) for taking an active interest in my work and for being a constant source of encouragement. Lastly, I would like to thank my collaborators at BARC-TIFR and IUAC for their tireless work in all the experiments.

On the personal front, I would like to thank those people who may not have contributed directly to this work but their contributions been immense both in my life and in realizing the thesis. Firstly, I would like to thank my parents for unconditional support and love which have pushed me harder in my professional life. I would like to thank my sister for all the joshing and support. I also convey gratitude to Dr. Aditi Nag Chaudhuri, my pisi, for laying the foundation and aptitude for basic sciences in me right from school days. I would also like to pay my heartfelt gratitude to Late Kalyani Chaudhuri (Grandmother), Late Samar

Sen (Maternal Grandfather) and Mrs Priti Sen (Maternal Grandmother) for sowing the seeds in me for scientific research.

Apart from the above mentioned people, there were countless people at VECC who have directly or indirectly contributed to all the experiments and I sincerely apologize for any omission in my acknowledgment.

Abhirup Chaudhuri

Contents

SUMMARY

This study is focused on understanding the basic fusion-fission reaction mechanism which may may have its use in finding an optimum entrance channel condition for the synthesis of super heavy elements (SHE). Since the production of super heavy nuclei requires fusion of two heavy elements, the dynamical hindrance to fusion (quasi-fission) is large, which has a detrimental effect on the overall fusion cross-section. On the other hand, the shell correction energies to the fission barrier is large in the super heavy region which ensures that the alpha or fission half-lives of these nuclei are enhanced by several orders of magnitudes. Thus it is evident that a complete understanding of both quasi-fission as well as shell effects in fission-fission are crucial to understand the fission process in it's totality. The present study is aimed at probing deeply into these two aspects of the fusion fission process in order to throw new light on the enigmatic dynamics of fusion fission process. Using the major accelerator facilities available in India (Kolkata, Mumbai and Delhi), three experiments were carried out in this thesis work.

In all the experiments, fission fragments were detected with two large area position sensitive multi-wire proportional counters (MWPC) which were indigenously developed in our laboratory at VECC. The detectors were placed in two rotatable arms on either side of the beam axis with their centers so arranged, so as to match the folding angles of the complementary symmetric fission fragments. The masses of the correlated fission events was extracted from flight times, the position of the impact points of the fragments on the detectors, and the energy losses in the gas detectors in an event by event basis.

In the first experiment at VECC Kolkata, a systematic study of fission fragment mass distribution of ^{236}U in alpha induced fusion-fission reaction of ^{232}Th

target at an excitation energy range of 21 - 64 MeV was carried out and a direct evidence was shown for the first time that the shell effect is washed at an excitation energy of 40 MeV in ^{236}U.

In the second experiment at TIFR Mumbai, the role of shell correction at the saddle point was explored for a neutron shell closed nucleus ^{210}Po. Fission fragment mass distribution was measured for the systems ^{206,210}Po at an excitation energy range of 40 - 60 MeV using ^{12}C beam on ^{194,198}Pt. It was found that there is no anomaly in the nature of the fragment mass distributions between the two systems and all the distributions were symmetric and devoid of any structures in both the reactions. As the fission fragment mass distribution is directly correlated to the saddle ridge structure for single barriered distributions, our findings suggests that fission dynamics of ^{206,210}Po could be well explained without inclusion of any shell correction at saddle ridge.

In the third experiment at IUAC New Delhi, the role of entrance channel dynamics on fusion-fission and quasi-fission have been studied for ^{200}Pb. The mass distributions of ^{16}O + ^{184}W and ^{19}F + ^{181}Ta populating the same nuclei ^{200}Pb at an excitation energy range of 50 MeV to 80 MeV were found to be symmetric and the width of the mass distributions were found to increase monotonically suggesting absence of any quasi-fission and fast fission.

List of Figures

Chapter 1

Introduction

1.1 Nuclear Fission Process

The nuclear fission process was discovered about 80 years ago. Lise Meitner, Otto Hahn and Fritz Stassmann [1] made the startling discovery that irradiation of U by neutrons produced elements of much smaller atomic weight and charge. This new type of reaction was consequently named “fission” by Meitner and Frisch [2] in 1939. The fission process was immediately related to the disintegration of a uniformly charged deformed liquid droplet exploiting the saturation property and low compressibility of nuclear matter [3] where the deformation energy of a highly deformed nucleus provided a guide to understand nuclear fission process. A similar model, describing the nuclei as a liquid droplet, was in place before the discovery of fission [4].

The Liquid Drop Model (LDM) [3] and its variants have stood the test of time and have been quite successful in describing the gross properties of nuclear masses and deformation energies. Since then, the general properties of nuclei have been studied quite extensively and close inspection of nuclear masses with respect to LDM prediction showed deviations for certain nuclei that were found to be more bound. The deviation is more pronounced at the so called “magic numbers”. The shell model with the implementation of spin-orbit coupling predicted the gaps in the single particle level densities corresponding to the magic numbers 2, 8, 20, 50, 82, 126 [5, 6] and was very successful in evaluation of nuclear ground-state deformations [7]. However, when this treatment was extended to large distortions in fission process, the calculations became very intensive. Thus it became essential to incorporate large scale deformations into bulk properties of the nucleus along with the addition of single-particle structural descriptions. This was precisely achieved by Strutinsky [8, 9] in which shell correction energy was added with LDM energy. The smooth part of the total energy of the nucleus was described by the phenomenological LDM expression and the remaining oscillations in the energies were described due to non uniformity in the single particle level densities. The inclusion of shell effects in LDM could describe new experimental observables like fission isomers, super deformed nuclei and asymmetric mass distributions. The inclusion of shell effect into nuclear mass also led to an interesting prediction in the form of the possibility of an "island of stability" in the super heavy region. These super heavy elements, could never have existed if shell effects were not dominant in this region and LDM alone fails miserably in explaining the experimentally observed half lives of these nuclei [10]. Recently experimental evidence for isotopes of elements up to Z = 118 [11] has been confirmed, though it is still a long way to reach the island of stability.

Most of the early nuclear fission studies were with neutron bombardment on actnides or spontaneously fissioning nuclei. With the advent of heavy ion accelerators and advancement of experimental techniques new observables could be introduced with access to higher excitation energies and angular momentum brought in by heavy projectiles. The new experimental probes of angular distribution of fragments, total kinetic energy carried by the fragments and neutron multiplicities could be exploited to study the dynamical history of fusion fission reactions. Even though the gross features of nuclear fission reactions are well understood but close examination of the finer aspects of fusion fission reactions still throw some new surprises. The gap in our understanding of nuclear fission process lies in the dynamical evolution that the system undergoes after the two heavy colliding nuclei comes into contact. The reason for this being the involvement of a very large number of nucleons, as well as the role played by macroscopic and microscopic forces in the fission process.

A large number of experimental investigations have established the broad aspects of heavy ion induced fusion-fission reactions. Fusion occurs when the projectile is absorbed by the target nucleus to form a single composite system called a compound nucleus (CN) equilibrated in all degrees of freedom. Classically, when the projectile-target system overcomes the one dimensional potential barrier created by the interplay between the long range coulomb forces and the short range nuclear forces, it gets captured inside the barrier, which leads amalgamation of the two nuclei into a single CN. The initial experimental conditions like mass and kinetic energy of the individual reaction partners are completely obliviated. The CN produced in a heavy ion reaction is highly excited with large angular momentum values. The excitation energies and angular momentum are decided by initial reaction parameters like Q-value, beam energy and the range of impact parameters contributing to fusion. The hot and rapidly rotating compound nucleus thus created is not stable and usually decays either by light particle evaporation [12] or by fission [3]. Light particle evaporation leaves behind an evaporation residue (ER) which is similar (N,Z) to the compound nuclei except for the evaporated particles.

The competition between the decay modes of fission and ER is completely governed by statistical factors. Increase in excitation energy and angular momentum causes an increase in the centrifugal energy of the system thereby reducing the depth of the potential. With further increase in energy and angular momentum the potential trap vanishes and non compound nuclear processes and inelastic reactions begins to dominate. In lighter CN, the major decay mode is evaporation. For intermediate systems fission competes with evaporation and in heavier systems fission is the dominant channel as fissility increases with atomic number.

The classical picture is not without its flaws. According to the classical picture, no fusion was expected at below barrier energies but subsequent investigations have revealed that there was appreciable cross-section at these energies [13, 14]. This could not be explained simply by invoking quantum mechanical tunneling as the experimental cross sections were found to be several orders of magnitude larger than what was expected. The assumption of a local, one-dimensional real potential was found to be inadequate [15] and a more microscopic description of the potential was called for to explain sub-barrier fusion. One such successful theory is the coupled channel theory [16] according to which the relative motion degree of freedom is coupled with internal degrees of freedom which results in a distribution of barriers [17] with different barrier heights, instead of a single barrier. In order to understand fusion mechanism, fission measurements were conveniently carried out in past, particularly for highly fissile systems in which fusion and fission cross sections are similar.

A statistical theory of fission [18] (Statistical Saddle Point Model), conceptualized on the equilibrium properties of a hot and rotating nuclei could successfully explain the angular distributions of fission fragments. Heavy ion induced fission fragment angular distribution was found to be anisotropic in nature. The differential fission cross section was found to be more forward and backward focused with respect to the beam axis and a minima in cross-section was seen in the direction perpendicular to it. Symmetric distribution around

90 degree in centre of mass frame is a signature of compound nuclear fission.

1.2 Non Compound Nuclear Fission Processes

Statistical Saddle Point Model (SSPM) [19] was successful in explaining the fission fragment angular distribution data in reactions induced by lighter projectiles like protons and alpha particles where excitation energies are low and fission barrier heights are appreciable. However, in heavier systems the observed angular anisotropies were found to be higher than SSPM predictions [20]. This was attributed to dynamical effects in fusion-fission process with an admixture of statistical fusion process. These dynamical effects are manifested by certain non-compound nuclear processes along side statistical fusion fission. These non-compound nucleus processes are fast fission [21, 22], pre equilibrium fission [23] and quasi fission [24, 25].

In heavy ion reactions, with high total angular momentum J the fission barrier is depleted to the point where the compound nucleus was spontaneously unstable against fission. The system is trapped into the pocket of entrance channel potential and escapes after the reorganization of the densities of the constituent ions. This process appears mainly at high energies in heavy ion induced fission and is a kind of a delayed deep inelastic process and is named fast fission. This resulted in forward peaked angular distributions and wider mass distributions.

Anomalously large angular anisotropy were also observed in energies in and around coulomb barrier which was against SSPM predictions and quickly became an area of intense experimental and theoretical scrutiny in the 1980's and 1990's. This is particularly interesting because the systems were well within reasonable excitation energy and angular momentum ranges and were fully expected to follow compound nuclear fusion fission paths. This ambiguity was resolved by Kapoor and Ramamurthy [23] in their pre-equilibrium fission model. According to this model, in systems with entrance channel mass asymmetry α, larger than Businaro-Gallone critical mass asymmetry α_{BG} [26], a more compact shape is favoured by the driving force and the system coalesces to form a CN. On the other hand systems with mass asymmetry lesser than the critical mass asymmetry the driving force favours more and more symmetric configurations and fission occurs before $8 * 10^{-21} s$ which is insufficient for K equilibration (K is the projection of total angular momentum on the symmetry axis). This results in smaller value of K_0^2 and according to SSPM this will lead to larger anisotropies.

Quasi fission arises when the saddle point configuration required for formation of CN is more compact than contact configuration. In quasi fission, the di-nuclear system formed during the initial phases of fusion re-separates after an exchange of a few nucleons towards more symmetry but never complete mass equilibration. Quasi fission is a dynamical mechanism which depends on the entrance channel properties of the target projectile system like ground state deformations and mass asymmetry as opposed to fusion fission. An admixture of quasi fission and CN fission can lead to larger fragment mass widths, supression of ER cross-section and strong mass angle correlations. Hinde et al. [27] put forward an entirely new postulate that the process of quasi fission depends on the relative orientation of the target and projectile during di-nuclei formation and is more probable for the projectile hitting the polar region of the deformed target as opposed to the equatorial region. Collision along the polar region favours more elongated intermediate di-nucleus which may eventually reach the saddle shape on a asymmetric mass ridge in the energy landscape following the path of least resistance. A compact mono-nucleus is preferably formed for the later configuration (collision in equatorial configuration), ending up in a nearly spherical compound nucleus. At lower energies, orientation dependent quasi fission dominates.

1.3 Motivation and organization of the thesis

Quasi fission, as described above, is the most important mechanism that poses a hindrance to the formation of heavy and super heavy elements. Again shell effects in CN in the super heavy region is the reason for appreciable fission barriers which ensures survival of the super heavy elements.

One of the major aspect of today's nuclear physics research is to search for the initial conditions that are optimal for the production of super heavy elements. This requires systematic understanding of dynamics of quasi-fission and evolution of nuclear shell effects with excitation energy, for a wide range fissioning nuclei of pre-actnides, actinides and super heavies.

In the present thesis work, we have explored both shell effects and quasi fission in the pre-actinides and actinides region using mass distribution of fission fragment as the probe. This work depicts the need for similar studies in the super heavy region.

The work to be presented in this thesis is divided into seven chapters. After a brief introduction presented in this chapter, the *second chapter* describes in brief the theoretical models relevant to this thesis work.

The *third chapter* presents the details of the experimental technique and the data analysis procedure. The method to determine the mass distributions of fission fragments using the two position sensitive MWPCs used by us are discussed.

The *fourth chapter* reports on the experiment carried out to study of shell effects for the fissioning nucleus ^{236}U. It is known that asymmetric mass distribution in actinides is an artifact of shell effect. We have measured the fission fragment mass distribution in α induced reaction on an ^{232}Th target over a wide excitation energy range in close energy intervals. We have found direct evidence that nuclear shell effect is washed out at an excitation energy of about 40 MeV wherein the mass distribution changed from asymmetric to symmetric. A statistical model calculation also showed that the second peak of the fission barrier, which arises due to shell effects, is also diminished at similar excitation energies. As shell effect is critical in super heavy element formation, constraining the excitation energy at which the nuclear shell effect washes out has important implications on the production of super heavy elements.

The *fifth chapter* reports another investigation on nuclear shell effects. Fission fragment mass distributions in the fission of ^{206}Po and ^{210}Po have been measured. ^{210}Po is a $N = 126$ neutron shell closed nucleus. As opposed to previous studies (discussed in the chapter in detail) of angular anisotropy and pre-scission neutron multiplicity no significant deviation of mass distributions between ^{206}Po and ^{210}Po have been found which can be pinned to heightened shell effect at saddle point due to $N = 126$ neutron shell closure. This result provides an important benchmark data to test new fission dynamical models and to study the effect of shell correction on the potential energy surface particularly at the saddle ridge.

The *sixth chapter* deals with the study of quasi-fission. To test the dependence of quasi fission on entrance channel mass asymmetry, mass distribution of fission fragments have been measured in the reactions $^{16}O +^{184} W$ and $^{19}F +^{181} Ta$ which populates the same compound nucleus $^{200}Pb^*$. The excitation energy ranges for both the systems have been kept similar. The width of the mass distributions were measured at different excitation energies and it was found that the widths increase monotonically with excitation energy, which is an indication of absence of quasi fission for both reactions. Our results are contrary to two recent claims which points to the presence of quasi fission in the above-mentioned reactions. The findings call for the development of dynamical calculations to understand the fusion dynamics of pre-actinide nuclei.

The *seventh chapter* is devoted to present a summary, conclusions and future outlook of the thesis work.

Chapter 2

Theoretical models

In this chapter, a brief overview of the theoretical models relevant to this thesis work is presented.

The nuclear force which is a short range force holds neutrons and protons together in a nucleus thus modifying the initial system of interacting nuclei into a finite many body system with many degrees of freedom. The peculiarity of the nuclear many body system lies in the fact that the number of degrees of freedom is neither very small to be treated deterministically nor very large to be treated statistically. Thus there is an array of microscopic and macroscopic effects that determine the gross properties of nuclear reactions.

With the availability of new particle accelerators and heavy ion beams it became possible to collide two heavy ions and produce compound nucleus as well as the reaction products with high excitation energies and angular momenta. This lead to new avenues of nuclear physics research which includes the possibility of creating new elements. Apart from the originally known nuclear fusion-fission process other non compound nuclear processes were discovered which includes fast fission and quasi fission.

2.1 Formation of compound nuclei

In nuclear reaction, long range repulsive Coulomb interaction and short range attractive nuclear forces come into play. In case of reactions involving heavy ion projectiles centrifugal forces also have a significant part to play effectively lowering the depth of the energy pocket and thus the barrier associated with it. The interplay of these forces brings about the various phenomena related to heavy ion collision.

To a first approximation, the heavy ion collision can be described by classical trajectories using the impact parameter. If the impact parameter is very large, the collision process is dominated by elastic scattering. Due to Coulomb repulsion some flux may be lost due to Coulomb excitations. The impact parameter below which the reaction partners begins to feel the nuclear force is called the grazing impact parameter b_{gr}. Trajectories with $b \approx b_{gr}$ is associated with quasi elastic reactions in which a small part of the internal energy gets converted to internal excitation. With further decrease in impact parameter the Coulomb repulsion is overcome by nuclear interaction which may result in a net exchange of a few nucleons and a large amount of kinetic energy may be transferred to internal excitation energy of the reaction partners. This type of reaction is called deep inelastic collision. Central collision results in fusion to form a compound nuclei. A prerequisite to the formation of compound nuclei is complete equilibration of mass, kinetic energy and angular momentum between the reaction partners so as all the entrance channel memory is lost. The compound nuclei stays together for a time sufficient for complete statistical equilibration of all the degrees of freedom (N/Z, kinetic energy, mass, shape etc). Thus a compound nucleus is formed and its decay is completely independent of the formation process. The lifetime of a compound nucleus varies between $10^{-19}s$ to $10^{-16}s$. The compound nuclei formed is highly excited with a high angular momentum. Such an unstable system may deacy through particle emission leaving behind an evaporation residue [12] or by fission [3]. It is a general observation that fission is a dominant channel for system with higher fissility.

2.1.1 The classical treatment of the fusion problem

Classically the effective nuclear potential can be written as sum of nuclear, Coulomb and centrifugal potential:

$$V_{eff} = V_n + V_c + l\,(l+1)\,\frac{\hbar^2}{2\mu^2} \tag{2.1}$$

If it is assumed that the target projectile system either fuses or elastically scatters the effective potential for any impact parameter (b) can be given by

$$V_{eff} = V\,(r) + \frac{Eb^2}{r^2} \tag{2.2}$$

When the effective potential is such that it coincides with the energy of the given trajectory E, the corresponding impact parameter is called the grazing impact parameter b_{gr} and the radial distance is called R_B. So

$$E = V_B + \frac{Eb_{gr}^2}{R_B^2} \tag{2.3}$$

Using the fusion cross section $\sigma_F = \pi b_{gr}^2$ and substituting the value of b_{gr} we arrive at

$$\sigma_F\,(E) = \pi R_B^2 \left(1 - \frac{V_B}{E}\right) \tag{2.4}$$

Quantum mechanically the fusion cross-section is given by

$$\sigma_F\,(E) = \frac{\pi}{k^2} \sum_{l=0}^{\infty} (2l+1)\,T_l \tag{2.5}$$

According to the sharp cutoff model transmission coefficient T_l is defined by

$$T_l = \begin{cases} 0, & \text{if } l > l_{gr} \\ 1, & \text{if } l < l_{gr} \end{cases} \tag{2.6}$$

In the classical limit taking $l_{gr} = kb_{gr}$ the above equation can be reduced to

$$\sigma_F(E) = \frac{\pi}{k^2} l_{gr}^2 = \pi b_{gr}^2 \tag{2.7}$$

assuming $l_{gr} >> 1$.

Experiments have shown that trajectories which pass over the barrier may not necessarily lead to compound nuclear formation, instead may lead to direct channels or other deep inelastic processes. To incorporate the effects of non compound nuclear processes into the above model, another selection criterion, the critical angular momentum l_{cr} was introduced [28]. For $l \leq l_{cr}$ (as shown in Fig. 2.1) the projectile gets trapped in the potential and equilibrate in all degrees of freedom to fuse into a single compound nucleus. At higher l values deep inelastic reaction occurs.

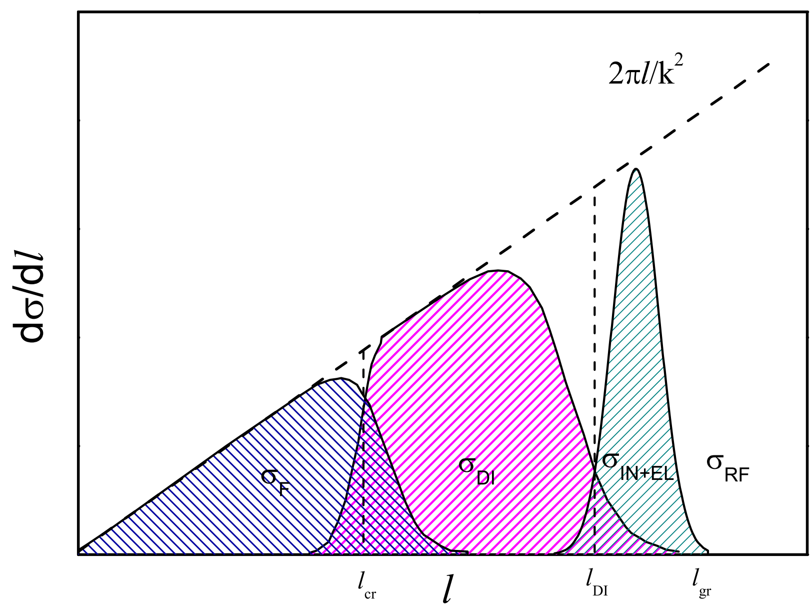

Figure 2.1: *Spin distributions in heavy ion reactions*

2.1.2 Fusion below Coulomb barrier through barrier penetration

The classical sharp cutoff model agrees well with the experimental fusion cross sections in the above barrier region, but at below barrier energies this model grossly underestimates the experimental cross sections [29, 30]. This suggests that there is a need to introduce the phenomenon of barrier penetration through quantum mechanical tunneling. To calculate the fusion cross section for quantum mechanical tunneling, the radial part of the Schrödinger's wave equation is used.

$$\frac{d^2\psi_l\left(r\right)}{dr^2}+k_l^2\psi_l\left(r\right)=0 \tag{2.8}$$

where $k_l\left(r\right)=\sqrt{\frac{2\mu}{\hbar^2}\left[E-V_l\left(r\right)\right]}$ is the local wave number. The transmission coefficient is calculated for passage either through or over the outer maxima in interacting potential using WKB approximation

$$T_l\left(E\right)=\frac{1}{\left[1+e^{\left(-2k_l\left(E\right)\right)}\right]} \tag{2.9}$$

and

$$k_l\left(E\right)=\int_{r_a}^{r_b}\sqrt{\frac{2\mu}{\hbar^2}\left[V_l\left(r\right)-E\right]}dr \tag{2.10}$$

where r_a and r_b are the inner and outer turning points of the barrier. The analytical form of the barrier potential was given by Hill Wheeler [31] in which the barrier was replaced by an inverted harmonic oscillator potential. Thus the transmission coefficient comes out to be

$$T_l\left(E\right)=\frac{1}{1+exp\left[\frac{2\pi}{\hbar\omega_l}\left(V_B\left(l\right)-E\right)\right]} \tag{2.11}$$

where $V_B\left(l\right)$ is the barrier height for the lth partial wave and $\hbar\omega_l$ is the barrier curvature. Using 2.5 and replacing the summation by integration and approximating $\hbar\omega_l=\hbar\omega_0$, $V_B\left(l\right)=V_B+\frac{\hbar^2 l(l+1)}{2\mu R_B^2}$ we arrive at the famous Wong's formula for fusion cross section [32]

$$\sigma_F(E) = \frac{R_B^2 \hbar\omega_0}{2E} ln \left[1 + exp\left\{\frac{2\pi}{\hbar\omega_0}(E - V_B)\right\}\right] \tag{2.12}$$

for $E << V_B$ the equation is reduced to

$$\sigma_F(E) = \frac{R_B^2 \hbar\omega_0}{2E} exp\left\{\frac{2\pi}{\hbar\omega_0}(E - V_B)\right\} \tag{2.13}$$

So according to the above equation the fusion cross section decreases exponentially with decrease in energy below the Coulomb barrier and at above barrier energies the fusion cross section shows linear dependence with 1/E.

In the above treatment, only one variable i.e; the distance between two fusing nuclei was considered. So, this model is called the One-Dimensional Barrier Penetration Model (1-DBPM). The basic premise of 1-DBPM is the assumption of an inert spherical nuclei interacting through an one dimensional potential. While this could adequately describe the fusion of light systems, the basic assumption of the one dimensional potential was inadequate in explaining fusion cross sections for heavier systems [33]. The reason for this being that the contribution from non-elastic channels increases significantly which includes transitions from ground state to excited states and transfer of particles among the reaction partners. Other internal degrees of freedom like static deformations and neck formations play a significant part in enhancing or lowering the fusion barrier. This led to the coupled channel formulation [16] in which all the main reaction channels are simultaneously described starting with a real potential that provides the bare interaction for the elastic scattering. Coupling interactions are added on to it to describe the transfer reactions and inelastic excitations. The effective fusion cross section is accounted for by imposing the ingoing-wave boundary in all channels.

2.2 Decay of the compound nuclei

The basic premise of the compound nuclei formation is complete oblivion of entrance channel parameters. The nuclei formed after capture has to traverse a long dynamical path equilibrating in all degrees of freedom. While, for lighter projectiles overcoming the Coulomb barrier ensures formation of a compound nuclei, for heavier systems entrance channel dynamics play a major role as opposed to statistical factors.

The first theory of decay of an equilibrated compound nuclei was put forward by Bohr and Wheeler [3]. According to this theory, fusion-fission is a two step process. In the first step, a compound nucleus is formed with an excitation energy, with equilibration of all degrees of freedom. In the second step, the compound nucleus disintegrates emitting neutrons or light charged particles or through fission.

In the Bohr Wheeler treatment, the fission probability is determined by considering a micro-canonical ensemble of nuclei with intrinsic excitation energy between E^* to $E^*+\delta E^*$. The number of quantum states between E^* to $E^*+\delta E^*$ is given by $\rho\left(E^*\right)\delta E^*$, where

$$E^* = E_{cm} + Q - V - E_{rot} \tag{2.14}$$

E_{cm} is the centre of mass energy of the target projectile combination, Q is the Q-value of the reaction, V is the ground state potential energy of the nucleus and E_{rot} is the rotational energy. The number of nuclei fissioning per unit time (R) is given by

$$R = \frac{\Gamma_{BW}}{\hbar}\rho\left(E^*\right)\delta E^* \tag{2.15}$$

According to the transition state definition, the number of fission events per unit time may be defined as the number of nucleons in the transition state with

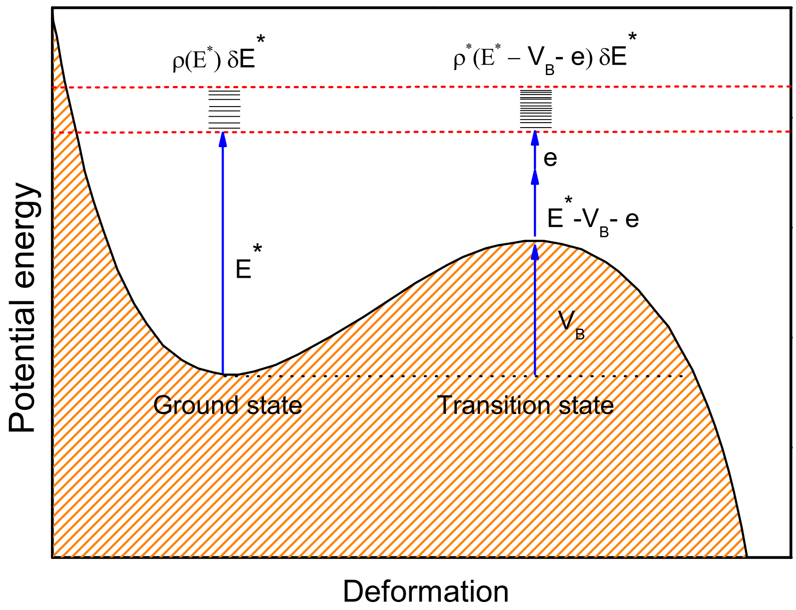

Figure 2.2: *Deformation vs potential energy plot in Bohr Wheeler theory of fission*

kinetic energy e passing over the fission barrier. The number of quantum states in and around the saddle configuration is given by $\frac{dp}{h}\rho\left(E^{*}-V_{B}-e\right)\delta E^{*}$ and the number of nuclei passing over the saddle point per unit time with momentum in the interval $(p, p+dp)$ is given by $v\left(\frac{dp}{h}\right)\rho^{*}\left(E^{*}-V_{B}-e\right)\delta E^{*}$, where v is the velocity of fission distortion. The fission rate can be given by

$$R=\delta E^{*}\int v\left(\frac{dp}{h}\right)\rho^{*}\left(E^{*}-V_{B}-e\right) \tag{2.16}$$

comparing 2.15 and 2.16 and using $vdp = de$ we get

$$\Gamma_{BW}=\frac{1}{2\pi\rho\left(E^{*}\right)}\int_{0}^{E^{*}-V_{B}}\rho^{*}\left(E^{*}-V_{B}-e\right)de \tag{2.17}$$

The nuclear level density parameter $\rho\left(E^{*}\right)$ plays a major role in describing the decay of a hot nuclei. It has been studied for many years and still extensively studied both experimentally and theoretically. Analytically, the Back Shifted Fermi Gas Model (BSFGM) [34] has been widely used in level density calculations. The model includes shell effect, pairing and deformations through different parameters. The standard form of level density can be written as

$$\rho\left(E^{*}, l\right)=\frac{2l+1}{24}\left(\frac{\hbar^{2}}{2I}\right)^{3/2}\frac{\sqrt{a}}{E^{*2}}exp\left(2\sqrt{aE^{*}}\right) \tag{2.18}$$

The quantity a has been introduced as an adjustable parameter which is used to fit experimental data. The parameter a is called the level density parameter and is related to the nuclear temperature T by $E^{*}=aT^{2}$. The value of level density parameter is $a \sim A/9\ MeV^{-1}$. However a linear variation of a cannot account for observed variation in level density in highly excited nucleus arising due to shell effects and pairing. Some microscopic calculations have suggested that shell effects are "washed out" at higher excitation energies. To incorporate the damping of shell effects in level density parameter Ignatyuk et. al [35] modified the parameter as

$$a\left(E^{*}\right)=\alpha\left(1+\frac{1-exp\left(\frac{-E^{*}}{\Delta_{E}}\right)}{E^{*}}\delta M\right) \tag{2.19}$$

where Δ_E is the rate of disappearance of shell effects on level densities and δM is the shell correction in LDM masses and α is the empirical level density parameter. Other modifications in the level density parameter a includes modification of α to include shape dependence and surface diffuseness.

By substituting 2.18 into 2.17 for $j=0$ and by assuming that the moment of inertia I and a is shape independent, the expression for standard level density can be written as:

$$\rho\left(E^{*}\right)\propto\frac{\sqrt{a}}{E^{*2}}exp\left(2\sqrt{aE^{*}}\right) \tag{2.20}$$

and Bohr Wheeler fission width is

$$\Gamma_{BW}=\frac{1}{2\pi}\int_{0}^{E^{*}-V_{B}}\frac{E^{*2}}{\left(E^{*}-V_{B}-e\right)^{2}}e^{2\sqrt{a\left(E^{*}-V_{B}-e\right)}-2\sqrt{aE^{*}}}de \tag{2.21}$$

The integration 2.21 yields a simple solution with the condition $E^{*} >> V_B$

$$\Gamma_{BW}=\frac{T}{2\pi}e^{-\frac{V_{B}}{T}} \tag{2.22}$$

where T is the Fermi gas temperature $\left(T = \sqrt{E^*/a}\right)$

2.3 Nuclear potential energy

The phenomenon of fission requires drastic rearrangement of nuclear matter i.e; nucleons (neutrons and protons). However, describing the complex nuclear matter in terms of effective interactions between two nucleons becomes quite cumbersome. Hence it becomes necessary to develop a simpler model which could describe the qualitative and quantitative aspects of nuclear matter satisfactorily. One such model is the Liquid Drop Model (LDM) put forward by Meitner and Frisch [36] and was put into quantitative terms by Bohr and Wheeler [3]. The model enabled us to define the process through nuclear shape dependent potential energy. In this description, volume conservation, i.e saturation property of nuclear matter is assumed, so the dominant term, which is proportional to the nuclear volume does not appear in this description. The Coulomb and the surface energy terms, which are shape dependent determine the potential energy of a nucleus at a particular configuration. With this approach the fission barrier heights and the corresponding shapes can be easily determined through computation of Coulomb and surface energy terms for various shapes by numerical integration.

2.3.1 The Liquid Drop Model and its modifications

The liquid drop model in its simplest form assumes that the nucleus is a uniformly charged liquid drop with sharp boundary and made up of incompressible matter. The changes in Coulomb and surface energies with change in shapes are of comparable magnitude and opposite sign.

Assuming azimuthal symmetry, the distortions to the sphere can be approximated as

$$R(\theta) = \frac{R_0}{\lambda_0}\left[1 + \alpha_2 P_2(cos\theta) + \sum_{n=3}^{\infty}\alpha_n P_n(cos\theta)\right] \tag{2.23}$$

here θ is the angle of the radial vector, $\alpha_n s$ are the amount of distortions from the sphere, R_0 is the radius of the undistorted sphere and λ_0 is the volume conserving factor $\left(= 1 + \frac{1}{5}\alpha_2^2 + ...\right)$. The Coulomb and surface term can be expressed as

$$\begin{aligned} E_c &= E_c^0\left(1 - \frac{1}{5}\alpha_2^2 + ...\right) \\ E_s &= E_s^0\left(1 + \frac{2}{5}\alpha_2^2 + ...\right) \end{aligned} \tag{2.24}$$

The difference between the energy of the distorted sphere and a normal sphere can be expressed as

$$\begin{aligned} \delta &= E_c - E_c^0 + E_s - E_s^0 \\ &= E_s^0\left[\frac{2}{5}\alpha_2^2 + ...\right] - E_c^0\left[\frac{1}{5}\alpha_2^2 + ...\right] \\ &= \frac{2}{5}E_s^0\left[\alpha_2^2\left(1 - \frac{E_c^0}{2E_s^0}\right) + \frac{E_c^0}{2E_s^0}f(\alpha_3, \alpha_4, ...)\right] \end{aligned} \tag{2.25}$$

Now $\chi = \frac{E_c^0}{2E_s^0}$ is called the fisility parameter. When $\chi \geq 1$, the nucleus becomes spontaneously unstable with respect to fission. Extensive investigations were performed by Cohen and Swiatecki [37] for different saddle point energies corresponding to different shapes and they arrived at a simple formula which can approximately mimic the barrier heights of different systems.

$$B_f = \begin{cases} 0.38\,(0.75 - \chi)\,, & \text{for } 1/3 < \chi < 2/3 \\ 0.83\,(1 - \chi)^3\,, & \text{for } 2/3 < \chi < 1 \end{cases} \tag{2.26}$$

The simple liquid drop model was, however seen to over predict the heights of fission barriers and fission half lives. An attempt was made to tackle this problem by including the effects of angular momentum. Cohen et. al. [38] added a correction term to account for the centrifugal forces. This centrifugal force plays a disruptive role and in effect reduces the fission barrier heights. This, however was still found to over predict the fission barrier heights and a scaling factor of 0.83 was suggested to fit the experimental cross sections [39, 40, 41]. Sierk [42] critically analyzed all the assumptions of LDM and proposed a macroscopic model of rotating nuclei. It was found that the main assumptions of LDM that the surface thickness and the range of forces are much smaller than nuclear dimensions breaks down in case of highly deformed nuclei where the nuclear dimension becomes comparable to the neck thickness. The model, thus called the Finite Range Liquid Drop Model (FRLDM) replaced the surface energy by Yukawa plus exponential potential energy to model the finite range of nuclear forces. In addition to this, a finite diffuseness term was added for charge distribution [43] and the rotational moments of inertia was calculated for nuclei with realistic surface density profiles.

The Yukawa plus exponential potential can be written as

$$E_n = \frac{-c_s}{8\pi^2 R_0^2 a^3} \int d^3r \int d^3r' \left[\frac{\sigma}{a} - 2\right] \frac{e^{-\sigma/a}}{\sigma} \tag{2.27}$$

where $\sigma = |\vec{r} - \vec{r'}|$ $c_s = a_s\left(1 - \kappa_s I^2\right)$, I is the neutron proton asymmetry $\left(N - Z\right)/A$, a_s and κ_s are the LDM surface energy and asymmetry constants respectively. a and r_0 are the diffuseness and average charge radii of the nucleus respectively. In the Coulomb energy the diffuseness was introduced by folding the Yukawa function with range a_c over a sharp surface liquid drop distribution.

$$E_c = \frac{Z^2 e^2}{\left(\frac{4}{3}\pi R_0^3\right)^2} \int d^3r \int d^3r' \left[\frac{1}{\sigma} - \left(1 + \frac{\sigma}{2a_c}\right) \frac{e^{\sigma/a_c}}{\sigma}\right] \tag{2.28}$$

In the same way, the rotational energy is also made diffuse by imposing an Yukawa function over a sharp surface

$$I = I^{sharp} + 4M_0 a_m^2 \tag{2.29}$$

where M_0 is the nuclear mass, a_m is the range parameter ($\approx a_c$) and I is the largest principal axis moment of inertia. The rotational energy of the nucleus is given by

$$E_R = \frac{l^2\hbar^2}{2I} \tag{2.30}$$

With these modifications in place, the fission barriers have been found to be within 1 MeV of the barriers inverted from fission and evaporation residue cross section data for a variety of nuclei of intermediate masses [42].

2.3.2 Nuclear shape parametrization

One of the prerequisite of fission is a highly deformed nuclei. Thus any description of fission would require a good description of nuclear shapes using appropriate collective coordinates. The first attempt at describing nuclear shape was through spherical harmonics [3], used for describing low lying collective oscillations. However, description of saddle shapes would require more number of harmonics which brings in more parameters and complicates the calculations.

One of the most popular parametrization of a group of azimuthally symmetric spheroids which can describe the saddle point shapes successfully is the funny hill parametrization [44] $\{c, h, \alpha\}$. The parameter c describes the elongation of the nucleus with respect to a sphere, h describes the thickness of the neck and α is loosely based on the mass asymmetry at the saddle point. The surface of a deformed nuclei with this parametrization is given by

$$r^2(z) = \begin{cases} \left(1 - \frac{z2}{c^2}\right)\left(ac^2 + bz^2 + \alpha cz\right) & b \geq 0 \\ \left(1 - \frac{z2}{c^2}\right)\left(ac^2 + \alpha cz\right) e^{\left(bcz^2\right)} & b < 0 \end{cases} \tag{2.31}$$

where z and r belong to the cylindrical coordinate system. By invoking the condition of volume conservation the constants a and b can be derived to

$$b = \frac{c-1}{2} + 2h \tag{2.32}$$

$$a = \begin{cases} \frac{1}{c^3} - \frac{b}{5} & b \geq 0 \\ -\frac{4}{3}\frac{b}{e^{bc^3} + \left(1 + \frac{1}{2bc^3}\right)\left(\sqrt{-\pi bc^3} erf\left(\sqrt{-bc^3}\right)\right)} & b < 0 \end{cases} \tag{2.33}$$

For physically accepted shapes the parameter a has to be positive. In the

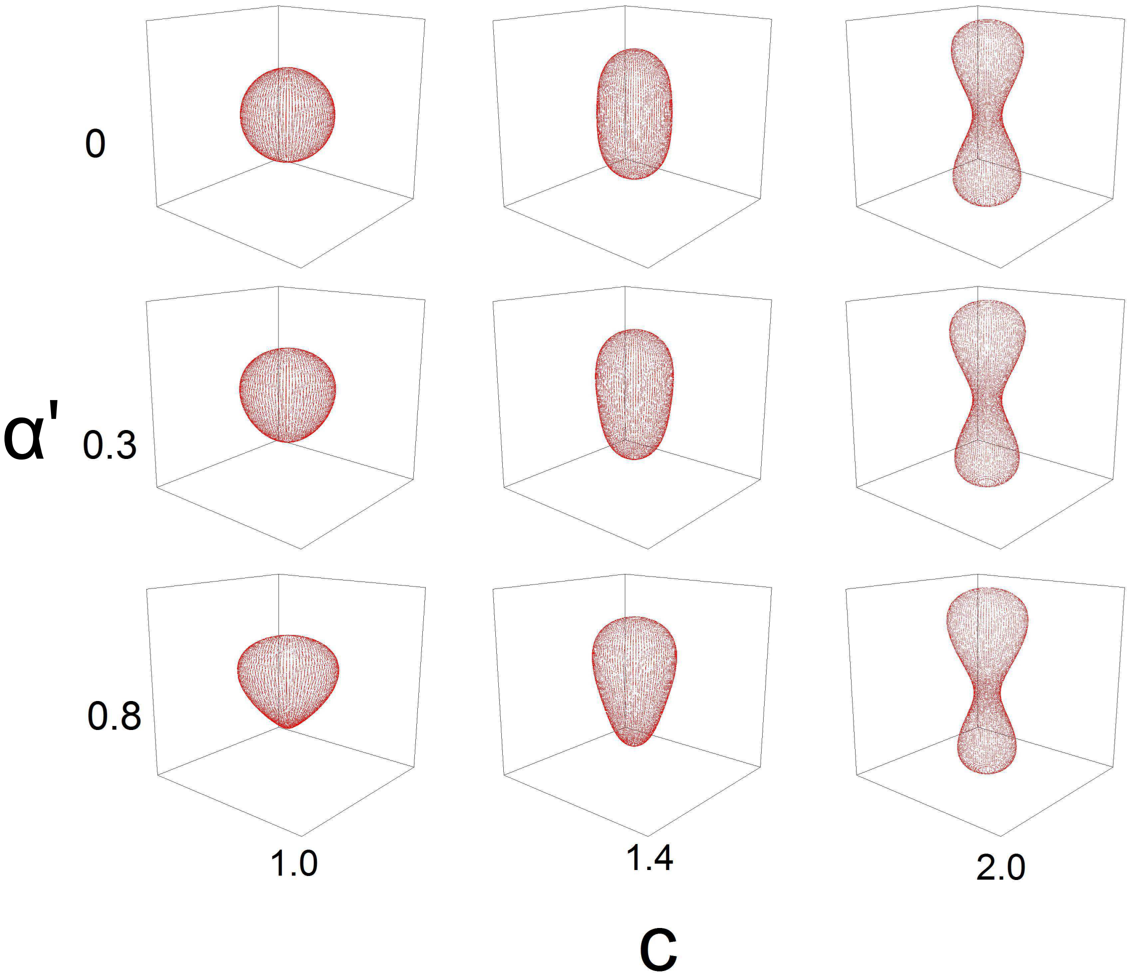

Figure 2.3: *Shapes of nuclei corresponding to different values of c and α' and with $h = 0$*

present work h has been set to 0 and the mass asymmetry at the saddle was set through $\alpha' = ac^3$. The advantage of using α' is that, there are no forbidden and unphysical shapes within $\alpha' \epsilon [-1, 1]$. The mass asymmetry at the saddle can be related by [45]

$$\frac{A_1}{A_2} = \frac{1 + \frac{3}{8}\alpha'}{1 - \frac{3}{8}\alpha'} \tag{2.34}$$

The shapes corresponding to different c and α' combination are shown in Fig. 2.3. The mass asymmetry was also computed by dividing the nucleus at the neck and numerically integrating the two parts at the saddle point. To address the problem of non physical shapes Nadtochy [46] introduced the collective coordinate system $\{q_1, q_2, q_3\}$. However, in this thesis work funny hill shape parametrization approach was used.

2.3.3 Strutinsky's shell correction

The LDM was based on uniform distribution of particles in phase space. According to the basic quantum description of nucleons or the shell model approach, every nucleon moves in an effective potential well created by the effective interaction of all other nucleons. This leads to energy quantization and emergence of so called magic numbers where the nucleus is more stable due to shell closure and low level density close to the Fermi level. The LDM and its later modifications could describe the binding energies and barrier heights of various nucleus with reasonable accuracies. However, it fails to account for large scale deviations from its predictions at certain intervals. Strutinsky [44, 8, 47] developed a prescription in which shell effects were considered as a small deviation from uniform single particle energy level distribution. In this approach, LDM gives the general trend of the energy and a shell correction term is added, which is computed with the deformed shell model. In a similar fashion, a correction term was also added to the pairing strength based on deformation.

The total energy of a nucleus can be written as the sum of LDM energy E_{LDM} which describes the smooth part of the energy and the shell correction term E_{Shell} which describes the single particle states in the vicinity of the Fermi energy.

$$E_{Total} = E_{LDM} + E_{Shell} \tag{2.35}$$

where

$$E_{Shell} = \textstyle\sum_{p,n} \delta U \tag{2.36}$$

The shell correction δU is the the difference between sum of single particle energies of a realistic shell model with non uniform level density and degeneracies and an uniform distribution. Thus

$$\delta U = 2 \sum_{\nu} \epsilon_{\nu} \eta_{\nu} - 2 \int_{-\infty}^{\lambda} \epsilon \tilde{g}\left(\epsilon\right) d\epsilon \tag{2.37}$$

here ϵ_{ν} is the single particle energies in a realistic shell model, η_{ν} are their degeneracies and $\tilde{g}\left(\epsilon\right)$ is an uniform distribution of states.

The shell corrected potential energy could successfully explain ground state deformations and double humped fission barriers seen in actinide nuclei. The inclusion of shell correction in the potential energy also led to an interesting prediction of existence of an island of stability around Z = 114 [48].

2.4 Non compound nuclear processes

The basic assumption in the formation of compound nuclei is the complete oblivion of the initial parameters of the target and projectile. The target and projectile fuse together and the composite system thus formed equilibrates in all degrees of freedom. Since the compound nuclei is formed at a high temperature and angular momentum comparable to the fission barrier heights, the compound nuclei is highly unstable and thus reach the saddle configuration and eventually fission occurs. Even though the LDM and its improved form could describe the gross properties of nuclear fission, it failed in describing certain aspects like asymmetric mass distribution, existence of fission isomers, super deformed nuclei etc. The inclusion of a macroscopic microscopic shell correction term to the LDM potential energy surface could properly describe doubly humped fission barrier seen in many actinide nuclei [44] and also predicted the existence of relatively stable super heavy elements around $Z = 114$ to 120.

With the advancement of advanced accelerator technologies in the nineties, it was possible to accelerate heavier projectiles to higher energies. This opened up new challenges as it became apparent that fusion/fission observables were diverting from statistical model predictions and warranted a deeper look into the dynamics of compound nuclear formation.

The occurrence of these non-compound nuclear processes can be understood in terms of the potential energy between two interacting nuclei as a function of internuclear distance (r) as shown in Fig. 2.4. When the two nuclei approach close to each other with the growth of a neck, the simplest form of interaction potential as a function of separation between two nuclei keeping all other internal degrees of freedom frozen is termed as sudden potential. Subsequently, the di-nuclei thus formed evolves in mass and shape degrees of freedom and the potential energy evolves with the new density distribution. The exit channel potential to fusion fission is approximated through the minimum potential energy in the potential energy surface corresponding to each distance of separation. This is called the adiabatic potential. The adiabatic and the sudden approximations provides a conceptual framework for understanding fusion-fission and associated non compound nuclear processes.

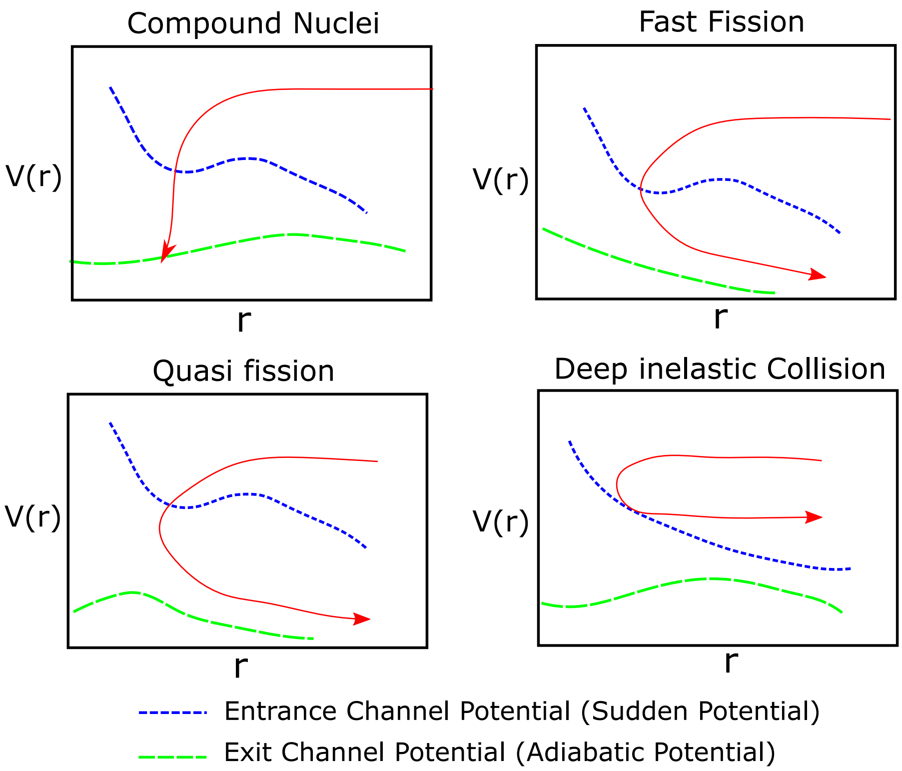

Figure 2.4: *Simplified diagrams of different reaction mechanism in terms of sudden potential and adiabatic potential as a function of internuclear distance*

In case of fusion-fission reactions, the di-nucleus is trapped in the entrance channel and equilibrates in all degrees of freedom evolving into a compound nucleus. In case of quasi fission, the di-nucleus attains the conditional saddle configuration in the entrance channel and subsequently evolves into more symmetry in such a way that the composite system reaches the mass asymmetric saddle directly without crossing the equilibrium potential energy in the adiabatic potential. In other words, there is full energy relaxation and incomplete mass and shape relaxations. Deep inelastic collisions are characterized by incomplete energy relaxation and fast fission occurs at higher energies and angular momentum, where the fission barrier vanishes due to higher angular momentum.

To understand the mechanism of non-compound nuclear fission processes, fission fragment angular and mass distributions are used as experimental probes. Several phenomenological models were also proposed to understand these process that are discussed in the following sub-sections.

2.4.1 Fission fragment angular distribution

Angular distribution of fission fragments is one of the most effective probes in studying the dynamics of fusion fission reactions. Angular anisotropy is the ratio of differential fission cross-section in the direction parallel to the beam with the direction perpendicular to the beam.

$$A = \frac{W\left(0^o\right)}{W\left(90^o\right)} \tag{2.38}$$

In the case of lighter ions, the statistical saddle point model (SSPM) was very

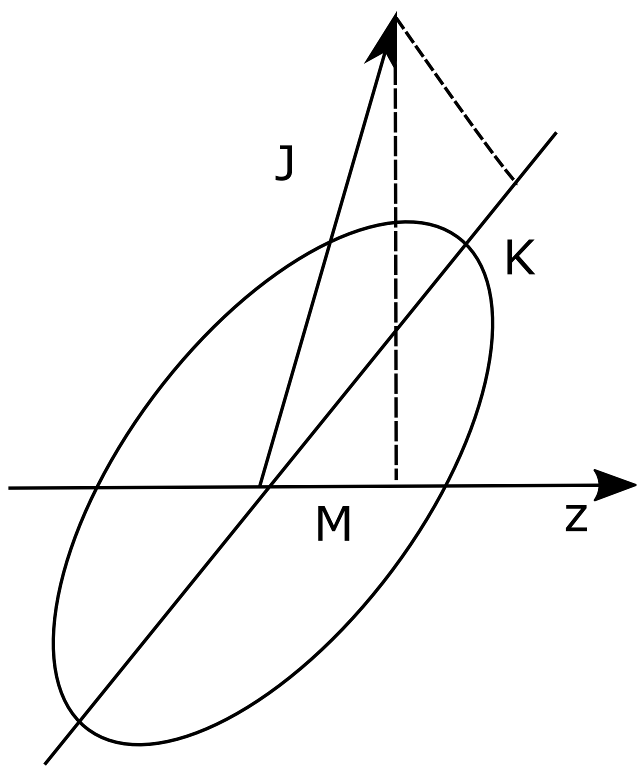

Figure 2.5: *Schematic representation of quantum numbers of a deformed nucleus*

successful in explaining the observed anisotropy [19]. According to the model the angular distribution of fission fragments depend on the angular momentum brought in by the projectile and the angular momentum transferred to the fragments. The transition state model assumes that the fusing nuclei separates along the nuclear symmetry axis and the total angular momentum (**J**) and its projection on the space axis defined by the beam direction (**M**) are conserved throughout the passage of the fissioning nucleus from an initial state of stability to final state of scission through the saddle point configuration. The orientation of the symmetry axis remains unaltered from saddle to scission. The projection of **J** on the symmetry axis (**K**) (Fig. 2.5) is not conserved. During the fission process the nucleus undergo many changes in shape and the K-value at the transition state is unrelated to the initial K value. However, after the nuclei reaches the saddle point it was postulated that **K** becomes a good quantum number. The probability of emitting a fission fragment at an angle θ after the transitioning nuclei has passed the scission is given by

$$P^J_{M,K}(\theta) = \frac{2J+1}{2}|d^J_{M,K}(\theta)|^2 sin\theta d\theta \tag{2.39}$$

where $P^J_{M,K}(\theta)$ is the emission probability of fission fragments at angle θ into a conical volume $d\theta$. The probability is normalized to unity for the limits of integration from 0 to π. The probability $P^J_{M,K}(\theta)$ is arrived at by considering the area of an angular ring on a sphere of radius R of width $Rd\theta$ through which the fission fragments are passing divided by the total area of the sphere, $4\pi R^2$. The area of the ring can be arrived at by width times the circumference of the ring which comes to $2\pi R^2 d\theta$. The $d^J_{M,K}$ functions is given by the following relation

$$d^J_{M,K} = [(J+M)!\,(J-M)!\,(J+K)!\,(J-K)!]^{\frac{1}{2}} \sum_{x=0,1,2,3..} \frac{(-1)^x \left(sin\frac{\theta}{2}\right)^{K+2x} \left(cos\frac{\theta}{2}\right)^{2J-K-2x}}{(J-K-x)!\,(J-x)!\,(x+K)!x!} \tag{2.40}$$

The angular distribution $W^J_{M,K}$ is obtained by dividing the fission fragment emission probability at angle θ by $sin\theta d\theta$

$$W^{J}_{M,K}\left(\theta\right) = \frac{2J+1}{2}|d^{J}_{M,K}\left(\theta\right)|^{2} \tag{2.41}$$

The angular distribution of the fission fragments is determined by the angular momentum brought into the system by the projectile and the fraction of this angular momentum converted into the fragment orbital angular momentum. This fraction is called K, the projection of J on the symmetry axis of the nucleus. According to Statistical Saddle Point Model (SSPM) the orientation of the symmetry axis of the saddle point nucleus, which is determined by the symmetric top wave function, is the fission axis and the orientation remains unchanged from saddle to scission of a fissioning nucleus. The K distribution is the distribution of K values at the saddle point and K_0^2, the variance of this distribution, remains unchanged, according to the assumptions made. The simplified theoretical expression for K_0^2 can be found by considering the level density in the transition state nucleus which is given by the approximate expression

$$\rho\left(J,K\right) \propto e^{\frac{\left(E-E^{J,K}_{rot}\right)}{T}} \tag{2.42}$$

$E^{J,K}_{rot}$, the rotational energy of the nucleus at the saddle point is given by

$$E^{J,K}_{rot} = \frac{\hbar^2}{2I_{\perp}}\left(J^2-K^2\right) + \frac{\hbar^2}{2I_{\parallel}}K^2 = \frac{\hbar^2}{2I_{\perp}}J^2 + \frac{\hbar^2K^2}{2}\left(\frac{1}{I_{\parallel}} - \frac{1}{I_{\perp}}\right) \tag{2.43}$$

Where $I_{\parallel}$ and $I_{\perp}$ are the moments of inertia parallel and perpendicular to the symmetry axis. For fixed E and T and J,

$$\rho\left(K\right) \propto e^{\frac{-E^{K}_{rot}}{T}} = e^{\frac{-\hbar^2K^2}{2I_{eff}T}} \tag{2.44}$$

where $\frac{1}{I_{eff}} = \frac{1}{I_{\parallel}} - \frac{1}{I_{\perp}}$. For

$$K_0^2 = \frac{I_{eff}T}{\hbar^2} \tag{2.45}$$

the equation 2.44 is equivalent to a Gaussian distribution with a width of K_0^2. The saddle point temperature is given by

$$T = \sqrt{\frac{E_{cm} + Q - B_f\,(l) - E_{rot} - E_{pre}}{a}} \tag{2.46}$$

where Q is the Q-value of the system, $B_f\,(l)$ is the angular momentum dependent fission barrier, E_{rot} is the average rotational energy of the nucleus at equilibrium deformation and E_{pre} is the energy lost due to pre-scission neutrons, respectively. a is the level density parameter. In the case of heavy ion reactions, the spins of the target and projectile is negligible in comparison to the orbital angular momentum, so, $M = 0$. Hence the angular distribution in this case is given by,

$$W^J_{M=0}\,(\theta) \propto \sum_{K=-J}^{J} \frac{(2J+1)\,|d^J_{0,K}\,(\theta)\,|^2 exp\,(-K^2/2K_0^2)}{\sum_{K=-J}^{J} exp\,(-K^2/2K_0^2)} \tag{2.47}$$

and by integrating over all J and K states we get

$$W\,(\theta) \propto 1 + \frac{< J^2 >}{4K_0^2} cos^2\theta \tag{2.48}$$

hence

$$A = \frac{W\,(0^o)}{W\,(90^o)} = 1 + \frac{< J^2 >}{4K_0^2} \tag{2.49}$$

The equation 2.49 thus gives a quantitative relationship between the J value and the CN temperature at the saddle point to the observed angular anisotropies. While the SSPM could successfully describe the angular anisotropies for lighter projectiles, for heavier projectiles it was found to underestimate the observed angular anisotropies [20, 49, 50]. This was attributed to the presence of non compound nuclear processes like quasi-fission [51, 21, 24, 25], fast-fission [21] and pre-equilibrium fission [23, 18]. These processes have entrance channel memory intact in them and an admixture of these events with regular fusion fission process can lead to large angular anisotropies [23], anomalous increase in width of the mass distribution of fission fragments with a strong mass angle correlation [52, 53] and suppression of evaporation residue cross section [54]

2.5 The pre-equilibrium fission model

To address the issue of anomalous fission fragment angular anisotropy, Ramamurthy and Kapoor [23] proposed the pre-equilibrium fission model. The criterion for anomalous fission fragment angular anisotropy was based on the Businaro-Gallone critical mass asymmetry (α_{BG}) [26]. According to this model, when the entrance channel mass asymmetry $\alpha > \alpha_{BG}$ the di-nuclear system after capture forms a more compact shape than the elongation of the conditional saddle. This results in a driving force favouring larger asymmetry ultimately leading to a compound nuclei. On the other hand when $\alpha < \alpha_{BG}$ the driving force favours more symmetric configuration leading to separation after mass equilibration. In this case the di-nuclear system separates before K equilibration leading to a smaller value of $\langle K_0^2 \rangle$ than that predicted for a finite rotating liquid drop model and thus leading to larger angular anisotropies. Ramamurthy and Kapoor proposed that anomalous fission fragment anisotropy can arise due to an admixture of compound nucleus events and non-compound fission events in which K degrees of freedom have not been fully equilibrated. This mechanism, called the pre-equilibrium fission is dominant when the fission barrier height B_f is comparable to the saddle point temperature (T).

Though Ramamurthy and Kapoor adequately addressed the occurrence of anomalous angular anisotropy, it was found that almost all systems with deformed targets, mainly actinides, showed anomalous angular anisotropies at near barrier energies irrespective of the mass asymmetry. This was explained by invoking orientation dependence of the relative compactness of the target projectile di-nuclear system by Hinde et. al [27]. In these systems quasi fission is more probable for projectiles hitting the polar region of a deformed target as it favours more elongated mono-nuclear shapes which is prone to a conditional saddle which is asymmetric and thus passing over a mass asymmetric fission barrier producing a characteristic K distribution. On the other hand, projectiles hitting the equatorial regions favours a more compact di-nuclear shape which favours passing over the fusion barrier and fully equilibrating in all degrees of freedom to form a compound nuclei. An admixture of these two events gives the observed K distribution.

2.6 Quasi fission and Swiatecki's criterion

Quasi fission is the phenomenon of total energy equilibration between the reaction partners and lack of mass equilibration before the composite di-nuclear system separates. This is found to occur in systems with high $Z_P Z_T$ values which means that quasi fission is dominant in systems which have heavy nuclei and more symmetric target and projectile. In terms of time scale, quasi fission lies between deep inelastic scattering and compound nucleus formation. In a dynamical model Swiatecki [51] proposed that for reactions involving heavy ions, merely overcoming the fusion barrier does not necessarily lead to formation of compound nuclei. The system requires an "extra push" to fuse and an "extra-extra push" to form a compound nuclei. According to this model there are three milestone configurations that the system has to overcome to form a compound nuclei.

1. The contact configuration in which the reaction partners come into contact and a growth of a neck is favorable. The reactions which do not overcome this threshold lead to elastic and quasi-elastic reactions for heavy systems. For lighter systems overcoming this threshold leads to compound nuclei formation.

2. The conditional equilibrium configuration in a multi-dimentional potential energy landscape at a frozen mass asymmetry. The trajectories that over-

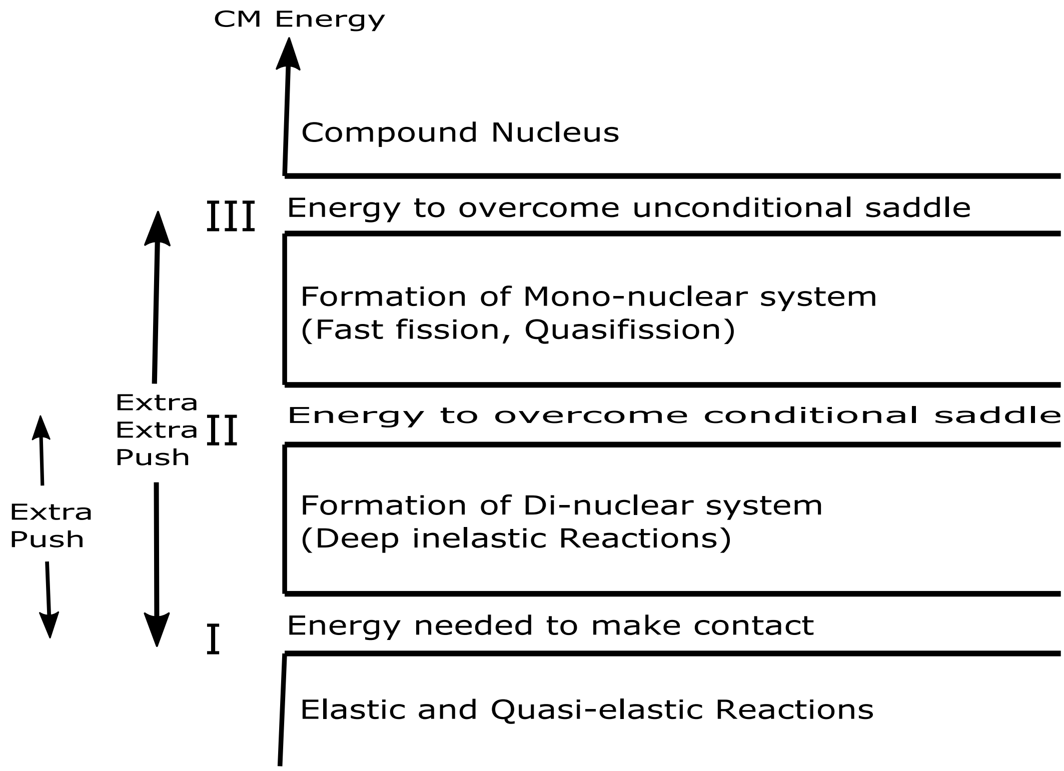

Figure 2.6: *Threshold energies and two types of extra push energies*

come the the type I configuration but not this one lead to deep inelastic scattering.

3. The configuration of unconditional equilibrium. The trajectories that overcome the type I and type II configuration but not type III corresponds to quasi fission. The trajectories that overcome all the three milestone configuration lead to compound nuclei formation.

For heavier ions an "Extra push" energy is required to overcome type II configuration and an "Extra-extra push" to overcome type III configuration. A schematic representation of the same is shown in Fig. 2.6. Even though Swiatecki's model predicts an onset of non compound nuclear processes for systems with $Z_P Z_T > 1600$, signatures of non compound nuclear processes were seen for much lighter systems with $Z_P Z_T \geq 800$.

2.7 Fission fragment mass distribution

Fission fragment mass distribution was one of the first measurable, studied after the discovery of fission. The experimental results of thermal neutron induced fission indicated that the fragment mass distribution in actinides are predominantly asymmetric. The first attempt at theoretical calculation of mass distribution was carried out by Peter Fong [55]. Fong argued that the internal excitation energy of the fragments at the breaking point is larger for the asymmetric than for the symmetric mode. Fong adopted a form of excitation energy at breaking point which includes a deformation parameter and an electrostatic repulsion parameter. A quantitative relationship was derived between excitation energy and the number of quantum states at saddle and the fission fragment mass distribution could be reproduced satisfactorily for slow neutron induced fission for ^{236}U.

Through out the years mass distributions have been studied for numerous nuclei and many target projectile combinations. From these experiments one could arrive at a general classification of mass distributions viz. nuclei with mass heavier than radium at low excitation energies have predominately asymmetric fission and pre-actinides in the Pb and Fr region have predominantly symmetric fission and mass distributions. The line between symmetric and asymmetric fission was not strictly adhered to and with the advent of better spectrometer it was found that nuclei in the Po and At region have an asymmetric component which becomes more prominent at sufficiently low temperatures. The asymmetry in the fission fragment mass distribution arises mainly due to shell effects which gives rise to a barrier structure in the saddle ridge. This barrier structure as well as the shell effects seems to disappear with increasing excitation energies. Saddle to scission dynamics can also play a role in distribution of masses to the nascent fragments. However the closeness of the deformation at the saddle point and scission for pre-actinides permits us to ignore the change in mass distribution during the descent stage.

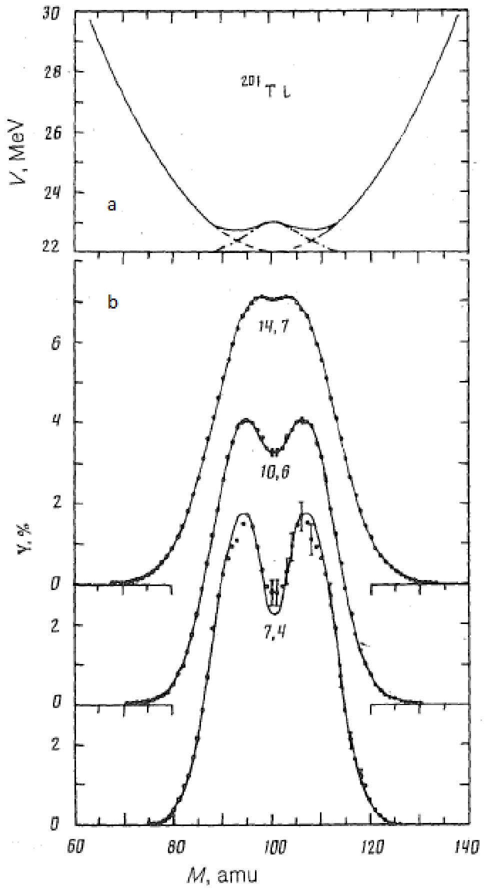

Figure 2.7: (a) *Potential energy* $\widetilde{V}(c, \alpha)$ *as a function of mass asymmetry showing both the liquid drop contribution to the barrier and the contribution by shell correction at the saddle* (b) *Calculation of mass distribution of* ^{201}Tl *with 2.55 [56]*

For fission of highly heated nuclei, the mass distribution is generally Gaussian type distribution.

$$Y(\alpha) = \frac{1}{\sqrt{2\pi\sigma_m^2}} e^{-\frac{\alpha^2}{2\sigma_m^2}} \tag{2.50}$$

where $\alpha = \frac{A_1 - A_2}{A_1 + A_2}$. This form of mass distribution is predicted by the liquid drop model potential $V(c, \alpha)$. With the decrease in excitation energy, shell correction comes into play. Thus the liquid drop potential has to be modified to incorporate shell correction. The new potential $\widetilde{V}(c,\alpha)$ is given by

$$\widetilde{V}(c,\alpha) = V(c,\alpha) + \delta w(c,\alpha) - \delta w_g \tag{2.51}$$

$\delta w(c,\alpha)$ is the contribution due to shell correction at the transition state and δw_g is the contribution at the equilibrium state. Expanding $V(c,\alpha)$ around $\alpha \to 0$ we have,

$$V(c,\alpha)_{\alpha\to 0} = V(c,0) + \frac{\delta V(c,\alpha)}{\delta\alpha}\alpha\mid_{\alpha\to 0} + \frac{1}{2!}\frac{\delta^2 V(c,\alpha)}{\delta^2\alpha}\alpha^2\mid_{\alpha\to 0} + ... \tag{2.52}$$

Ignoring the odd terms in the expansion so as to keep the symmetric nature of the barrier with respect to mass asymmetry, we have

$$V(c,\alpha) = V(c,0) + \frac{1}{2}q\alpha^2 \tag{2.53}$$

where $q = \frac{\delta^2 V(c,\alpha)}{\delta^2\alpha}$ is the stiffness parameter of the nuclei with respect to the asymmetric variation in the shape of the nuclei on its journey from ground state to the saddle point. In terms of the transition state model 2.22, using 2.53 we have the total mass distribution

$$Y(\alpha) \sim e^{-\frac{V(c,\alpha)}{T_{sp}}} \sim e^{-\frac{q\alpha^2}{2T_{sp}}} \tag{2.54}$$

Comparing this to 2.50 we get $\sigma_m^2 = \frac{T_{sp}}{q}$. T_{sp} is the temperature at the saddle point $\sqrt{\frac{E^* - B_f(\alpha)}{a}}$ and B_f is the liquid drop fission barrier height. It is well known that the contribution of shell effects falls off rapidly with excitation energy and for a sufficiently excited nuclei shell effect is non existent. To model the effect of disappearance of shell effect with excitation energy $\delta w(c,\alpha)$ is modified with an additional term $e^{-\lambda E^*}$ where $\lambda = 1/\Delta_E$ in 2.19. So 2.51 stands

$$\widetilde{V}(c,\alpha) = V(c,0) + \frac{1}{2}q\alpha^2 + \delta w(c,\alpha)\, e^{-\lambda E^*} - \delta w_g \tag{2.55}$$

and

$$\widetilde{Y}(\alpha) \sim exp\left[\frac{-\frac{1}{2}q\alpha^2 - \delta w(c,\alpha)\, e^{-\lambda E^*}}{T_{sp}}\right] \tag{2.56}$$

It is easy to see that for $E^* >> 1/\lambda$ 2.56 reduces to 2.54.

$$lnY(\alpha) - ln\widetilde{Y}(\alpha) = \frac{\delta w(c,\alpha)}{T_{sp}} e^{-\lambda E^*} \tag{2.57}$$

The above equation gives a possibility of evaluating the parameters of 2.55 by comparing the degree of departures from symmetry at different excitation energies. Mass distribution of different pre actinides were compared [57] for different nuclei at different excitation energies and it was found that observed departures of $\widetilde{Y}(\alpha)$ from $Y(\alpha)$ is localized in a region of $A/2 \pm 15$. A unified parameter for shell correction at the bottom of the symmetric valley which could successfully describe the observed mass distribution is given by [56, 57]

$$\delta w(c,\alpha) = \delta w(c,0)\, e^{-\gamma\alpha^2} \tag{2.58}$$

The parameter γ is free and from experimental masses, it was found to be varying from $0.015A^2/4$ to $0.020A^2/4$ [57]. The mass distribution for ^{201}Tl using this procedure is shown in Fig. 2.7

The theoretical models, described briefly in this chapter, have been used to understand the results of the experiments carried out in the thesis work.

Chapter 3

Experimental setup and data analysis

As discussed in the previous chapter, the fusion-fission process starts with damping of the projectile-target relative motion and eventual capture of the projectile into the target which is followed by equilibration in various kinematic and microscopic degrees of freedom to form a compound nucleus. The hot rotating compound nucleus is relatively unstable. The compound nuclei may lose energy by evaporation of a few light particles to leave an evaporation residue or, if the fissility is large, the compound nuclei may undergo binary fission. Apart from this, fusion-fission dynamics is also dependent on the entrance channel parameters at near barrier energies. Usually, apart from complete fusion the total reaction cross section consists of admixture of various events like elastic, inelastic, deep inelastic, transfer and non-compound nucleus processes like quasi fission, fast fission and pre-equilibrium fission. So, it becomes essential to separate the fission fragments arising from a compound nuclear reaction from these contaminants.

Experimentally fission fragments can be separated from some of these processes by keeping the detectors at proper folding angles for the complimentary fragments. Folding angle between complementary fission fragments is an experimental signature of the linear momentum transferred in the reaction process.

Silicon detectors are used in many experiments for detection of fission fragment induced by lighter ions. However, these detectors have limited count rate handling capability and are very prone to radiation damage. Added to this is the high cost and small active area make them unsuitable for fragment mass and kinetic energy measurement.

Most of the drawbacks of silicon detectors mentioned above are not present in large area position sensitive gas detectors like multi wire proportional counters (MWPCs). Due to small radiation length they are transparent to elastic and quasi-elastic particles. They are also insensitive to radiation damage and show good timing and position resolution which are critical for fission fragment mass detection. They are also inexpensive and can be fabricated in the laboratory. In this work large area position sensitive multi wire gas detectors were extensively used for fission fragment mass distribution studies.

3.1 Position sensitive multi wire proportional counters

The experimental study of the dynamic aspects of the fission process in which a sufficiently heated compound nucleus moves from the equilibrium state to scission via the saddle requires accurate measurements of mass, energy and angular distributions of fission fragments. Fission fragment yields are low at below barrier energies and have to be separated from a large background of unwanted channels like elastic, quasi-elastic and other non-compound reactions. The separation of these channels requires precise measurements of linear momentum transferred to the compound nuclei which is experimentally manifested by the folding angle distribution of fission fragments. Measurements of folding angles and masses of complementary fission fragment requires precise measurements of velocity, position and energy in a correlated fashion. The above pre-conditions dictates the necessity of large area position sensitive detectors. The position sensitive detectors can detect fragment mass ratios by either a combined velocity-energy measurement completely independent of each other [59] or by accurate measurements of time of flight difference between the correlated fission fragments [60]. The former requires good individual resolving powers of time and energy.

In this work two large area position sensitive multi-wire proportional counters [61] were used for Time Of Flight (TOF) measurements. These detectors have been proven to handle high event rates without any radiation damage and have shown good position resolution, high gain and fast rise time. Further, theses detectors can be modified to suit individual experimental needs by modifying the type of gas, gas pressure and voltage between the electrodes [62]. In our experiment a detector [63], similar to the Breskin type detector [64], was used. These detectors were fabricated in our laboratory at Variable Energy Cyclotron Centre.

3.1.1 Construction of the detector

Our detector is a modified version of the detectors described in [64, 63]. It consists of two parallel plate avalanche counter (PPAC) stage coupled to a low pressure MWPC with an active area of $20cm \times 6cm$. Our detector consists of five wire planes, one anode (A), two position sensitive wire planes (X, Y) and two cathode (C) wire planes separated by spacer planes. The separation between anode and any of the position sensitive X or Y planes were $1.6mm$ while separation of any of the position sensitive planes and a cathode plane was $3.2mm$. A schematic diagram of the cross sectional view of the detector is shown in Fig. 3.1.

The wire planes were made of G-10 quality double sided epoxy, copper plated

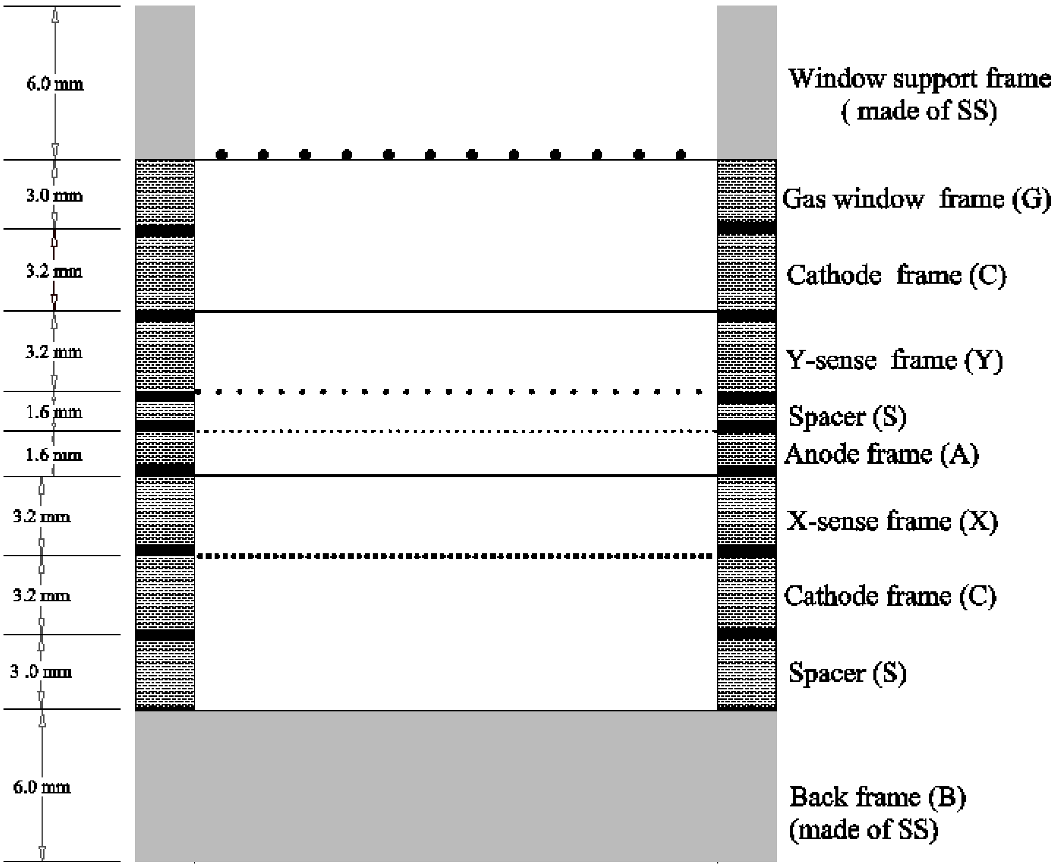

Figure 3.1: *Vertical arrangement of the gas detector*

PCB boards. The anode plane was wired with $10\mu m$ diameter gold plated tungsten wires soldered $1mm$ apart to a conducting strip at either end of the wire plane. The cathode planes were similarly wired with $20\mu m$ diameter gold plated tungsten wires perpendicular to the anode wire plane. The position sensitive X and Y planes were soldered to delay readouts. The X wire plane consisted of 100 wires of pitch $2mm$ and the Y wire planes consisted of 30 wires of pitch $2mm$. The delay between successive X-sense wires and Y-sense wires were $2ns$ and $5ns$ respectively. The delay chips used were of Rhombus Industries, USA make and has a fast rise time. The delay line was terminated by a 50Ω resistance and the signal was taken from the other end. The cathode wire planes were connected in parallel to a power supply through a charge sensitive pre-amplifier. The whole assembly of wire planes and spacers were vacuum sealed with RTV88 sealant. Stretched polypropylene films of thickness $50\mu g/cm^2$ was used as entrance window frame of the detector. The window frame was supported by a stainless steel wire frame. The detector was operated in continuous flow mode and gas flow was controlled by an external flow control system (MKS, USA make)

3.1.2 Offline calibration for operating parameters

The newly fabricated detectors were tested in laboratory for uniformity of the position readouts and to fine tune the operating parameters. A ^{252}Cf source was mounted in front of the detector inside an evacuated chamber. The voltages required for cathode and anode is provided by a over current protected high voltage supply module (N471A,CAEN). In all our experiments Iso-butane was used. The gas pressure and the operating voltages were fine tuned for maximum pulse height and rise time. The optimum voltage for cathode was found to be $\sim -250V$ and that of anode $\sim +300V$. The optimum gas pressure for our detector was $3torr$. To check the correlation between the X and Y readouts and the timing pulses an electronic setup similar to Fig. 3.2 was used. The electronic setup used is discussed in detail in the next section.

3.2 Experimental setup

In fission fragment mass distribution measurements, it is necessary to separate out complete fusion fission events from competing processess like elastic, quasi-elastic and and transfer channels. Experimentally this is done by keeping the detectors at proper folding angles for complimentary fragments as calculated from Viola's systematics. Conventionally fragment mass ratios were deduced

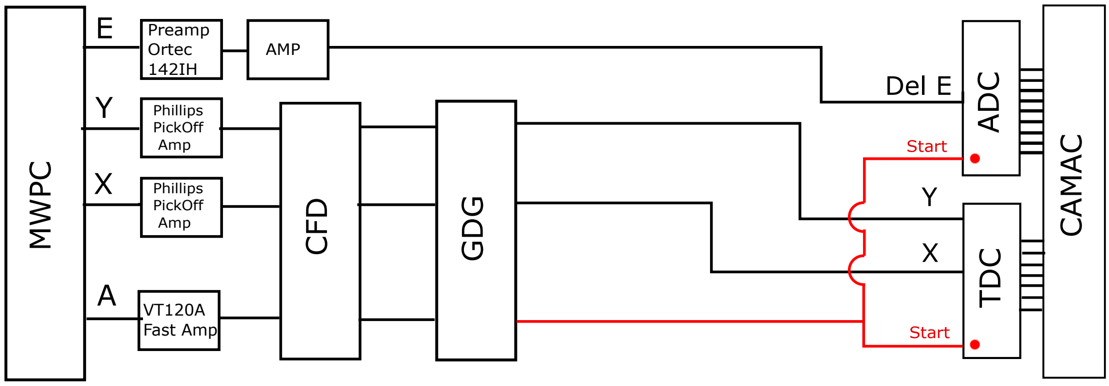

Figure 3.2: *Block diagram of electronics set up for laboratory calibration*

from kinetic energy measurements of complementary fission fragments by solid state detectors. Unfortunately these types of experiments have the inherent difficulties in addressing energy losses of the complementary fragments in the target and energy loss due to prompt neutron emissions from fragments. Further these detectors are prone to show pulse height defects which further dilutes the mass resolution. Another approach to measure the kinematics of fission fragments is the time of flight (TOF) method. In this approach the time of flight for a given fragment is measured through its flight path. The achieved mass resolution depends on the time resolution of the devices measuring the timing at the beginning and end of the flight path. The start time is usually picked up from the pulsing of a bunched beam. The stopping time is usually picked up by a position sensitive detector placed at the end of the flight path.

In the course of this work, to measure the TOF and the folding angle between two complementary fission fragments, two large area position sensitive detectors were placed at folding angles for complementary fragments. The experiments were performed at K-130 cyclotron at Variable Energy Cyclotron Center, Kolkata, 15UD Pelletron at Inter University Accelerator Center, New Delhi and Tata Institute of Fundamental Research, Mumbai. In all the experiments, the detectors were placed inside a large volume scattering chamber on two movable arms. The distances of the forward and backward detectors were fixed in such a way that their angular coverage ensured that all complementary fission fragments were detected by both the detectors. The two arms in the scattering chamber can be rotated all over the reaction plane through a motor driven pulley. The angular position of the arms with respect to the beam axis can be read from outside, either digitally or thorough varnier scale placed beneath the scattering chamber. Two detector stands were made to provide stability to the detector during movement of the arms and to isolate the detectors from electrical interferences. Care was taken so as to align the detectors and target along a central line. The detector needs to be placed absolutely perpendicular with respect to the beam axis so as to avoid any deviations in polar and azimuthal directions which may produce systematic errors in calculation of flight paths. The target was mounted on a target ladder which is placed at the

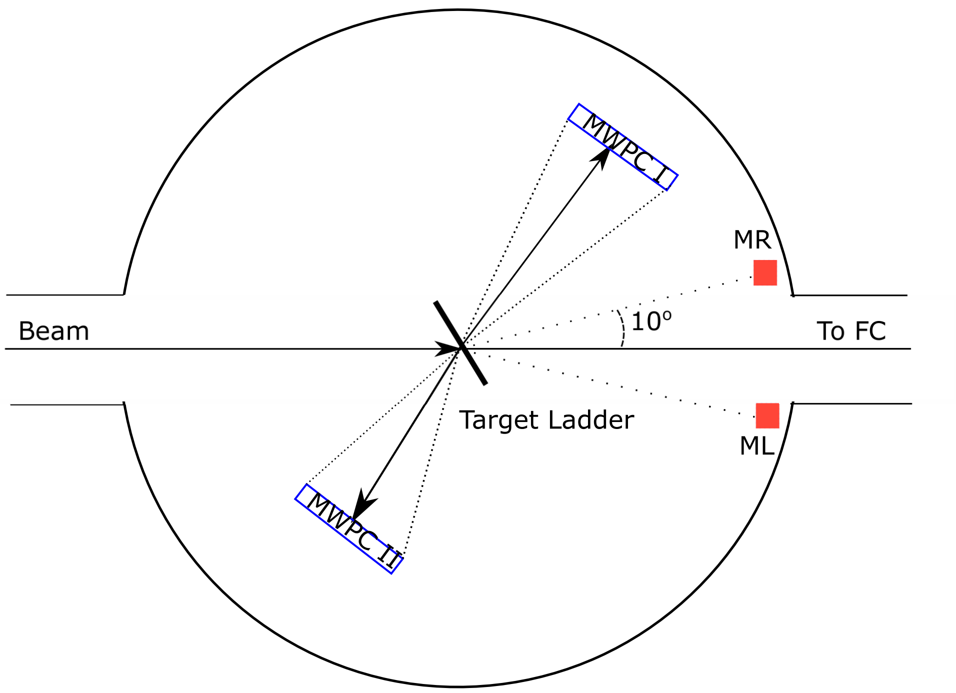

Figure 3.3: *General experimental setup for TOF measurements*

center of the scattering chamber. The ladder can be rotated along its own axis and usually can house more than one target. The suitable target was selected by varying the height of the target ladder. All these could be achieved without breaking the vacuum in the scattering chamber. The residual beam was dumped on a Faraday cup with good neutron shielding to suppress secondary neutrons. The current integrator at the Faraday cup is used to normalize the fission fragment yields. In addition to this two silicon surface barrier detectors of thickness $300\mu m$ are kept at angle $\pm 10^o$ with respect to the beam. This are used to monitor the elastic scattering yields which could be later used to normalize the fission events and for on-line monitoring of the time structure of the beam. A schematic representation of the experimental setup and the actual experimental setup is shown in Fig. 3.3 and Fig. 3.4 respectively. The position sensitive MWPCs within the chamber works in continuous gas flow mode. The flow rate is controlled by a gas handling system through an inlet and outlet pipe attached to the detector. The pumping down process of the scattering chamber to rough vacuum $10^{-3} mbar$ is attained gradually to protect the detector window and the target. The scattering chamber is capable of attaining $10^{-6} mbar$. In all the experiments the detectors were operated at a steady pressure of 3 Torr by using a digital flow rate controller.

3.3 Detector Electronics

The fast timing signal from the anode (A1 and A2) was used to obtain the TOF of the fragments with respect to the beam. The timing signals from both the MWPC1 and MWPC2 were first pre-amplified by ORTEC VT120A pre-amplifier and were then processed through a constant fraction discriminators (CFD). Similarly, the X and Y signals of both the MWPCs were amplified by PHILLIPS 6955B picked off amplifier (PO) and then fed to CFDs. The energy

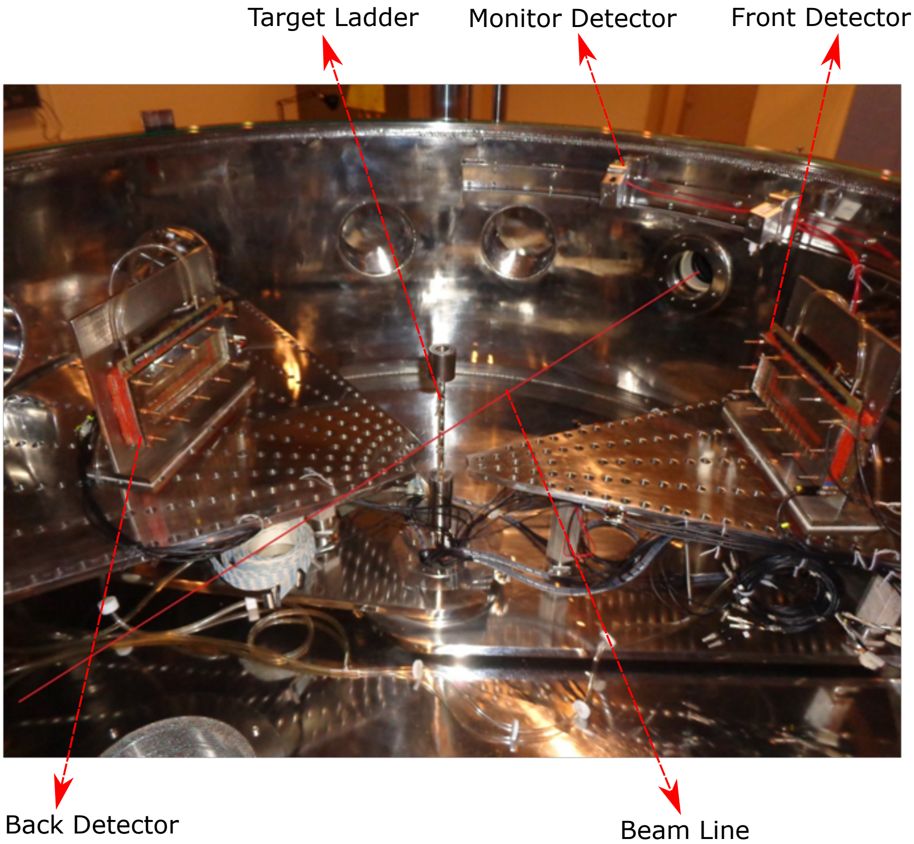

Figure 3.4: *Experimental setup for mass distribution measurements at TIFR, Mumbai*

loss signal in both the detectors, E1 and E2 were pre-amplified by a charge sensitive ORTEC 142IH preamplifier. Care was taken to keep the pre-amplifiers as near as possible to the detector to prevent any attenuation and unnecessary delay introduced due to long wires. The pre-amplifiers were electrically shielded to prevent any unnecessary noise from creeping in. The master trigger was created using the **.OR.** of the discriminated pulses of A1 and A2 in coincidence with RF pulse from the beam buncher $M = (A1 + A2)\,.RF$. This "Master" triggers the data acquisition system (CAMAC) to start acquiring the signal from A1, A2, X1, Y1, X2, Y2, E1 and E2. The signals from anode and X,Y readouts of both the detectors were then time analysed using a 12 bit Time to Digital Converter (TDC) after introducing required delay by a Gate and

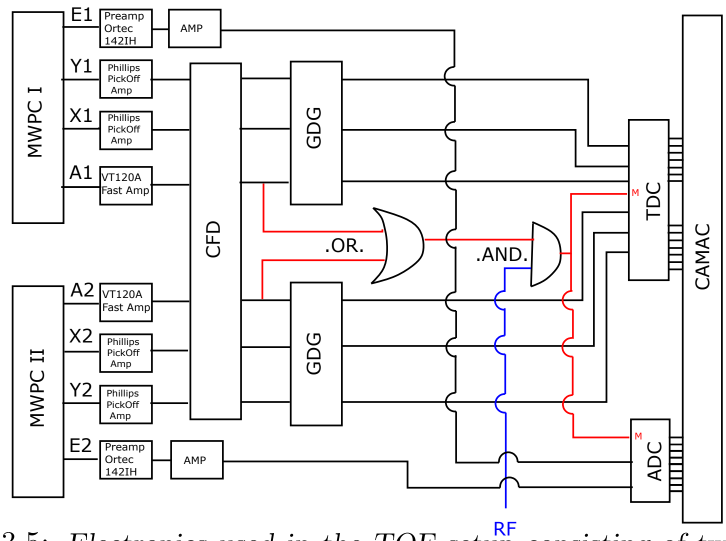

Figure 3.5: *Electronics used in the TOF setup consisting of two detectors MWPC I and MWPC II to obtain fission fragment of mass distribution. RF line is shown in blue and the master trigger signal is shown in red. A, X-Y and E are the anode, position detection and cathode pulses respectively.*

Delay generating module. The energy loss signal was amplified by ORTEC 572 spectroscopic amplifier. The amplified signal was digitized by a 12 bit Analog to Digital converter (ADC) connected to the CAMAC. Real time control and monitoring of data quality was obtained through a standard control software VME-DAQ at VECC and Linux Advanced Multi-Parameter System (LAMPS) [65] at TIFR and IUAC. A simplified schematic diagram of the electronic setup is shown in Fig. 3.5

3.4 Time and position calibration

As discussed earlier, the timing signal viz. A1, X1, Y1 and A2, X2, Y2 were time analyzed using a 12 bit Time to Digital Converter (TDC). The TDC sets a digital representation of time interval between two pulses (the start and stop signal). The digitization process is started following a common start input and the range of the digitizer was kept at 400 ns. The digitization can also be done on a common stop input. In that case all the time spectra obtained are reversed. The calibration of time was accomplished using a ORTEC 462 time calibrator. The Time Calibrator generates pulses at precise time intervals within a set range randomly. The spectra generated is used to test the linearity and to calibrate the TDC. Each output from the Time Calibrator consists of a pair of start and stop pulses. Fig. 3.6 shows the time calibrator spectra and its linear fit in a

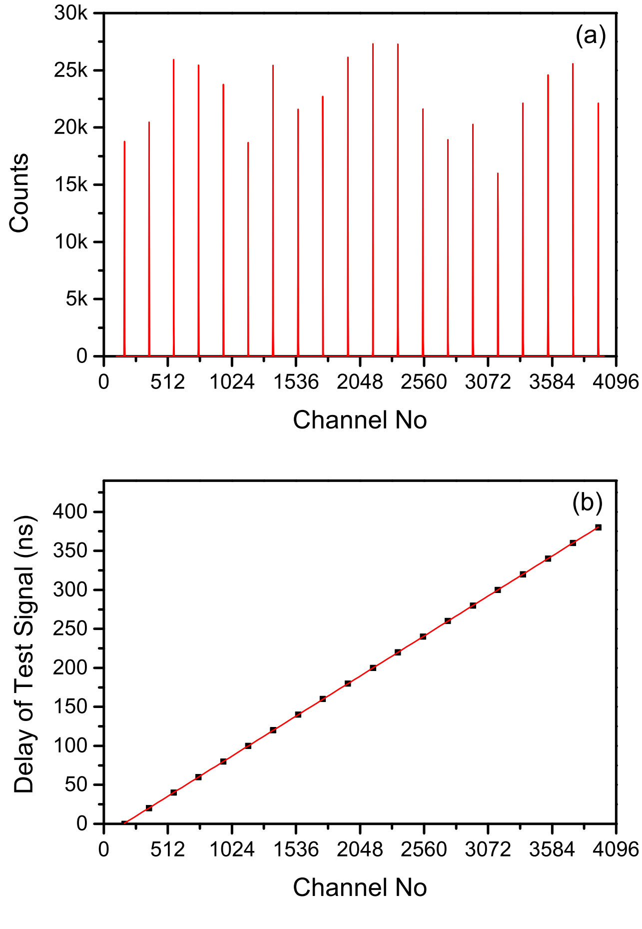

Figure 3.6: *(a)Time calibrator spectra of A1 spectra in a 400ns range with 20ns interval and (b) Linear fit of time calibrator pulse of A1 spectra with respect to TDC channel number.*

20ns interval of A1 pulse in one of the experiments. The channels were perfectly linear and a linear fit was found to be adequate. All the six spectra A1, X1, Y1 and A2, X2, Y2 were put through the time calibrator with 20ns interval across its range of 400ns and was linearly fitted. The coefficients of the fits would give a conversion between channel number of spectra and its time difference.

The position signal of a detected particle is obtained by measuring the delay of the sense wire signal with respect to the anode pulse. The position signal is used to determine the length of flight and the folding angle between the two complementary fission fragments. In order to accurately determine the position, the delay information obtained through time calibration has to be corresponded to angles or actual position within the detector. There are two ways of achieving the relationship between delay and actual position in the detector. The detectors are supported by 14 support wires of 0.4 mm thickness and these produce well defined dips in the X spectra. From these dips the position or angle to the beam can be correlated from the timing spectra of X and Y as discussed in [66]. Secondly we can use a theodolite to exactly know the angle of the edges of the detector from the center and the 14 support wires by rotating the vernier scale of the detector arm and aligning the cross hair of the theodolite with the edges and support wires. The second approach was taken in the current work as it gives better correlation between detector angles and position of detector. As discussed earlier the active area of the detector is 20cm by 6cm and is supported by 14 support wires. The central part of the detector was kept at a predetermined angle with respect to the beam direction and was assigned $l = 0$. The left and right edges were assigned $l = +10$ cm and $l = -10$ cm respectively. The correlation between the X-position of the detector and the off-sets $\Delta\theta$ of the wire positions from the central position for the experimental setup involving ^{210}Po is shown in Fig. 3.7. The plot shows slight non linearity so third order polynomial was used to fit the curve. The time and position calibration is described in more detail in [66, 67].

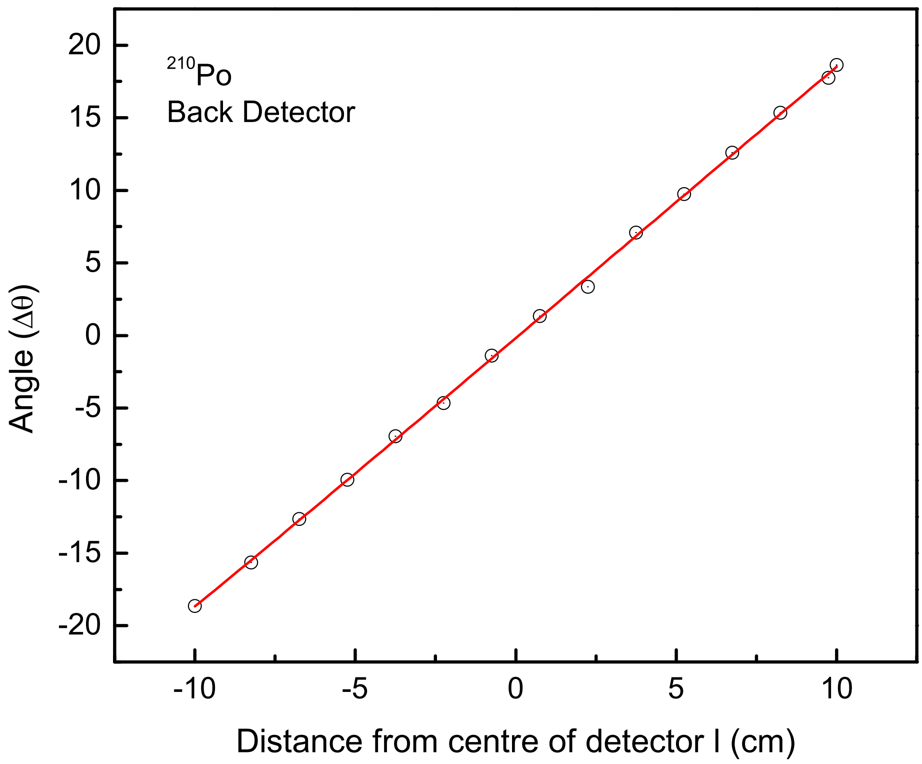

Figure 3.7: *Correlation between the detector X position of the detector fixed through the position of the support wires and the edges and the offset angle of the detector from the central position.*

3.5 Fragment mass distributions

Fragment velocities and thus mass ratios in the laboratory frame can be reconstructed using accurate time of flight measurements, folding angle (θ) and azimuthal angle (ϕ) measurements. The mass distribution can be obtained from simple kinematics of mass and momentum conservation. Form the illustration below, by applying the principle of conservation of momentum we get

$$P_1 cos\theta_1 + P_2 cos\theta_2 = M_{CN} V_{CN}$$
$$P_1 sin\theta_1 = P_2 sin\theta_2 \tag{3.1}$$

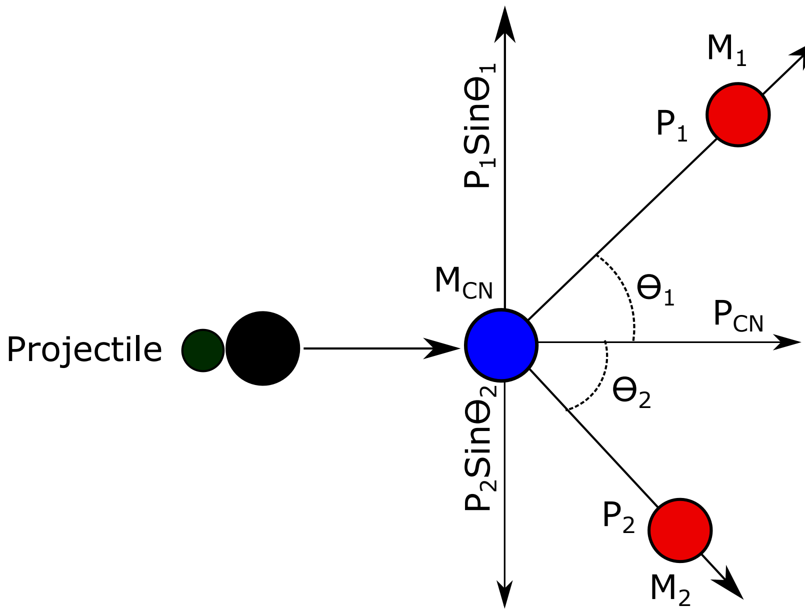

Figure 3.8: *Fusion fission kinematics*

where M_{CN} and V_{CN} is the mass and velocity of the CN. 3.1 leads to

$$P_1 = \frac{M_{CN}V_{CN}}{sin\,(\theta_1 + \theta_2)} sin\theta_2 \tag{3.2}$$

and

$$P_2 = \frac{P_1 sin\theta_1}{sin\theta_2} \tag{3.3}$$

The time of flight difference between the emitted fragments can be expressed as

$$\begin{aligned} t_1 - t_2 &= \frac{d_1}{v_1} - \frac{d_2}{v_2} = \frac{d_1 M_1}{P_1} - \frac{d_2 M_2}{P_2} \\ &= \frac{d_1 M_1}{P_1} - \frac{d_2}{P_2}\left(M_{CN} - M_1\right) \end{aligned} \tag{3.4}$$

where d_1 and d_2 are the flight path lengths of the complementary fission fragments. Rearranging the terms we get

$$M_1 = \frac{(t_1 - t_2) + M_{CN}\left(\frac{d_2}{P_2}\right)}{\left(\frac{d_1}{P_1} + \frac{d_2}{P_2}\right)} \tag{3.5}$$

The experimentally measured time of flight of fission fragments also contain delays introduced by electronic modules and cables and also the time structure of the beam pulse. To tackle this issue t_1 and t_2 is replaced by $t_1 + \delta t_1$ and $t_2 + \delta t_2$ respectively in 3.5. The difference of δt_1 and δt_2 denoted as δt_0, is independent of the beam profile. The finite delay δt_0 introduces a linear shift in the mass distribution. δt_0 is adjusted by using the identity property of the complementary mass distributions. The flight paths d_1 and d_2 are determined from the exact distances L_1 and L_2 of the centres of the respective MWPCs from the target and precise measurements of impact points on the detectors through X_1, Y_1, X_2 and Y_2 of MWPC1 and MWPC2 respectively.

The fragments lose a part of their energies in the target itself. So very thin targets were used so as to minimize the error in TOF calculations.

3.6 Folding angle calculation

In binary reactions, the emitted fragments are separated by 180^o with respect to each other in the centre-of-mass frame. In the laboratory frame, the angle of emission between the two fragments, called the folding angle, depends on the velocity of the emitted fragments and also on the recoil velocity of the fissioning nucleus. Compound nucleus (CN) formation involves complete linear momentum transfer in the beam direction from the projectile to the fissioning nucleus as opposed to direct reactions and incomplete fusion reactions. Thus in CN formation the two fragments will be separated at a characteristic angle less than 180^o in the laboratory system. Fission fragments following other processes which involves incomplete linear momentum transfer will be separated by an angle greater than that of two fragments formed after CN formation. Hence, by knowing the proper folding angle of the complimentary fragments, the fragments from two competing processes can be separated easily. As shown in the figure,

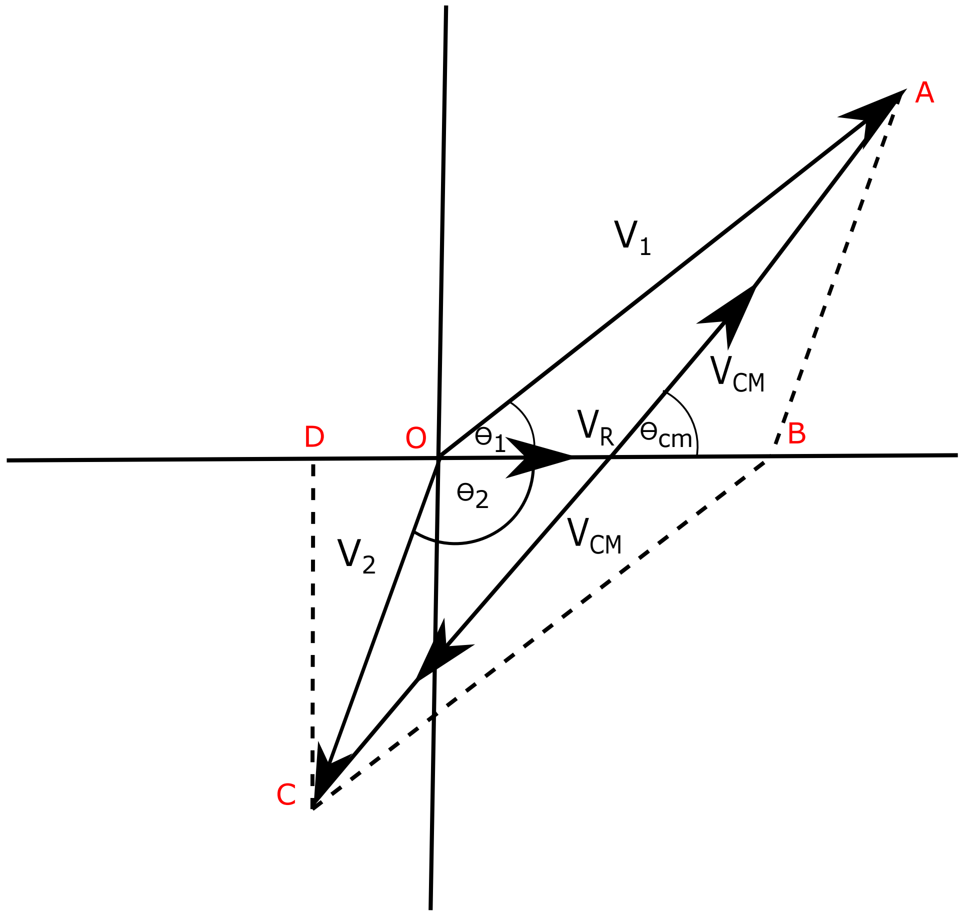

Figure 3.9: *Kinematics of complete fusion followed by fission*

V_1 and V_2 are the velocities of the fission fragments in the lab frame and V_{CM} is the velocity in the center of mass frame. V_R is the recoil velocity of the compound nuclei. θ_1 and θ_2 are the angles of emission of the complementary fission fragments such that

$$\theta_{fold} = \theta_1 + \theta_2 \tag{3.6}$$

The angle at which the forward detector is placed, θ_1 is known apriori. θ_2 can be calculated by

$$tan\theta_2 = -tan\,(\pi - \theta_2) = -\frac{DC}{DO} = -\frac{DC}{DB - OB} \tag{3.7}$$

substituting the values DC, DB and OB we get

$$tan\theta_2 = \frac{V_1 sin\theta_1}{2V_R - V_1 cos\theta_1} \tag{3.8}$$

thus

$$\theta_{fold} = \theta_1 + tan^{-1}\left[\frac{V_1 sin\theta_1}{2V_R - V_1 cos\theta_1}\right] \tag{3.9}$$

from the above figure we may say $\overrightarrow{V_{CM}} = \overrightarrow{V_1} - \overrightarrow{V_r}$ which unfolds into

$$V_{CM}^2 = V_1^2 + V_R^2 - V_1 V_R cos\theta_1 \tag{3.10}$$

Rearranging the equation and solving the quadratic equation for V_1

$$V_1 = \left[V_R cos\theta_1 \pm \sqrt{V_R^2 cos^2\theta_1 + (V_{CM}^2 - V_R^2)}\right] \tag{3.11}$$

Only the positive root is considered as with increasing value of θ_1, V_1 becomes negative which is unphysical.

$$V_1 = \left[V_R cos\theta_1 + \sqrt{V_R^2 cos^2\theta_1 + (V_{CM}^2 - V_R^2)}\right] \tag{3.12}$$

The recoil velocity V_R can be calculated from the recoil energy E_R which in turn can be obtained from the incident angular momentum P_i

$$V_R = \sqrt{\frac{2E_R}{A_{CN}}} \qquad\qquad E_R = \frac{P_i^2}{2A_{CN}} \tag{3.13}$$

where A_{CN} is the CN mass.

The centre-of-mass velocity V_{CM} of the fragment is obtained using Viola systematics [58] which assumes symmetric fission between two spheres in contact.

$$< E_K >= \left[0.01189\frac{Z^2}{A_{CN}^{1/3}} + 7.3\,(\pm 1.5)\right] \tag{3.14}$$

Experimentally observed folding angle distribution is Gaussian in shape for CN fission. The width of the folding angle distribution depends on several kinematic factors such as asymmetric mass splitting and pre-scission and post-scission neutron emissions. Any contribution from incomplete fusion following fission such as transfer-fission gets adequately resolved as humps on both sides of the full linear momentum transfer events in the folding angle distribution.

3.7 Data analysis techniques

The main aim of data post processing is the elimination of events arising from elastic, quasi-elastic reactions and incomplete fusion and to adjust the machine time delays of the anode pulses from the beam buncher pulse. The machine time delays of the anode pulses ($\delta t_{01}\&\delta t_{02}$) from the buncher of the Pelletron varies with beam energy. This could be obtained from the timing spectra of elastically scattered projectiles from the target at very forward angles. However, in most cases, the machine time delays $[(\delta t_{01} - \delta t_{02}) \rightarrow \delta t_0]$ is determined from the identity of the mass spectra of the two detectors.

One of the basic necessities in time difference method is the ruling out of

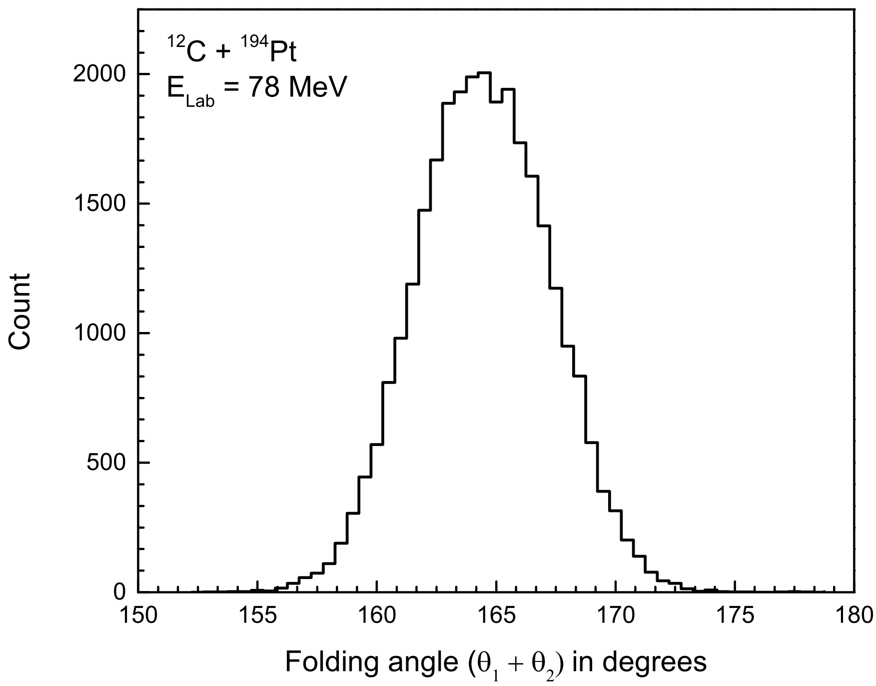

Figure 3.10: *Folding angle between two complementary fission fragments for* $^{12}C+^{194}Pt$ *at* E_{Lab} = *78 MeV*

events arising form incomplete momentum-transfer events such as transfer fission. In reactions involving non fissile targets, the transfer events are virtually absent but it is not the case in highly fissile actinide target. To get rid of this problem, the X and Y positions in the two detectors were transformed to polar angles. The polar angle obtained from the two detectors are added to yield the folding angle. The resulting folding angle distribution is shown in Fig. 3.10. If the fraction of transfer fission event is appreciably high, the resulting folding angle distribution gets resolved into two or more peaks depending on the linear momentum transferred. One of the peaks corresponds with the expected position calculated according to Violas systematics [58] which assumes symmetric fragment masses. These events are due to fission after full momentum transfer from the projectile to the target. Other structures in folding angle distributions (if any) are broad and may be on either side of the peak due to partial momentum transfer. Lower folding angles signifies larger momentum transfer than that of fusion fission and vice versa. Larger momentum transfer occurs due to the ejectiles emitted in the backward direction. Widely varying recoil angles and velocities makes the distribution for the transfer fission component broader than that of the fusion fission component especially at near and sub-barrier energies. The correlation of the polar and azimuthal angles of fission fragments is an effective way of separating events according to the linear momentum of the projectile transferred to the fused system. If transfer fission events are appreciable, two bands, representing the folding angle distributions of fusion fission and transfer fission, will be visible.

Contributions of elastic and quasi-elastic channels are virtually absent because the detectors are thin and operated at low pressure which makes the detectors almost transparent from the elastic and quasi-elastic channels. Residual elimination of elastic and inelastic channels from fission fragments were obtained by correlating the energy deposition signals (E1 and E2) of the two MWPCs. Fig. 3.11 shows the energy deposition by the coincident particles in the two detectors at a given energy.

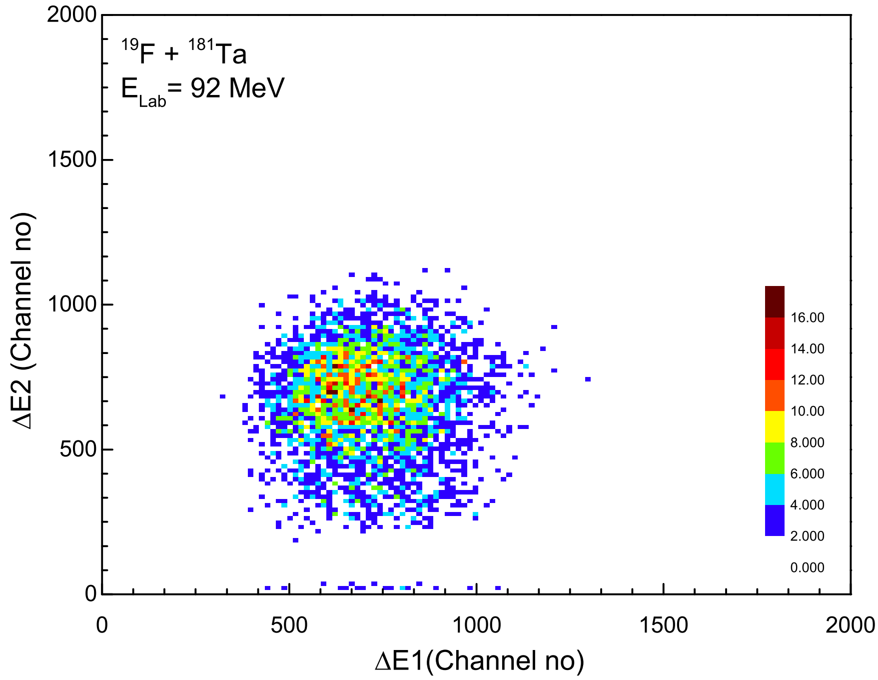

Figure 3.11: *Coincident spectra of cathode signals of the two detectors (energy losses $\delta E1$ and $\delta E2$) for $^{19}F +^{181} Ta$ at E_{Lab} = 92 MeV*

Mass distribution measurement requires determining the actual flight paths of the complimentary fission fragments. The local co-ordinates of the impact point of the fission fragments with respect to the centers of the detectors, (X1, Y1) and (X2, Y2) were used to find the precise flight path lengths of both the fragments. The timing signals t1 and t2 were recorded for each event and their difference $(t1 - t2)$ is calculated event by event. The time calibration coefficients are used to yield the actual time difference. Fig. 3.12 shows a typical plot of timing difference between two complementary fission fragments for $^{12}C +^{194} Pt$ at 78 MeV lab energy.

In this thesis work, three experiments were carried out. Each experiment had different setup (flight path, angular coverage etc) depending upon the reactions studied. These are discussed in detail in the next three chapters.

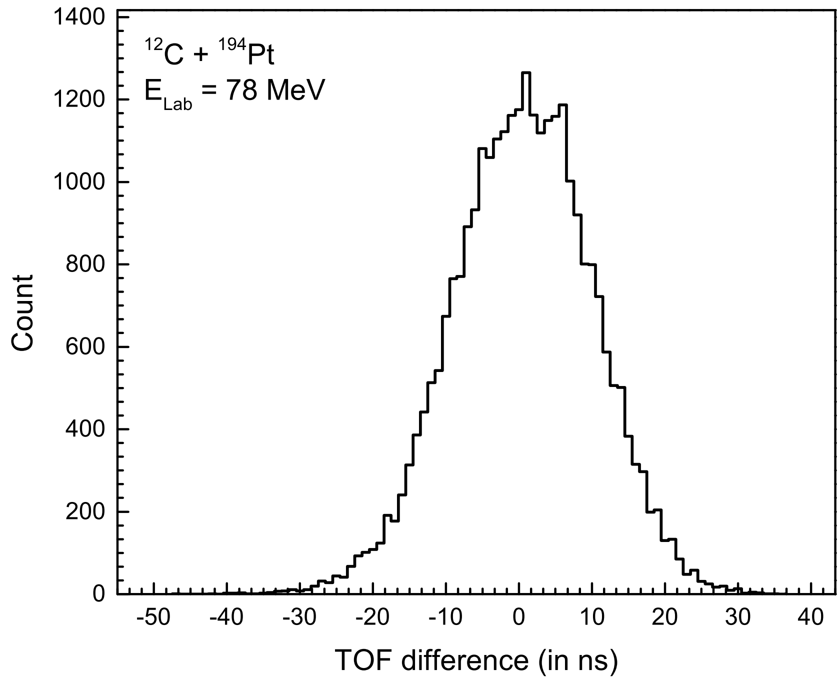

Figure 3.12: *TOF difference between two complementary fission fragments for* $^{12}C +^{194} Pt$ *at* E_{Lab} *= 78 MeV*

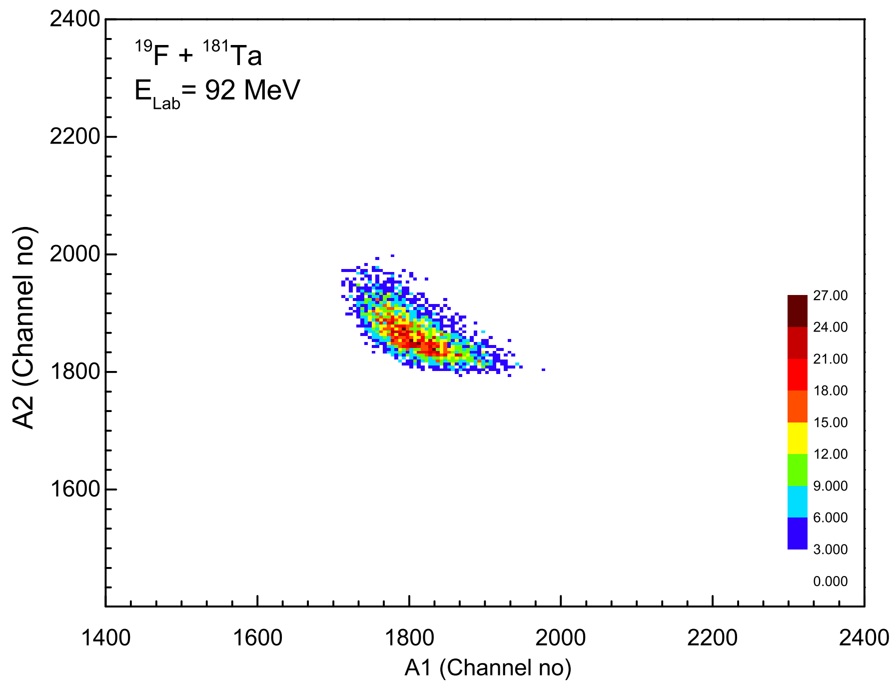

Figure 3.13: *Coincident spectra of anode signals between two complementary fission fragments for* $^{19}F +^{181} Ta$ *at* E_{Lab} *= 92 MeV*

Chapter 4

Washing out of shell effects with excitation energy

Determining the limits of the nuclear chart is an open and challenging question for both physicists and chemists. The Liquid Drop Model (LDM) of nucleus [3] predicts that element beyond Z = 104 can not exist. If the two fundamental nuclear parameters, the attractive nuclear surface potential and the repulsive coulomb forces are taken into account, then fissility of a nucleus ($\chi = \frac{E_C}{2E_S}$,ratio of Coulomb energy (E_C) and surface energy (E_S)) becomes 1 and fission barrier height [$B_f = 0.7(1-\chi)^3 a_s A^{2/3}$, where $a_s A^{2/3}$ is the surface term in binding energy formula] becomes zero. Thus nuclei with $Z \geq 104$ immediately fission as there is no barrier to prevent their decay. However, elements beyond that atomic number have been synthesized in laboratory [48]. The heaviest element synthesized in the laboratory with Z = 118 is known as Oganesson.

The observed stability of these heavy elements is originated from the microscopic shell effects. While the bulk properties of nuclei and their collective behavior are explained by LDM, nuclear Shell Model [68] takes into account the single-particle nature of nuclear states where shell gaps can be interpreted as regions of reduced level density. Both the macroscopic properties and the shell effects of nuclei can be incorporated by adding a shell-correction term to the LDM binding energy. Strutinsky [8, 44] used the shell averaged single particle energy as a correction term to the liquid drop model energy. The fission barriers predicted by the liquid drop model decreases with the increasing atomic number and nuclear fissility. However, the shell correction can become large even when the macroscopic barriers are vanishingly small. Thus, incorporation of the shell correction to the macroscopic barrier leads to alteration of the barrier height, leading to large fission barriers which can stabilize the ground state of nuclei against spontaneous decay. These purely shell stabilized nuclei show an increase in the alpha or fission half-lives by several orders of magnitude compared to that predicted by macroscopic theories. The possibility of purely shell stabilized nuclei gave rise to the possible existence of new elements in the super heavy domain. Other important nuclear phenomena such as super deformed nuclei [69], fission isomers [9] and new magic numbers in the exotic nuclei [70] are the consequences of the microscopic shell effects.

It is generally seen that shell effects are annihilated at higher excitation energies [19]. One of the ways of production of new super heavy elements is by bombardment of heavy ions on actinides targets and the compound nuclei are always formed with high excitation energies to the order of a few tens of MeV. Excitation energy is thus an important parameter and fine tuning the excitation energy may increase the production cross section of the SHE by several orders of magnitude. Therefore, it is really important to constrain the excitation energy at which shell effects get washed out.

Several authors [71, 72, 73] had studied previously the fission fragment mass distribution (FFMD) of actinides nuclei. Colby *et al* [71] carried out radiochemical study of fission fragments of alpha induced fission of ^{238}U and reported that the mass distribution in fission of ^{242}Pu are asymmetric up to a lab energy of about 40 MeV, indicating the presence of the shell effect. Back *et al* [72] showed that for ^{242}Pu, even at an excitation energy of 45-50 MeV, shell effect persists and the FFMD are asymmetric. But in 310 MeV ^{16}O inelastic scattering on ^{238}U, Back *et al* [73] observed symmetric mass distributions at high excitations signifying washing out of the shell effects, and asymmetric mass distributions at low excitations. However, for a particular actinides element, the exact energies at which the shell effects disappear could not be found out in the above experiments.

In this thesis work, an experiment was carried out to constrain the excitation energy at which nuclear shell effects washes out for an actinides nuclei. Fission fragment mass distribution in alpha induced fusion-fission reaction on ^{232}Th target at a wide excitation energy range of 21-64 MeV was measured. For the first time, a direct evidence is shown that the shell effect is washed at excitation energy of about 40 MeV in ^{236}U.

4.1 Experimental setup

The experiment was performed with alpha beam from the K-130 cyclotron at the Variable Energy Cyclotron Centre, Kolkata, India. The target used was a self-supporting ^{232}Th foil. Fission fragments were detected using two large-area (20 cm $\times$ 6 cm) position-sensitive multi-wire proportional counters (MWPCs) [63] as described in a previous chapter. These were placed at the folding angle of fission fragments on either side of the beam axis, covering an angular arc of 67° and 83°, respectively. The time difference of the fast anode pulses with respect to the pulsed beam, the X and Y positions and the energy loss of fission fragments were measured for each event. The detectors were maintained at an operating pressure of 3.0 torr of isobutane gas. The gas pressure was kept low to make the detectors almost transparent to elastic and quasi-elastic particles. The accuracy in measurement of polar angle and azimuthal angle of emitted fission fragments was found to be better than 0.2° and 0.8° respectively.

Beam flux monitoring as well as normalization was performed using the elastic events collected by a silicon surface barrier detector placed at forward angle and the total charge collected at the Faraday cup. The event data collection was triggered by the detection of a fission fragment in any of the MWPC detectors in coincidence with the beam pulsing of the Cyclotron.

4.2 Details of data analysis

The fission fragments were separated from quasi-elastic channels through coincident time spectra of both the detectors and energy loss spectra. The measured excitation function for fission is shown in Fig. 4.1. The measured fission excitation function is compared with the previous results of Ralarosy *et al.* [74] and was found to be in agreement with the present measurement. A coupled channel calculation (CCDEF) [75], as shown by the solid lines in the Fig. 4.1 was also done. In the CCDEF calculation, axially symmetric shape of the target, with nuclear quadruple and hexadecapole deformation parameters $\beta_2 = 0.217$ and $\beta_4 = 0.09$ [76] were used. The experimental and theoretical fission excitation function is mostly in agreement at all energies in and around and above the barrier.

The measurement of fission cross section was also carried out at deep sub-barrier energy (7.7 MeV), where no measurement have been reported so far. This low energy beam was obtained in 3rd harmonic operation of the cyclotron. Interestingly there is an enhancement in measured fission cross section as compared to the theoretical prediction in the deep sub-barrier region. The fission cross section measurement at deep sub-barrier energies is experimentally challenging and this phenomenon of enhancement of cross section is of particular interest for extreme sub-barrier fusion reactions of astrophysical interest [77, 78].

However, the mechanism of fission enhancement is not in the scope of the present thesis work and has not been discussed here.

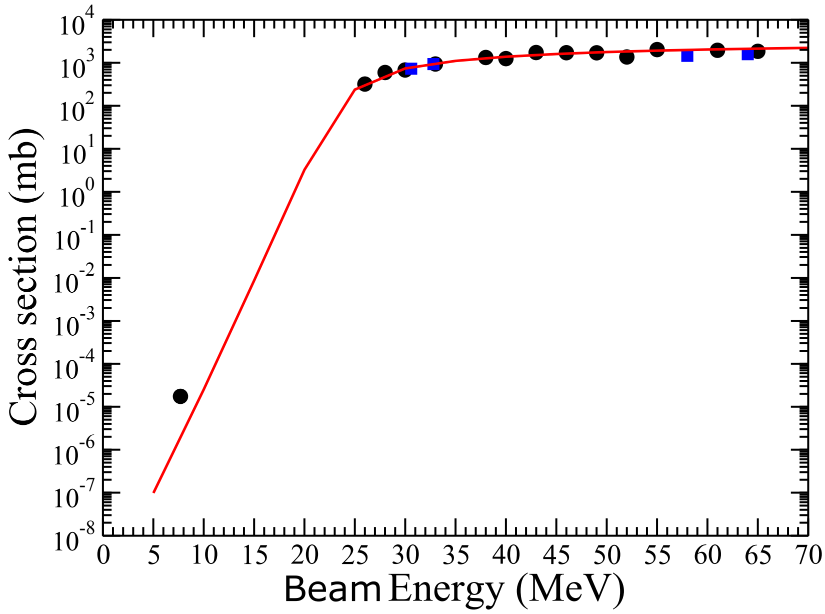

Figure 4.1: *The fission excitation function of ^{4}He+ ^{232}Th reaction. The solid (black) circles represent the present measurement. Measurement of Ralarosy et al. [74] is shown by solid (blue) squares.*

In Fig.4.2, a typical distribution of the complementary fission fragments in (θ, ϕ) plane at an excitation energy of E* = 23 MeV is shown. The polar and azimuthal angle correlation for the fission fragments shows that incomplete fusion is non-existent and the fission followed formation of compound nucleus. The spread in the polar and azimuthal angular correlations is due to fission reaction kinematics and neutron emission from fragments. It is quite possible that angular deviations due to neutron emissions can wash out kinematic correlations of the complementary fission fragments, so only the events within the high intensity region in the middle of the θ - ϕ correlation plot which corresponds to an angular cone of radius 4^{o}, as shown in Fig. 4.2 (black circle), were used for computation of mass distributions. Precise measurements of flight paths and time of flight differences of the complimentary fission fragments [63, 79] was used to

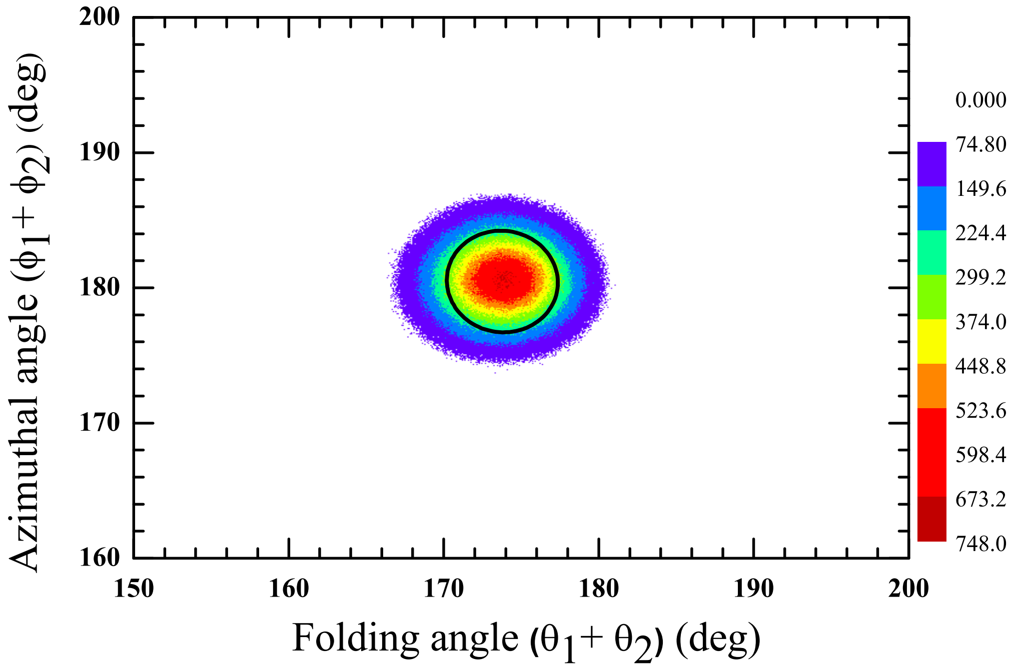

Figure 4.2: *Measured distributions of folding angles of the fissioning nuclei formed in the reaction $^{4}He+^{232}Th$ at an excitation energy of 23 MeV.*

determine the masses of the fission fragments. The details of the procedure has already been explained in chapter 3.

The FFMD extracted from the relevant events at different excitation energies are shown in Fig. 4.3. Since the cross section is very low, the FFMD at beam energy energy of 7.7 MeV could not be measured. It was observed that, for excitation energies between 43.6 - 64.2 MeV (Fig. 4.3 i-l), the measured mass distributions are symmetric and could be well described by a single Gaussian function peaking at half of the mass of the compound nucleus. Since in this highly fissile system, quasi-fission is not expected, the symmetric mass distributions are more likely to originate from a fully equilibrated compound nucleus passing through the saddle ridge defined by the macroscopic (LDM) barrier. Microscopic (shell) effects is not significant on the fission barrier at these energies. The widths of the FFMD is expected to be following statistical process and would be a smooth function of temperature or excitation energy. On the other hand, the shape of the FFMD changes from symmetric to asymmetric at excitation energies $\leq$ 40.5 MeV (Fig. 4.3 a-h).

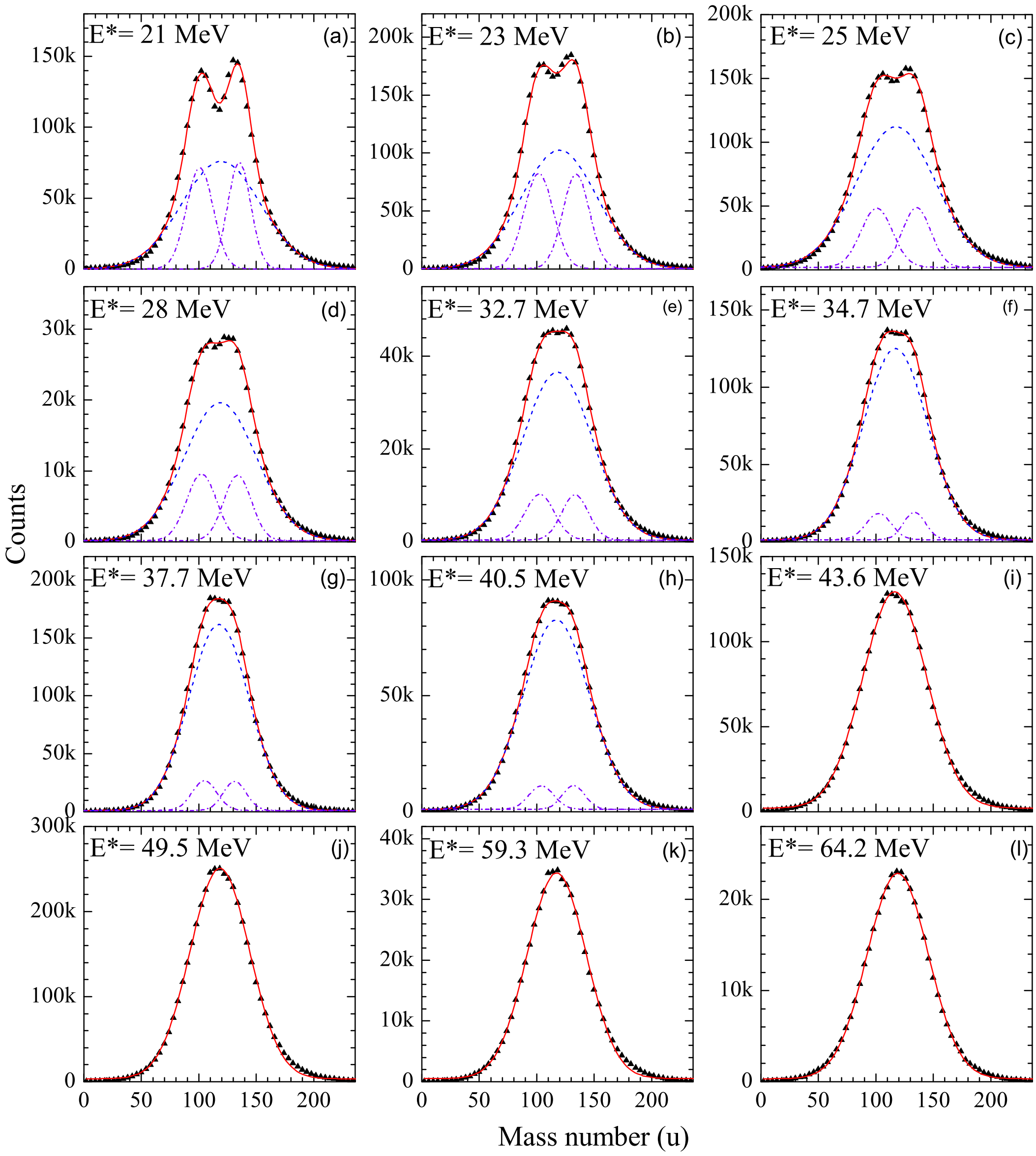

Figure 4.3: *Plots of fission fragment mass distributions at different excitation energies. These were fitting by three Gaussians for E^* = 21 MeV to 40.5 MeV are shown by dash blue (symmetric component) and violet dash-dotted (asymmetric components) lines. The overall fitting is shown by full (red) lines. The mass distributions at higher excitation energies ($\geq$ 43.6 MeV) are best fitted by a single Gaussian.*

The characteristic features of mass distributions have been further analyzed at lower excitation as shown in Fig. 4.4 using the data of 23 MeV excitation energy. In the top half of the figure marked (a), an attempt was made to fit the data by two Gaussian functions of equal area which would be the scenario assuming asymmetric fission as observed in the case of spontaneous or thermal neutron induced fission [19]. But based on both the relative χ^2 values and the visual inspection of the fits, it is clear that the fits are not satisfactory and the distribution could be best fitted by three Gaussian functions, with one of the peaks corresponding to the symmetric (A $\sim$ 118) division and the other two at A $\sim$ 132 and A $\sim$ 100. This suggests the simultaneous co-existence of both asymmetric and symmetric components of fission at this excitation energy.

4.3 Results and discussions

It can be seen from Fig. 4.3a-h that all FFMDs with E* $\leq$ 40.5 MeV are best fitted with three Gaussian functions as discussed previously in the case of E* = 23 MeV. However, it is observed that there is a steady decrease in the total area under the Gaussians for asymmetric division, with increase in excitation energy and at 40.5 MeV, the two asymmetric peaks were barely visible and are annihilated at 43.6 MeV, where the experimental data could be fitted with a single Gaussian. Thus, it can be concluded that symmetric fission is only mode above 43.6 MeV. The ratio of the areas of the symmetric to the total yields (G_{sym} / (G_{sym} + G_{asy1} + G_{asy2}), where G_{sym}, G_{asy1} and G_{asy2} are the areas under symmetric and two asymmetric components), as a function of excitation energy is shown in Fig. 4.5 to present a more quantitative picture of the above assertion. It can be easily seen that the probability of fission from the symmetric mode increases with excitation energy of the fissioning system. At an excitation energy $\sim$ 40 MeV, the value saturates to unity, indicating the annihilation of the asymmetric component of the mass distribution.

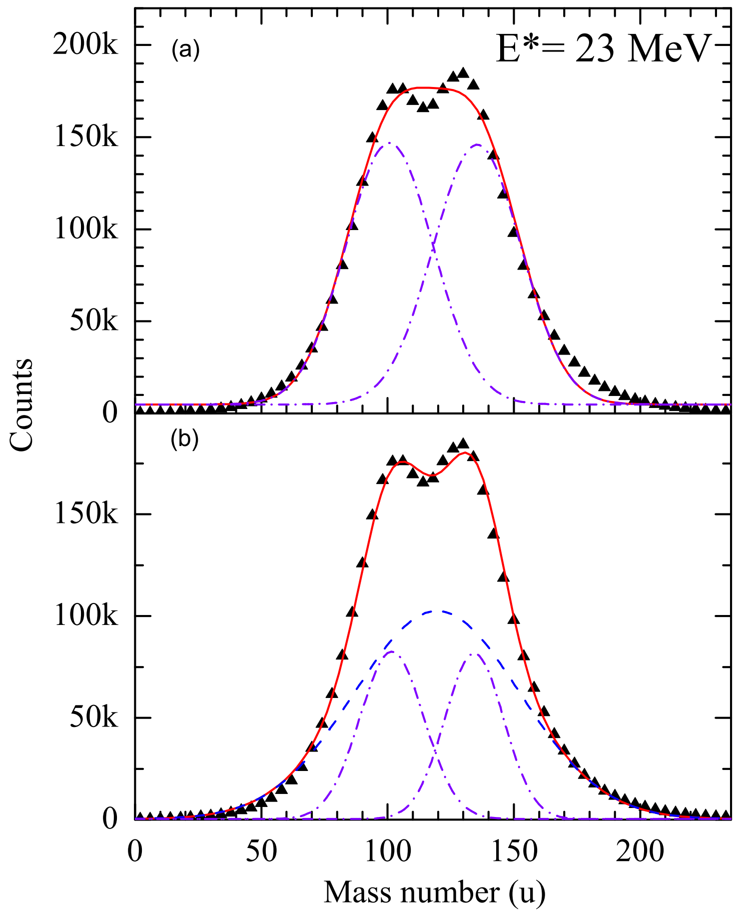

Figure 4.4: *Fission fragment mass distribution at excitation energy 23 MeV fitted by two Gaussian (upper panel) and three Gaussian (lower panel) distributions. The asymmetric components are shown by (violet) dash-dot line and symmetric component is shown by (blue) dash line. The overall fitting is shown by solid (red) lines.*

Study of the widths of the FFMDs can throw further insights into the fission process of the system. It is generally accepted that the width of any symmetric fission fragment mass distribution is proportional to the temperature [80, 81] of the hot and equilibrated compound nucleus (as discussed in Chapter 2). In Fig. 4.6, the red dotted lines show the expected variation of the width of symmetric FFMD with excitation energy. The widths of the symmetric mass distributions is represented by black triangles as shown in Fig. 4.3. It is easy to observe that only for energies above 43.6 MeV the widths follow

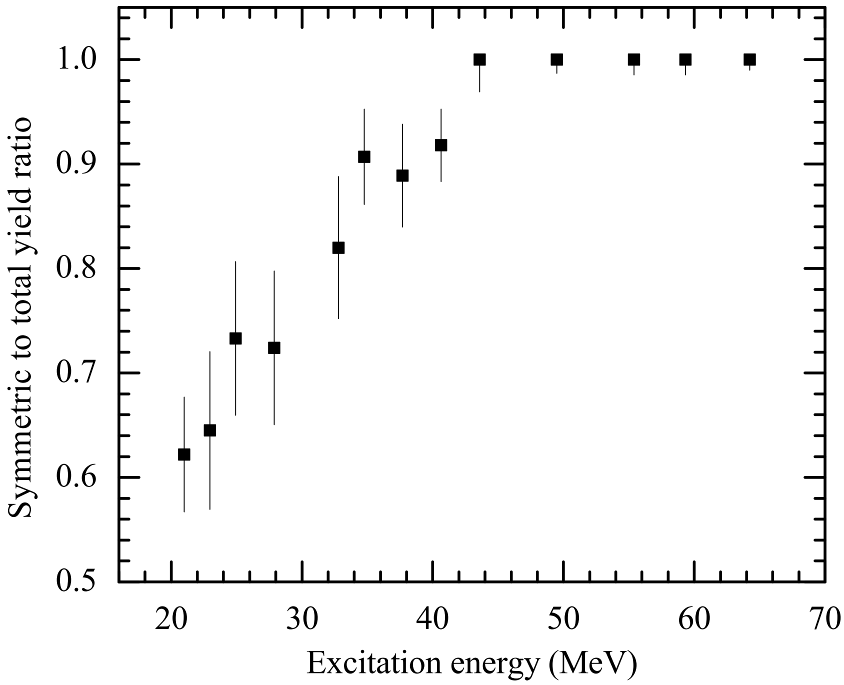

Figure 4.5: *The variation of the ratio (relative unit) of the yield of symmetric fission to the total fission yield at different excitation energies.*

the expected trend. An attempt was also made to fit the mass distributions by constraining the width of the symmetric part of the distribution around the expected trend (dotted line), represented by the red solid square. However, such fitting is associated with very large uncertainty (red vertical lines) and thus, are unphysical. At an excitation energy lower than 43.6 MeV, the best fitted width of the symmetric distribution (black triangles) increases with decrease in energy. This effect of increase in width of FFMD at low excitation energies, can also be interpreted as a signature of onset of shell effects. Such an effect has not been seen before and needs more detailed investigation. Thus co-existence of two fission modes in ^{4}He + ^{232}Th reactions at low excitation energies are clearly observed, one leading to symmetric mass distribution and the other leading to a mixture of both symmetric and asymmetric mass distributions. While the symmetric component can be conveniently explained by invoking only the liquid

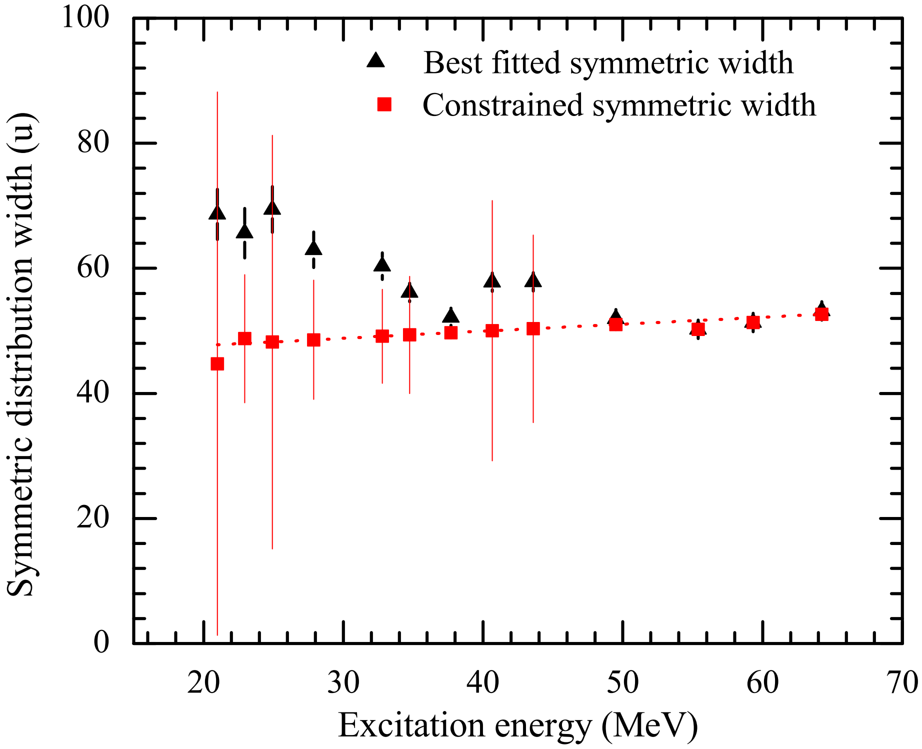

Figure 4.6: *Width of the fitted symmetric mass distribution as a function of excitation energy.*

drop model, the asymmetric component is due to microscopic shell effects. The compound nucleus passes over a fission barrier through shape oscillations, which is a combination of macroscopic (LDM) and a microscopic (shell effect) barrier. The minimum energy path to scission after the formation of a compound nucleus is a statistical mixture of paths in which the mass distribution is decided at LDM (symmetric) fission barrier or the LDM plus shell corrected (asymmetric) fission barrier. The experiment shows that at lower excitation energies both the fission modes co-exist, but the asymmetric component gradually decreases with increase in excitation energy and vanishes at around 40 MeV, as evident from the measurements of mass distributions. This vanishing of the asymmetric mode of fission at around 40 MeV can be considered as a direct signature of the washing out of shell effect in ^{236}U.

It is seen that during spontaneous fission and in most reactions involving fission of actinides and pre-actinides, the FFMD is predominantly asymmetric [19] at lower excitation energies. Following the framework of the shell correction method as proposed by Strutinsky [9], the total nuclear potential is obtained by the superposition of the macroscopic and smooth liquid drop part and a shell correction term, obtained from microscopic single particle model through a scaling factor. As a result, the potential energy surface is distorted for heavy nuclei like ^{236}U, and shows the characteristic double-humped structure as a function of deformation. Extensive potential energy surface calculation has shown that [82] the saddle point, corresponding to second barrier, has a mass-asymmetric shape for heavy nuclei. So, the FFMD should be asymmetric if the fragment passes over the shell corrected potential. Our observation points to the heavier peak to be around 132 - 134 which is close to the doubly magic ^{132}Sn spherical nuclei. It is evident that the nature of variation of fission mode and thus symmetric to total yield ratio critically depends on the nature of variation of the corresponding fission barrier with excitation energy. The evolution of this fission barrier with excitation energy can be understood from the nuclear free energy F which determines the collective dynamics of a hot compound nuclear system [83, 84]. The free energy is given by F =V$-(a - a_{gs})T^2$, where V is the nuclear potential energy, a is shape-dependent level density parameter with the value a_{gs} at the ground state deformation. The nuclear temperature T is calculated at the ground state deformation. Using the Fermi gas model, T can be obtained from the intrinsic excitation energy E^* by using $E^* = a_{gs}T^2$ [85]. The nuclear shapes were defined within the ellipsoidal shape parametrization in the present calculation, where c, the ratio of the axis of symmetry to any other principal axis of the ellipsoid and quantifies the amount of deformation. The shell corrected V which was obtained from a macroscopic-microscopic model [86]

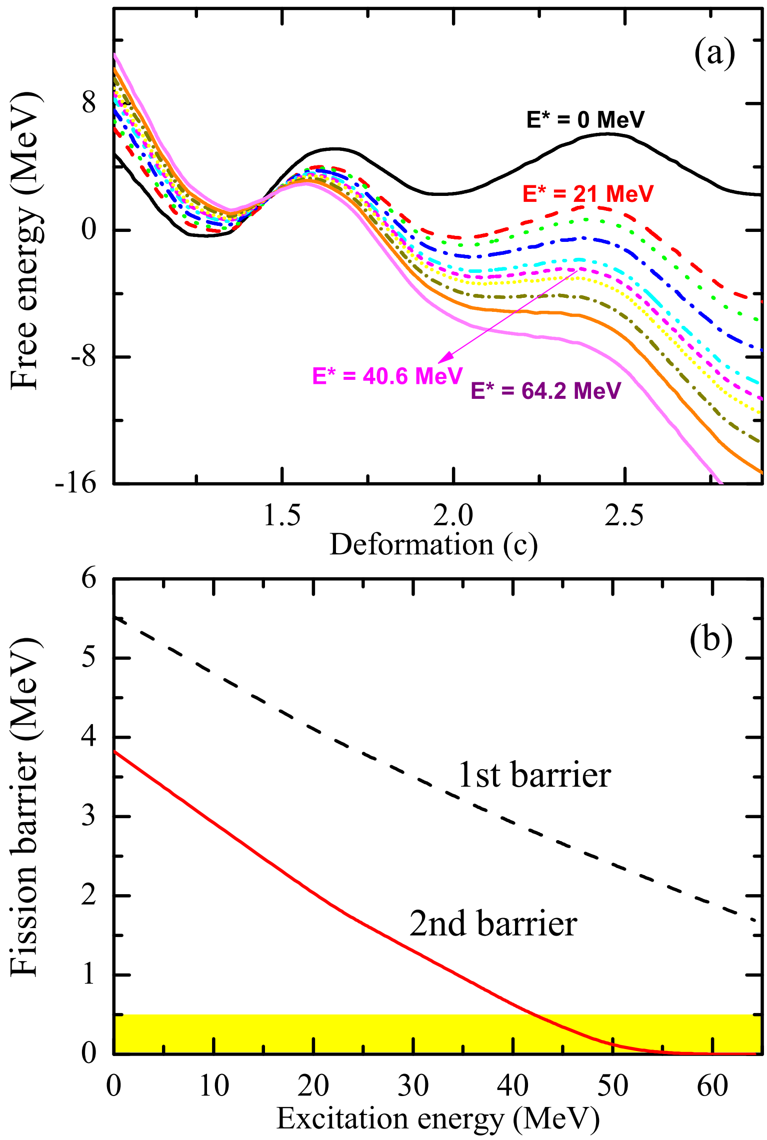

Figure 4.7: *(a): The variation of free energy as a function of deformation (c, see Chapter 2) for* ^{236}U *for ground state and excitation energies of 21, 24.9, 30.8, 37.7, 40.6, 43.6, 49.5, 55.3 and 64.2 MeV. (b): Variation of fission barrier as a function of excitation energy. The shaded (yellow) region ia the uncertainty in fission barrier calculation.*

was used in the present calculation. The value of a, the level density parameter, was calculated following the work of Ignatyuk *et al.*, [35, 87].

The variation of F, the free energy, as a function of deformation c of the system is shown in Fig. 4.7 (a) for varying E^*. It is evident form Fig. 4.7 that for the system ^{236}U, there exits two fission barriers separated by minimas. It is to be noted from Fig. 4.7 (a) that the effective heights of the two fission barriers decrease with E^*. The same variation of the fission-barrier height as a function of E^*, the excitation energy of the compound nuclei is shown in the lower panel (b) of Fig. 4.7. It can be clearly seen that the second barrier becomes insignificant (to less than 500 KeV) at around $\sim$ 40 MeV. It is interesting to note that in the FFMD measurement presented, the asymmetric fission fragment yield also vanishes at same excitation energy. So, it can be inferred that there is a clear correlation between the observed vanishing of asymmetric mass yield and the vanishing of the second barrier of the doubly humped fission barrier and thus the vanishing of shell effects for ^{236}U.

As mentioned earlier, nuclear level density (NLD) is affected by the persistence of shell effects. From fission fragment angular distribution measurement, it was shown [88] that the shell effect on nuclear level density parameter is damped with excitation energy and that the level density parameter saturates to its liquid drop value at a similar excitation energy ($\sim$ 40 MeV) where the asymmetric component of the mass distribution was found to vanish. From a measurement of proton evaporation spectra [89] in nuclei around ^{208}Pb at E^* $\sim$ 50 MeV, the extracted NLD was found to follow the expected liquid drop behavior. The present measurement, is therefore, in agreement with the above findings.

One of the advantages of measurement of masses of the fission fragments, using the present technique, is the less susceptibility to modification by secondary de-excitation of excited fission fragments. This is because the mean fragment velocity (as was measured here), unlike kinetic energy measurements, does not change due to light particle evaporation. The events in which the flight paths are greatly modified by secondary neutron evaporation were rejected. Moreover, another inherent advantage of the chosen system is that the angular momentum involved in α induced reaction is much less and thus the effect of angular momentum dependence of fission barrier does not significantly affect the barrier. As fusion fission reaction was chosen here, excitation energy estimation is also less ambiguous. Also, α induced fusion is completely free from other competing incomplete fusion processes (e.g; quasi-fission) which could otherwise contaminate the mass distribution as is the case in heavy ion induced fusion. And lastly, in the present experiment, the extracted results are completely model independent as opposed to the earlier results derived from either angular anisotropy [88] or proton/gamma evaporation studies [89] which requires specific model input to extract useful information about the persistence of shell effect with increase in excitation energy.

4.4 Conclusion

Though the weakening of shell effect with increase in excitation energy was known qualitatively from previous studies, for the first time, a direct evidence that nuclear shell effect gets washed out at $E^{*}\sim$ 40 MeV is shown in this thesis work. The asymmetry in mass distribution observed in this experiment, at lower excitation energies is due to the manifestation of shell effects. From the fission fragment mass distributions, it is clear that the symmetric distribution component increases with the increase in excitation energy, indicating that shell effects are more prominent at lower excitation energies. The change in shape of the mass distribution, from asymmetric to symmetric, at $E^{*}\sim$ 40 MeV is a direct evidence of the washing out of shell effects.

This thesis work calls for a systematic study along this line for other actinide elements to be carried out to understand the role of nuclear shell effect in a better way.

Chapter 5

Effect of shell correction at saddle point

As it was discussed in the previous chapter that nuclear shell effect play the central role on the stability of the super heavy elements (SHE). Probing the effect of shell correction on nuclear potential energy surface has an important impact on the activities in the production of SHE. Therefore, the role of nuclear shell effects on various nuclear reaction processes as a function of excitation energy, specially for the nuclei around the shell closure, has currently remained an issue of intense discussions. Apart from the basic understanding point of view, a large part of the recent activities were concentrated on the study of shell effect in fission of heavy nuclei with the aim to unveil the relationship between nuclear structure and nuclear stability.

There have been immense efforts, both theoretical and experimental, to address the burning question whether nuclear shell effects survives around the saddle point [90, 91, 92, 93, 94, 95, 96, 97]. The theoretical efforts are concentrated on calculating the potential energy surfaces (PES) in a multi-dimensional space. It is found, in general, while the ground state mass is strongly influenced by the shell correction, the saddle point mass should be rather close to its macroscopic value [95, 98]. In contrast, a few recent experimental studies indicated rather strong effect of shell correction at the saddle point, particularly around N=126 shell closed nuclei [99, 91, 93]. An anomalous increase in fission fragment angular anisotropy was observed in the fission of ^{210}Po at excitation energy ∼40-60 MeV, which was conjectured as an indirect evidence of shell correction at saddle due to neutron shell closure at N=126 [91, 99]. The pre-scission neutron multiplicity data for ^{206,210}Po also indicated the requirement of substantial shell correction not only in shell closed ^{210}Po but also in ^{206}Po [93]. These results, which are apparently indicative of a much stronger role of nuclear structure in fission process is bound to have implications on all future studies of the fission, and particularly will have vital impact on the production of spherical super heavy nuclei around the next closed neutron shell at N = 184. Therefore, it warrants independent attempt to estimate the role of shell correction at saddle point in the same mass/excitation energy region where the deviations were observed.

In this thesis work, the fission fragment mass distributions for the fissioning nuclei ^{206,210}Po were measured to look for signatures (if any) of shell correction on the potential energy surface at the saddle. No significant deviation of mass distribution was found between ^{206}Po and ^{210}Po and both the distributions could be explained using realistic macroscopic potential only, contrary to the reported angular anisotropy and pre-scission neutron multiplicity results.

It should be mentioned that all the available experimental probes (evaporation residue yield, fission fragment angular anisotropy, pre-scission neutron multiplicity) may, however, not be equally effective in studying the shell effect near the saddle point. Intuitively, evaporation residue yield would bear information about smaller (close to ground state) rather than saddle point deformation; whereas, the pre-scission neutron emission would only project an average effect of all deformations that the system has passed through in course of its dynamical evolution up to the scission point. Fission fragment anisotropy is considered to be sensitive to potential energy surface at the saddle point, though the correlation between anisotropy and PES is strongly model dependent and therefore, not quite straightforward. On the other hand, the fission fragment mass distribution may be a more direct and effective tool to probe the nature of PES at the saddle point, as the mass ratio of the nascent fragments depends on the structure of the potential energy surface at the saddle point only. The effectiveness of this probe was demonstrated in the study of washing out of shell effect in fission of ^{236}U, as discussed in the previous chapter.

5.1 Previous investigations on the same system

An anomalous increase in fission fragment angular anisotropy was observed [91] in the fission of ^{210}Po but not in ^{206}Po, with decreasing excitation energy. Similarly, the analyses of the pre-scission neutron multiplicity data for ^{206,210}Po have also indicated the requirement of shell correction of the fission barrier in both cases [93]. In both cases, the authors sought to explain this finding as an indirect evidence of shell effect due to neutron shell closure at N=126, which was present and even persisted up to about 60 MeV of excitation energy for the neutron shell closed nucleus ^{210}Po. However, unlike in the case fragment anisotropy, substantial shell modifications were required to explain neutron multiplicities for both ^{206,210}Po and contribution of dissipative dynamics was also not ruled out [93]. Interestingly, the recent four-dimensional Langevin calculations for the same systems raised question on the robustness of the SSPM analysis procedure and indicated that the above (multiplicity) data could well be explained with purely macroscopic potential energy landscape without considering any shell effect [92].

The analysis of both angular anisotropy and pre-scission neutron data mentioned above [91, 99, 93], were carried out within the framework of the well established statistical models [19, 100] which are fairly successful in explaining the gross features of the binary fission of a statistically equilibrated compound nucleus. As the gross effects of shell structure are already taken care of in the model calculations through the shell corrected level density term, any departure of the measured evaporation residue yield, anisotropy or pre-scission neutron multiplicity from the corresponding model predicted values may be construed either as the manifestation of shell structure on the PES or as the contributions from other non-compound fission channels. However, the robustness of the statistical model predictions was recently called into question [92]. With the advent of dynamical calculations using stochastic Langevin equation, Schmitt *et al.* [92] showed that the angular anisotropy and neutron data [91, 93], mentioned above, could well be explained with purely macroscopic potential energy landscape without considering any shell correction at saddle point. The prevailing dramatic ambiguity thus motivated us for the immediate evaluation of the problem through a new experimental observable, the fission fragment mass distribution, which would probe the PES directly at the saddle point, as the mass ratio of the emitted fragments largely depends on the structure of the potential energy surface at the saddle point [101].

5.2 Experimental setup

The experiment was performed at the Pelletron facility at BARC-TIFR, Mumbai, India using bunched beam of ^{12}C (58 - 78 MeV) on (96.5% enriched) isotopes of ^{194}Pt of thickness 260 μg/cm^2 (carbon backing 20 μg/cm^2) and ^{198}Pt (91.6% enriched) of thickness 170 μg/cm^2 (10 μg/cm^2). The targets were mounted at an angle of 45° with respect to the beam axis. Fission fragments were detected with two large area position sensitive MWPC [63] as described in chapter 3. The detectors were placed on either side of the beam axis at 48 cm and 37 cm from the target. The centres of the forward and backward detectors were kept at an angle of 45° and 121° to the beam axis respectively. The detectors were operated at a pressures of 3 torr of iso-butane gas in flow mode. The gas pressure was adjusted so as, the detectors were almost transparent to elastic and quasi-elastic particles. As in the earlier experiment, the flight times of the fragments, coordinates of the impact points of the fragments (θ, ϕ), and the partial energy losses of the fragments in the gas detectors were measured. From these measurements, the masses of the correlated fission events and the transferred momentum to the fissioning system was inferred. Normalization of the fission cross-section and beam flux monitoring were done using the elastic events collected by two silicon surface barrier detectors placed at 15° on either side of the beam axis and a Faraday cup placed at the beam dump.

5.3 Details of data analysis

The measured folding angle distributions of fission fragments (FF) at near the Coulomb barrier energies in the two reactions are shown in Fig. 5.1. The peak of the folding angle distributions are consistent with the expected value for complete transfer of momentum in each of the reactions. The symmetric shape of the folding angle distribution, as shown in the figure, ensures that admixture of transfer induced fission fragments are minimal and all the fragments have originated through fusion-fission reactions.

The fission fragments are separated from elastic and quasi-elastic reaction channels, both from the time correlation and energy loss spectra in the detectors. The masses were determined following the procedure of measuring the difference of the flight times in the two detectors, polar and azimuthal angles of the fragments with respect to the beam axis. The procedure for calculating mass distributions of fission fragments were discussed in details in Chapter 3.

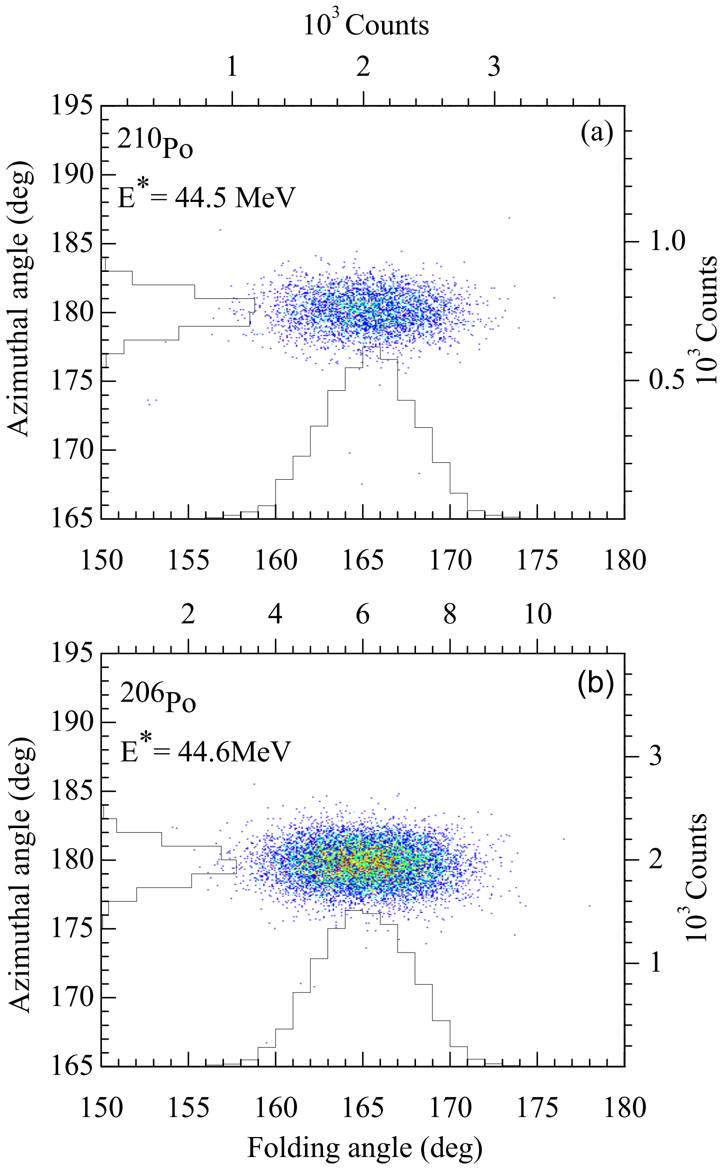

Figure 5.1: Folding angle distribution of complimentary fission fragments for the reactions (a) $^{12}C+^{198}Pt$ and (b) $^{12}C+^{194}Pt$ at similar excitation energies.

The mass resolution achieved in the experiment is $\sim$ 5 u.

Since the targets were not 100% pure and as there is no way to distinguish the origin of the fission fragments detected by the detectors (whether they originated from the compound nuclei formed in fusion of the projectile and the main targets

^{194,198}Pt or their isotopic impurities), the effect of the impurities was estimated by assuming proportionate number of the actual events coming from the isotopic impurities chosen randomly through a time seeded uniform random number generator. To estimate the dispersion in the variance of mass distribution due to the presence of isotopic impurities, the above process was repeated 2000 times. It is found that the dispersion in the variance of mass distribution due to impurities were negligibly small.

5.4 Results

Typical fission fragment mass distributions, measured at similar excitation energies for the two aforementioned reactions are shown in Fig. 5.2. The red (solid) lines are single Gaussian fits to the data. The good fits to the experimental data using a single Gaussian function in both the reactions are clearly confirming that the fission fragment mass distributions are completely symmetric, having nearly identical shapes at all excitation energies. The standard deviations (σ) of the fitted mass distributions for both the reaction channels of ^{12}C+^{194,198}Pt are plotted as a function of excitation energy in Figs. 5.3 (a),(b). For statistical fission of the compound nucleus, the standard deviation of the mass distributions follows the relation $\sigma = \sqrt{\frac{T}{k}}$, where T is the temperature at the saddle point and k is the stiffness parameter for the mass asymmetry degree of freedom [80] (as discussed in Chapter 2). From Fig. 5.3(c) it can be seen that the value of $\frac{\sigma}{\sqrt{T}}$ with excitation energy is almost constant, indicating purely statistical compound nuclear fission process in both the cases. The value of k, the nuclear stiffness constant, was found to be consistent with the comprehensive compilation of fission fragment mass distributions data presented in [102]. The non-compound fission processes and/or the presence of shell correction, both of which would have triggered an anomalous variation of σ [54, 81], are therefore

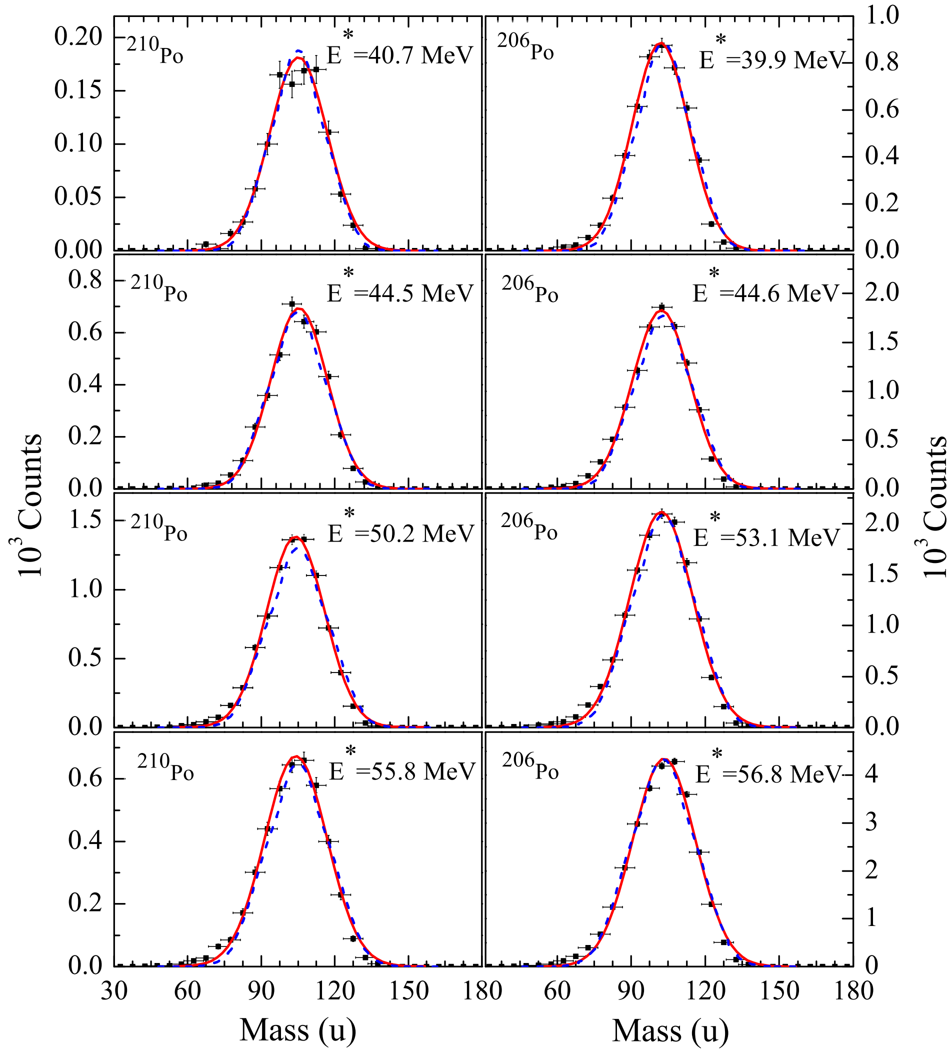

Figure 5.2: FFMD at different excitation energies. Single Gaussian fits are shown by solid (red) lines. The dashed (blue) lines show the theoretical calculations.

quite unlikely in either of the two reaction channels, which is clearly at variance with the earlier results for the same systems, using different probes [91, 93].

5.5 Discussions

The present experimental results of non-observation of any appreciable anomaly in mass distribution and thus, shell correction at the saddle ridge, in both

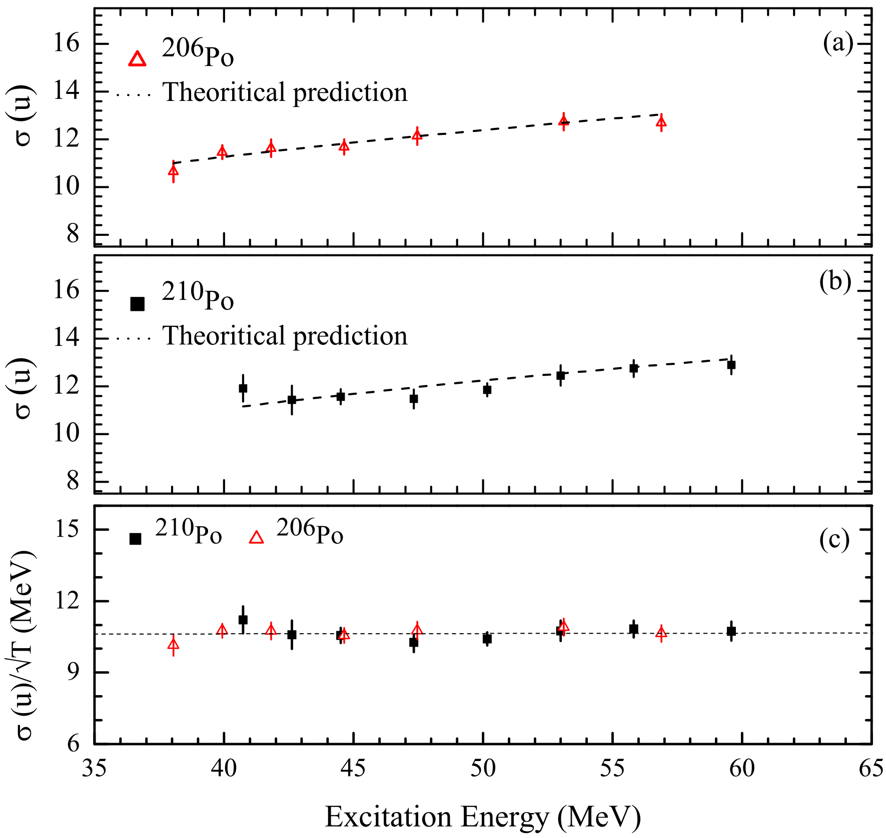

Figure 5.3: (a),(b):Plots of the standard deviation of the fitted symmetric mass distribution with excitation energy. Dotted lines shows the calculated standard deviations. (c) Variation of the standard deviation normalized by the saddle temperature. The dashed line is a guide to the eye.

the systems ^{206,210}Po was also justified theoretically. A detailed theoretical calculation of potential energy surface (PES) [103] found that fission barriers are single-humped for the systems under consideration. So, an attempt was made in this thesis work to reproduce the measured mass distributions theoretically, considering only realistic macroscopic potential without any microscopic shell correction. The PES was calculated using the Finite Range Liquid Drop Model (FRLDM) [42, 43, 104]. The nuclear shapes were defined using the Funny Hill [44] parameters in two dimensions viz. elongation (c) and mass-asymmetry (α). The fragment masses (M), with respect to a particular combination of c and

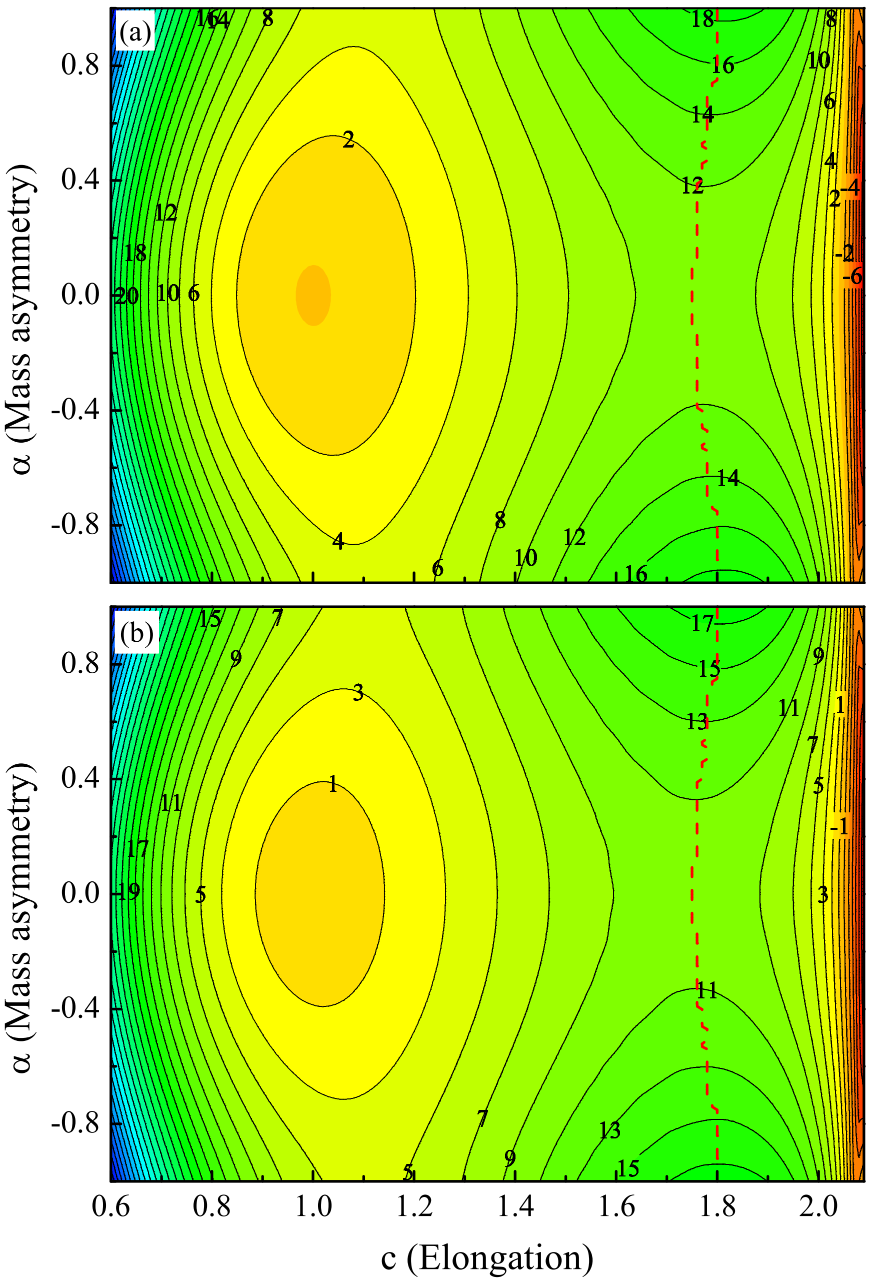

Figure 5.4: Potential energy surface for the compound nuclei (a) ^{210}Po and (b) ^{206}Po relative to the ground state energy of FRLDM. Contours plots are at intervals of 2 MeV. The computed saddle ridge is represented by (red) dashed line

α at the saddle ridge, were derived by dividing the compound nucleus at the neck of the deformed shape. Fig. 5.4 shows the calculated potential energy surfaces for ^{206}Po and ^{210}Po. The saddle ridge, defining the fission barrier $V(\alpha)$ as a function of α, is shown by (red) dashed line for each of the system. Multi-dimensional Kramers formula for the fission width [105, 106] was used to obtain the fission fragment mass distributions.

$$\Gamma_f = N(\alpha)exp(-V(\alpha)/T), \tag{5.1}$$

The coefficient $N(\alpha)$ depends on the detailed structure of the potential surface and T is the saddle point compound nuclear temperature. In the present calculation, for the purpose of simplicity, $N(\alpha)$ was assumed to be independent of α and $V(\alpha)/T$ was multiplied by a factor B to take care of the dynamical effects [107]. The constant values of B (1.93 and 1.82) reproduced the experimental data quite satisfactorily for ^{206}Po and ^{210}Po, respectively (as shown by blue dashed line in Fig. 5.2). The computed standard deviations of the theoretical FFMDs were also found to reproduce the experimental data reasonably well as shown (by dotted line) in Fig. 5.3.

As discussed earlier, the change in shape or width of the fission fragment mass distributions is a signal for the presence of shell correction at saddle point [101]. It is clearly obvious from the experimental data that, there is no anomaly between the fission fragment mass distributions of the two systems, ^{206}Po and ^{210}Po. Both of these systems exhibit symmetric Gaussian-like mass distribution without any appreciable change in shape (width) throughout the whole range of excitation energy under consideration. Theoretical mass distributions, without incorporating any shell correction in the PES were found to clearly reproduce the experimental data in both the cases. Thus, from this measurement, it is clear that the N=126 shell closure in ^{210}Po does not affect the fission fragment mass distribution.

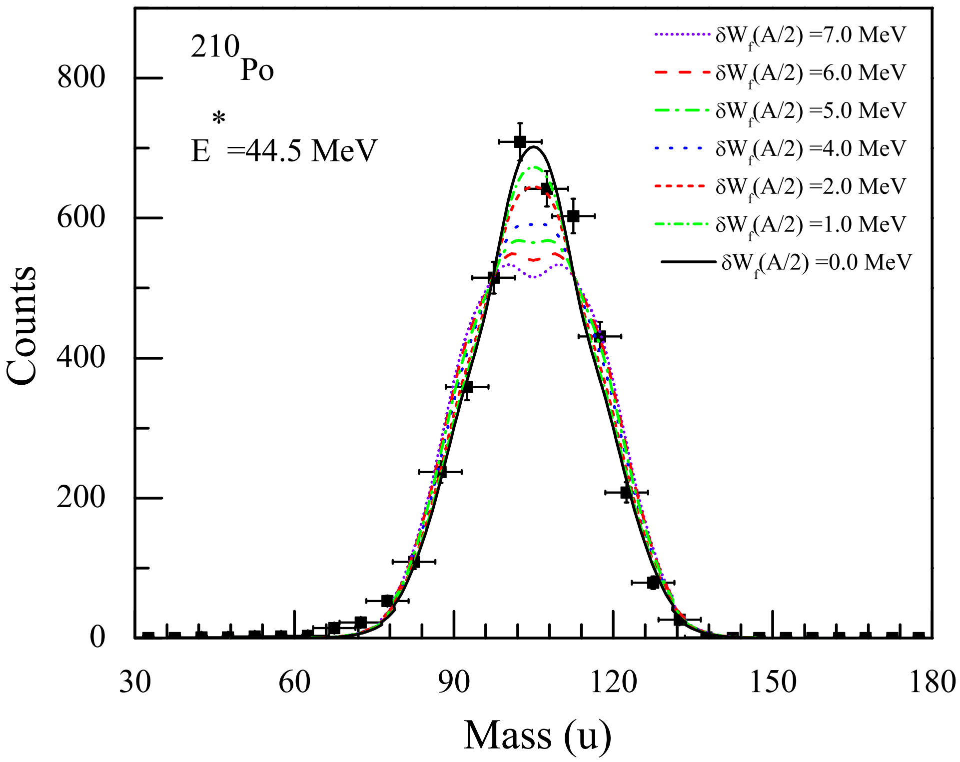

Figure 5.5: Effect of shell correction in the saddle ridge on the FFMDs. $\delta W_f(A/2)$ is the shell correction at symmetry.

In order to quantitatively workout the sensitivity of the fission fragment mass distributions on the magnitude of shell correction at saddle, the mass asymmetry dependent fission barrier was modified by adding a shell correction term $\delta W_f(M)exp[\lambda E^*]$, where λ is the shell damping factor which was taken to be 0.054, and $\delta W_f(M)$ was taken in the empirical form [101]

$$\delta W_f(M) = \delta W_f(A/2)exp[-\gamma(M - A/2)^2]. \tag{5.2}$$

The variation in the shape of the mass distribution for different values of $\delta W_f(A/2)$ is shown in Fig. 5.5 for a representative case of ^{210}Po fission, where $\delta W_f(A/2)$, the shell correction at symmetry, was varied over a range of 1-7 MeV. Even a visual inspection of Fig. 5.5 makes it clear that the measured mass distribution can be best fitted with no shell corrections at the saddle point. At

7 MeV of shell correction at the saddle point, which was necessitated in the neutron multiplicity data for the same system [93], the mass distribution in our calculation, is clearly asymmetric as opposed to our experimental observation. It is to be noticed that even a variation in $\delta W_f(A/2)$ of 1 MeV produces a perceivable change in the shape of the mass distribution.

The fission fragment mass distributions of ^{210}Po, populated through ^{4}He + ^{206}Pb reaction, was also reported by Itkis *et al.* [102, 108]. A comparative study of the width of the fission fragment mass distributions at the only overlapping excitation energy revealed slight suppression for the ^{4}He + ^{206}Pb reaction compared to the present measurement. This can be attributed to the lower angular momentum carried by ^{4}He as compared to ^{12}C. A very weak structure in the fission fragment mass distributions was reported by Itkis *et al.*, which was however absent in the present case. This may be due to the inherent sensitivity of our spectrometer. It is to be pointed out that the contributions of other non-compound fission channels are minimal in both the systems, as their presence would have appreciably broadened the mass distributions [81, 109]. The width of the mass distribution remained almost constant over the whole range of excitation energy without any anomalous increase (excluding temperature effects) which indicates that the contributions of non-compound nuclear fission channels are minimal.

An angular anisotropy measurement [110] for the nucleus ^{213}Fr was recently reported, which is also a N=126 neutron-shell closed nucleus. Interestingly, in this system, no such appreciable deviation from statistical model predictions at similar excitation energies were observed; and a reanalysis of the ^{210}Po data [91] including multi-chance nature of fission reduced the discrepancy in angular anisotropy. A systematic study of angular anisotropies for different isotopes were conducted for few other systems [111] and in none of the cases, large deviations in anisotropies were observed. Another recent calculation [96] for ^{210}Po, prescribed for minimal shell correction at saddle point but substantial dynamical effects, to explain concurrently the fission excitation function and neutron emission data. This reinforces our belief that the anomalous angular anisotropy and neutron multiplicity observed in the systems ^{206,210}Po may not be attributed to neutron shell closure or shell correction at saddle point - it could be due to the inherent limitations of the implementations of statistical models [92].

5.6 Conclusion

The direct probe of fission fragment mass distribution does not show any signature of the modification of the potential energy surface at the saddle point due to the effect of N=126 neutron shell closure in ^{210}Po. These results provide a benchmark for different models that are used to predict the fission barriers for the production of spherical super heavy nuclei around the next closed neutron shell at N = 184.

The present observation of the symmetric fragment mass distributions and smooth trend of their variances on the one hand and anomalous deviations of angular anisotropy and neutron multiplicity observed earlier for the same system on the other hand cannot be explained together with the assumption that PES is significantly modified due to neutron shell closure.

The present results also clearly demonstrate that, so far as the study of PES at saddle point is concerned, the fragment mass distribution has an advantage over the other probes as being selectively more sensitive towards changes around the saddle point only and less prone to model dependent ambiguities.

The present findings merits further investigation for the other regions of neutron or proton shell closure.

Chapter 6

Probing quasi-fission through fission fragment mass distributions

In the previous two chapters, it is discussed how fission fragment mass distributions (FFMD) is used to look for the presence of nuclear shell effects that helps to survive super heavy elements. One of the process that severely hinders the formation of heavy and super heavy element is quasi-fission. In this chapter, it is shown how fission fragment mass distributions is used to probe quasi-fission for the nucleus ^{200}Pb.

One of the major motivations in heavy ion nuclear physics research is to reach the postulated island of stability. While sustained efforts over the years have provided important insights into the mechanism of nuclear fission there is still a gap in our understanding of the dynamics of fusion of two heavy ions after formation of a contact di-nuclear system. The broad features of formation of a compound nuclei can be described by two nuclei having enough kinetic energy to overcome the repulsive coulomb barrier and reach the close range attractive nuclear potential to form a contact di-nuclear system. This di-nuclear system can either equilibrate in several collective degrees of freedom with different relaxation times thus reaching a compact mono nuclear shapes at equilibrium deformations or may dissociate without equilibrating in one or more collective degrees of freedom. This equilibrated nuclei is often formed at a very high excitation energy and may thus reach an unconditional saddle and undergo binary fission, or it may also de-excite through the evaporation of a few light particles to form a stable evaporation residue (ER). These non-equilibrium processes preceding complete fusion seriously hinders formation of ER and thus any plan into the production of SHE must take into account minimization of these processes. In terms of increasing relaxation times, these processes can be placed into three broad categories:

(a) Deep inelastic collision (DIC), which represent the energy relaxation mode without capture thus exhibiting a wide range of loss of kinetic energies with minimal deviations of mass distributions from the projectile and target masses.

(b) Quasi-fission, wherein the initial di-nucleus formed after equilibration in energy cannot amalgamate into a more compact shape through mass flow of the projectile into the target so as to equilibrate into mass degrees of freedom but rather the mass flows in the opposite direction leading to a more symmetric di-nuclear system before separating.

(c) Pre-equilibrium fission, which is characterized by non-equilibration of K degrees of freedom.

Swiatecki's dynamical model [51, 113] predicted the onset of quasifission (and pre-equilibrium fission) processes for heavy systems with $Z_P Z_T \geq 1600$ wherein the exit channel configuration is more compact than the contact configuration and an extra energy is required for such systems to fuse. However, much lighter systems with $Z_P Z_T \approx 800$ have shown signatures of quasifission. This can be explained on the basis of mass flow of the initial contact configuration. A phenomenological tipping point called the Businaro-Gallone critical mass asymmetry α_{BG} [114] is used to deduce the direction of mass flow of the initial di-nucleus.

In the process of unraveling the role of entrance channel dynamics on fusion fission processes, the nucleus ^{200}Pb has received a lot of attention recently. The evaporation residue (ER) cross sections and gamma multiplicity distributions for ^{16}O + ^{184}W and ^{19}F + ^{181}Ta reactions leading to the same compound nucleus ^{200}Pb* was measured by Shidling *et al.* [115, 116]. It was found that the measured ER cross section (normalised) and moments of gamma multiplicity distribution of the system ^{16}O + ^{184}W was notably enhanced [115] as compared to the other system ^{19}F + ^{181}Ta at higher excitation energies. This is a clear indication of entrance channel effects. The reduction of ER yield in the reaction ^{19}F + ^{181}Ta was accompanied by a selective suppression of contributions of higher spin events. This was attributed to the onset of pre-equilibrium fission [23, 118] in the ^{19}F + ^{181}Ta system. It is to be noted that, both the systems have a $Z_P.Z_T < 700$, much lesser than the suggested threshold value (≥ 1600) for the onset of entrance channel dependence as per Swiatecki's dynamical model [51, 113]. Although the value of the entrance channel mass asymmetry α of the two systems (0.84 and 0.81, respectively) are similar, they are on opposite sides of the Businaro-Gallone critical mass asymmetry ($\alpha_{BG} = 0.837$) [114]

It was claimed by Nasirov *et al.* [119] that the observed reduction in ER cross-section (σ_{ER}) at higher energies [115], in the reaction ^{19}F + ^{181}Ta could be an artifact of incorrect estimation of the total fusion cross-section (σ_{fus}). It could be due to an error in the reconstruction of σ_{fus} in the experiment [115] from fission like fragment yields wherein the contributions from quasi-fission and fast fission reactions, which does not arise from complete fusion, were not accounted for and subtracted from the measured fission yield. This led to an overestimation of σ_{fus}, thereby lowering the normalised (σ_{ER}/σ_{fus}) ER yield.

From a theoretical calculation of the same two systems, in the framework of the dinuclear system and advanced statistical models [120], it was shown that the magnitude of hindrance to complete fusion was more for ^{19}F + ^{181}Ta as compared to ^{16}O + ^{184}W. A dramatic increase in quasi-fission and fast-fission with increase in energy for the ^{19}F + ^{181}Ta reaction was also predicted by Nasirov *et al.*. Another calculation [121] using dynamical cluster-decay model (DCM) and Wong model found that, the experimental data for the system ^{19}F + ^{181}Ta could be explained without needing to incorporate any quasi-fission component. However, this work could not rule out the presence of quasi-fission in the case of the other system ^{16}O + ^{184}W. This widespread ambiguity between theory and experiment demanded a serious relook into the problem through another experimental observable, the fission fragment mass distribution, which is an established robust tool for direct detection of prevalence of quasi-fission in a system.

Variation of the width of the FFMD with excitation energies is a sensitive probe for studying quasi-fission [109, 81, 52]. In the case of statistical fusion fission, the compound nucleus proceeds through a mass symmetric unconditional fission barrier. Thus the FFMD is expected to be symmetric around $A_{CN}/2$ (where A_{CN} is the compound nuclei mass), if fine structures due to shell effect are neglected. Since, at the excitation energies under consideration, shell effects are expected to be washed out (as discussed in Chapter 4), the FFMDs should be symmetric in shape with a smooth increase in width (or standard deviation σ_m) of the distribution with excitation energy. Quasi-fission is a competing dynamical process which proceeds through a mass asymmetric conditional fission barrier, making the fragment mass distribution asymmetric. The mass distribution is also expected to be asymmetric for fast fission that occurs for the composite system when the angular-momentum-dependent fission barrier becomes extremely small. However, as indicated by Nasirov et al [119]; the contribution of fast fission is negligibly small for the measured energy range in this thesis work. Thus, an admixture of statistical fission events and quasi-fission will result in larger width of the mass distribution and the width of the mass distribution is expected to increase if there is an enhancement of quasi-fission with change in the excitation energy. Therefore, any sudden change in the width of the mass distribution would indicate departure from full equilibration, while onset of mass asymmetry or an increase in width of mass distribution would be a strong signal of quasi-fission.

In this thesis work, the fission fragment mass distributions of the two reactions, ^{19}F + ^{181}Ta and ^{16}O + ^{184}W populating the same compound nuclei ^{200}Pb* at similar excitation energies were measured to look for the extent of quasi-fission. No significant deviation was observed in the widths of the fission fragment mass distributions of the two entrance channels. The width (standard deviation) of the fission fragment mass distributions increases smoothly and monotonically which clearly points to the absence of quasi-fission in either of the reactions.

6.1 Experimental Setup

This experiment was carried out at the 15UD pelletron accelerator facility of the Inter University Accelerator Centre (IUAC), New Delhi. Pulsed beams of ^{19}F and ^{16}O on enriched isotopic targets of ^{181}Ta of thickness 200 μg/cm^2 with carbon backing of 20 μg/cm^2 and self supporting target of ^{184}W of thickness 100 μg/cm^2 respectively were used to produce the same compound nucleus. The width of pulse beam was 1.2 ns with a repetition rate of 250 ns. The fission fragments were detected with two large area X-Y position sensitive multi-wire proportional counters (MWPCs) [63] as described in Chapter 3. The MWPCs were mounted on two rotatable arms, at expected folding angles for complementary fission fragments. For measurement of mass distributions, the centre of the forward detector and the backward detector were kept at a polar angle (θ) = 75° and θ = 74° respectively on either side of the beam axis. However, at few energies, the detectors were rotated for mass angle measurements. To ensure complete coverage of complementary fission fragments, the forward detector and the backward detector were placed at 41 cm and 29 cm respectively from the centre of the target. The detectors were operated at a pressure of 3 torr of iso-butane gas. This pressure was optimized to obtain the best possible timing resolution and at the same time to keep the detectors insensitive to elastic and quasi-elastic events. The TOF difference of the complementary fragments, the X-Y coordinates of the fragments (impact points) on the detector (θ, ϕ) and the partial energy loss of the fragments inside the detector were measured event by event. From these measurements, the mass distribution of the correlated fission events and the momentum transferred to the fissioning system were derived, details of which are described in chapter 3. For the purpose of beam flux monitoring and normalization of the fission events, two silicon surface barrier detectors placed at ±10° with the beam axis were used. In addition, the Faraday cup placed at the beam dump was also used to normalize the observed fission events.

6.2 Data Analysis

Fig. 6.1 shows a typical polar and azimuthal angle correlation plot for ^{19}F + ^{181}Ta reaction. The peaks of the folding angle distributions was found to be consistent with the value expected for complete momentum transfer of the projectile. The symmetric θ and ϕ distribution indicates that there is no admixture of transfer induced fission with full momentum transfer events. However, the

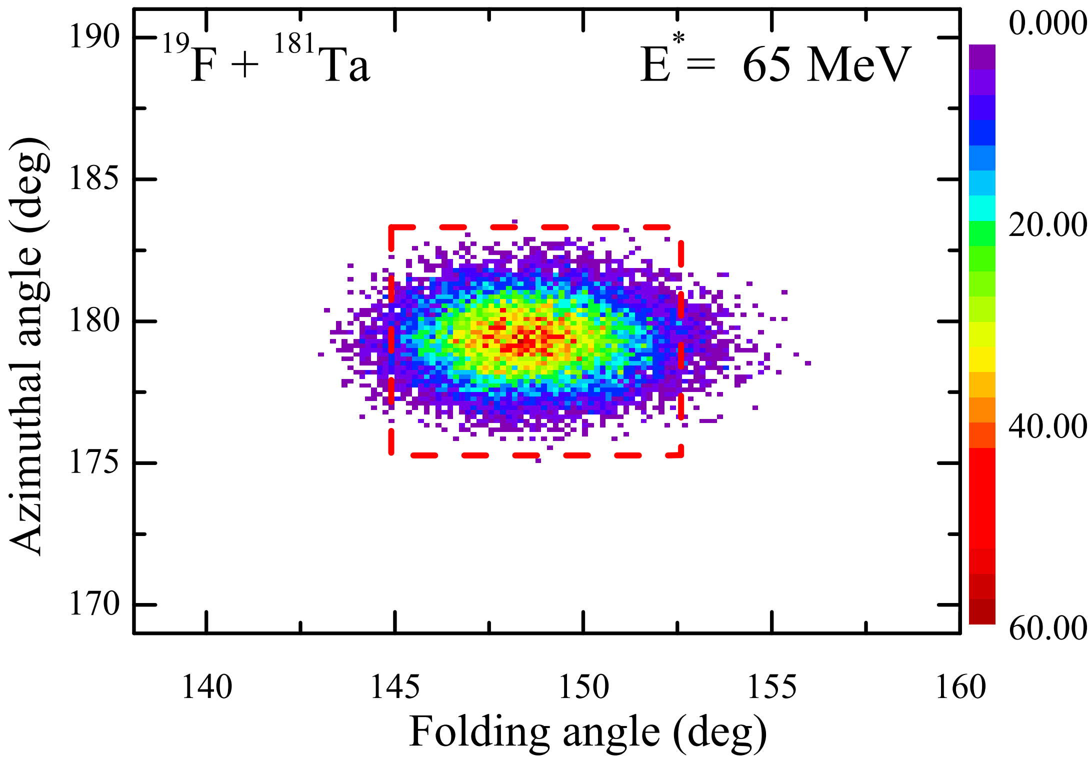

Figure 6.1: Distributions of folding angle of complimentary fission fragments for ^{19}F+ ^{181}Ta at an excitation energy of 65 MeV. A rectangular gate indicated by the red dashed line was used to select the FF events for mass distribution analysis.

kinematic spread in both θ and ϕ due to post scission neutron emission from the fragments cannot be ignored. So, events within a gate as shown in the figure by red dashed line were analyzed. The mass distributions obtained through narrower gates do not affect the width of the mass distributions within the error bar. A mass resolution of $\sim 4u$ in the present experimental set up was achieved.

While from the θ-ϕ distribution, it was found that transfer induced fission is minimal, any events from elastic and quasi-elastic reaction channels were well separated in the time correlation and energy loss spectra. The mass ratio of the complementary fragments were measured from TOF difference of complementary fission fragments, polar and azimuthal angles, recoil velocities and the momentum transferred. The procedure has been described in details in Chapter 3.

6.3 Results and Discussions

The measured fission fragment mass distributions for both the reactions at similar excitation energies are shown in Fig. 6.2. The mass distributions are symmetric in nature at all energies and single Gaussian fits with peaks close to the half of the combined target-projectile mass are satisfactory, as shown by solid (red) line. As discussed earlier, the presence of quasi-fission usually leads to asymmetry in the mass distribution (in the form of increased yields near target and projectile masses) and thereby causes additional broadening of the distribution. It will be apparent from the following discussions that there was no significant admixture of an asymmetric distribution in the measured mass distributions. The standard deviations σ_m(u) of the Gaussian fitted fission fragment mass distributions are plotted against excitation energy in Fig. 6.3. It can be observed that the σ_m(u) increases monotonically with excitation energy for both the reactions. No anomalous large scale deviation in σ_m(u) is seen at higher excitation energies between the two reactions ^{19}F + ^{181}Ta and ^{16}O + ^{184}W. The calculation of Nasirov *et al.* [119] is shown in the inset of Fig. 6.3. The calculation indicates appreciable influence of quasi-fission and fast fission in ^{19}F + ^{181}Ta system as compared to ^{16}O + ^{184}W. However, if that was the case as predicted from the calculation [119], quasi-fission and fast fission component should have been reflected in the behavior of the measured widths of the mass distribution with excitation energies, in the form of anomalous increase in widths at the onset of quasifission, which was not observed at all. At the present moment, no model exists that can reliably predict the widths of the mass distribution with changing quasi-fission fraction; however, FFMD has

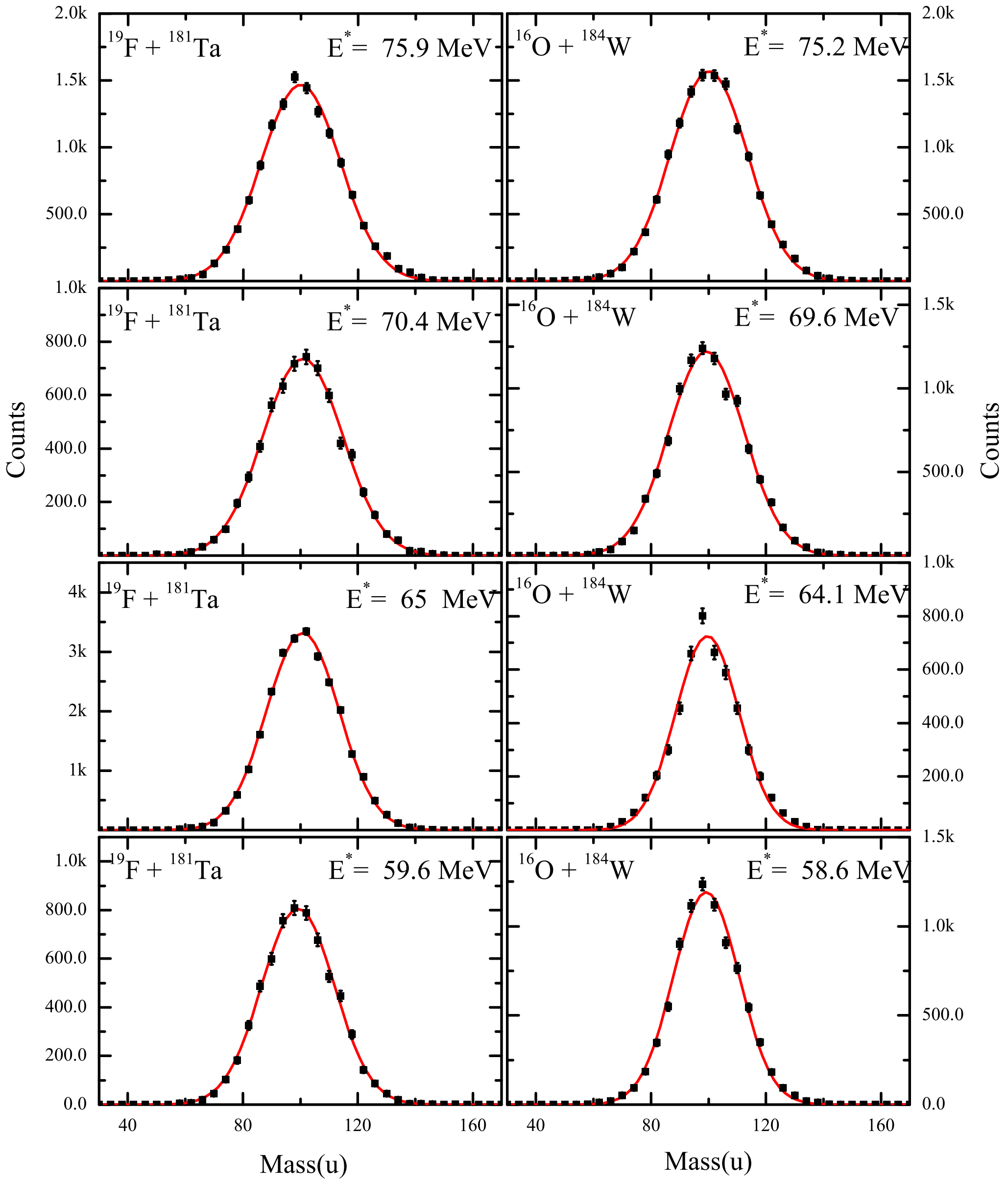

Figure 6.2: Experimental FFMDs for the reactions ^{19}F + ^{181}Ta (left) and ^{16}O + ^{184}W (right) at different excitation energies. Single Gaussian fits are shown by full (red) lines.

been found to be sensitive enough to detect an admixture of $\sim 5\%$ quasifission in a reaction [109].

In case of statistical fission from an equilibrated compound nucleus, the variance (σ_m^2) of the FFMD is a linear function of the nuclear temperature at

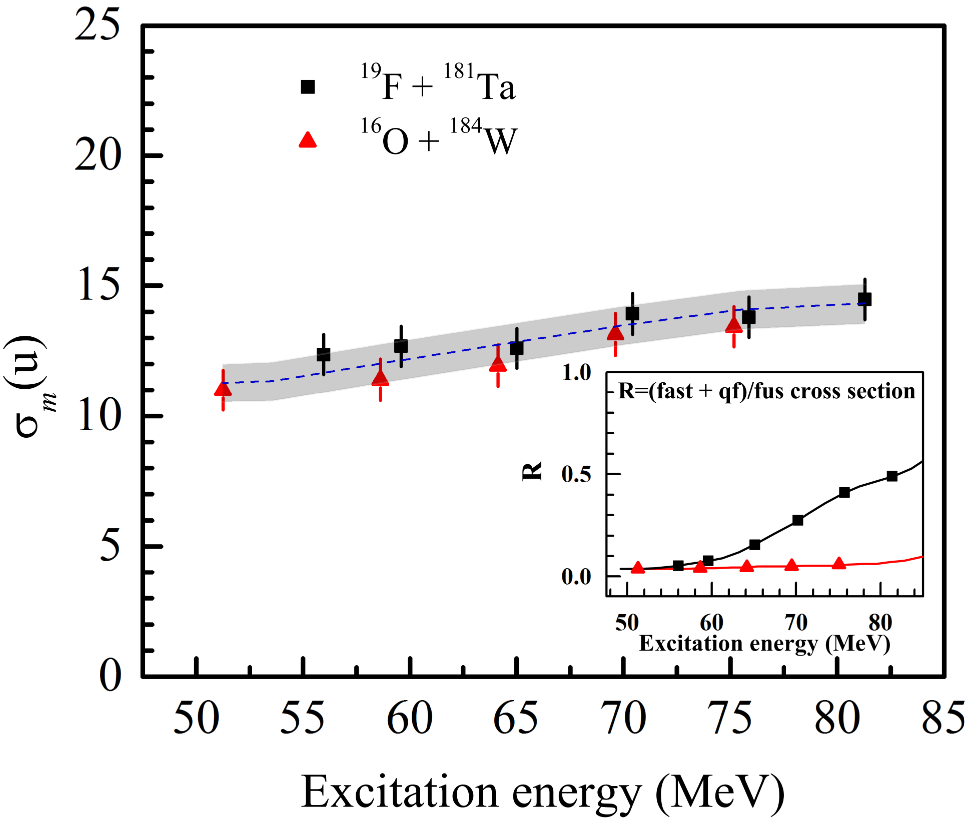

Figure 6.3: Plots of the standard deviation (σ_m(u)) of the Gaussian fitted symmetric mass distribution with excitation energy. The calculated widths are shown in (blue) dashed line, the uncertainties in the calculation are indicated by the shaded region. The theoretically predicted [119] variation of the sum of the fast fission and quasi-fission cross sections with excitation energy for the two systems (normalized with the total fusion cross sections) is given in the inset.

saddle point. Blue (dashed) line in Fig. 6.3 shows the calculated standard deviation from statistical theory [80] using the relation $\sigma_m = \sqrt{\frac{T}{k}}$, where T is the scission point temperature, k is the nuclear stiffness parameter for the mass asymmetry degrees of freedom. Since, for this system, the saddle and the scission point temperatures are very similar [125], we have used the saddle point temperature to calculate the standard deviation of the mass distributions. The saddle point temperature of the nucleus can be estimated by

$$T = \left[\frac{E^{\star}_{CN} - B_f(l) - E_{pre} - E_{rot}}{a}\right]^{1/2} \tag{6.1}$$

where $E^{\star}_{CN}$ is the excitation energy of the compound nucleus, $B_f(l)$ is the angular momentum dependent fission barrier height, E_{rot} is the rotational energy of the CN at the saddle point calculated according to the finite range rotating liquid-drop model [42], E_{pre} is the energy carried out by pre-fission neutrons, which is estimated from the empirical systematic [126] and a is the nuclear level density parameter.

It has been observed that the variance (or standard deviation σ_m(u)) of the mass distribution also has a weak dependence on the mean square average value of angular momentum $< l^2 >$ [126]:

$$\sigma_m(u) = \sqrt{(T/k + \beta < l^2 >)} \tag{6.2}$$

with the value of the constant $\beta \sim 0.05$ [125]. The angular momentum ($< l^2 >$) of the CN was calculated by CCFULL code [127]. A value of the inverse stiffness parameter $1/k = (98.1 \pm 15.1)u^2/MeV$ fitted the data well and was found to be consistent with the comprehensive compilation of the data [125, 128]. The uncertainty in calculation of σ_m due to the uncertainty in the compiled value of inverse stiffness parameter $1/k$ is shown by the shaded region in Fig. 6.3. It is evident that mass variances of both the systems followed the same trend within the limits of uncertainty. The admixture of fast and quasi-fission as predicted in the theoretical calculation [119] for the reaction ^{19}F + ^{181}Ta (as shown in the inset of Fig. 6.3), which gradually increases to as high as ~50% with the increase in excitation energy, should have made the trend of variation of the standard deviation (σ_m) of mass distribution drastically different as compared to that for the ^{16}O + ^{184}W reaction at higher excitation energies. On the contrary, the present measurement clearly indicates that, both the reactions follow fusion fission path and there was no appreciable difference in the fusion dynamics for the two reactions in the measured excitation energy range.

6.4 Theoretical Calculations of Fission Mass Width

A theoretical calculation was performed in this thesis work to better explain the absence of any appreciable quasi-fission in either of the two reactions. The mass distributions of both the target-projectile combinations were estimated using two-dimensional Langevin equations with elongation (c) and mass-asymmetry (α) as collective coordinates [107]. The spin distribution obtained from CC-FULL calculation was used to sample the input angular momentum for each Langevin event. The Langevin equations are written as [129]

$$\frac{dp_i}{dt} = -\frac{p_j p_k}{2}\frac{\partial}{\partial x_i}(M^{-1})_{jk} - \frac{\partial F}{\partial x_i} - \eta_{ij}(M^{-1})_{jk}p_k + g_{ij}\Gamma_j(t) \tag{6.3}$$
$$\frac{dx_i}{dt} = (M^{-1})_{ij}p_j$$

where x_i represents the collective coordinates c or α and p_i is the associated conjugate momentum. The driving force F is defined by $F = U - (a - a_0)T^2$, where U is the finite-range liquid drop model [42] potential energy with rigid rotor values for moment of inertia, a is the shape dependent level density parameter by Ignatyuk [35] with its value a_0 at the ground state deformation. The temperature T is the saddle point temperature calculated from excitation energy E^* by using $E^* = a_0T^2$. The inertia tensor $\mathcal{M}$ is calculated from the Werner-Wheeler prescription [130]. The dissipation tensor, given by η, the expression of which with proper reduction factor as prescribed in references [107, 131], was used in the calculation. In 6.3, $g_{ij}\Gamma_j(t)$ is the random (Langevin) force and $\Gamma_j(t)$ is the time-dependent stochastic variable with a Gaussian distribution, and random-force strength tensor is given by g_{ij}. The time-correlation property of the random force is assumed to follow the relation $\langle \Gamma_k(t)\Gamma_l(t')\rangle = 2\delta_{kl}\delta(t-t')$. The fluctuation-dissipation theorem: $\sum_k g_{ik}g_{jk} = \eta_{ij}k_{\mathrm{B}}T$ relates the strength of the random force to the dissipation coefficients.

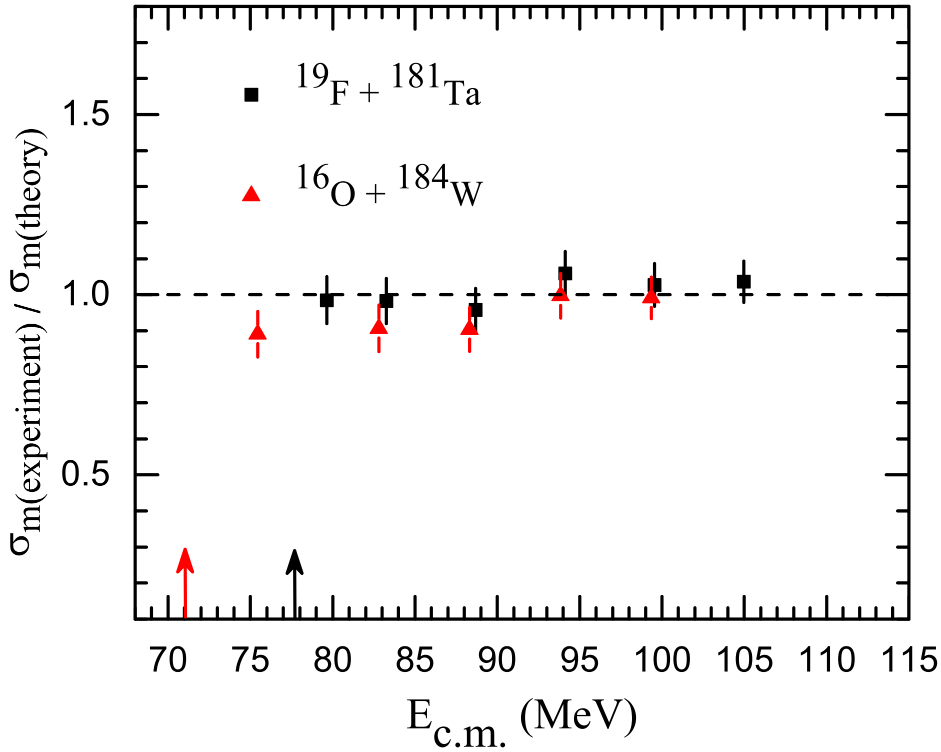

Figure 6.4: The ratio of the experimental (measured) and theoretically inferred standard deviation σ_m(u) of the fitted symmetric mass distribution with respect to the c.m. energy. The Coulomb barriers are shown by arrows for both the reactions, ^{19}F + ^{181}Ta (77.8 MeV) and ^{16}O + ^{184}W (71 MeV). The dashed line whith a constant value of 1 is a guide to the eye.

The σ_m was also calculated from the theoretically obtained mass distributions. The ratios of experimental and the theoretically obtained σ_m values are plotted in Fig. 6.4. It can be observed that there is a good overall agreement between the experimental results and the theoretical values of σ_m(u) in Fig. 6.4 for both the reactions. This clearly indicates the absence of quasi-fission in ^{19}F + ^{181}Ta reaction.

6.5 Mass Angle Correlation

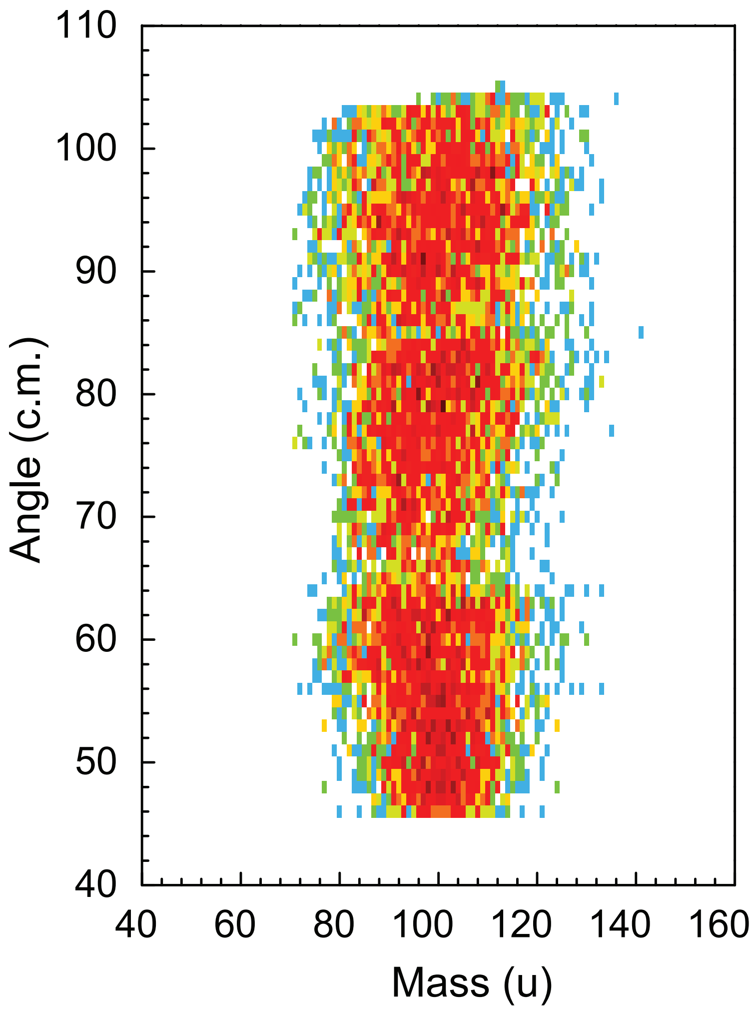

Figure 6.5: Measured mass angle distributions in the reaction ^{19}F + ^{181}Ta at an excitation energy of 75.9 MeV

One of the signatures of quasi-fission is a strong correlation between the fragment mass and centre of mass angle. This is because, quasi-fission occurs when the composite system breaks before completing a full rotation [132] and the resultant mass angle distribution retains this correlation. To look for the possible signature of quasi-fission, the mass angle correlation for the reaction ^{19}F + ^{181}Ta is plotted at an excitation energy of 75.9 MeV in Fig. 6.5. At this energy a large amount of quasi-fission cross section were predicted by Nasirov *et* *al.* [119]. However, there was no significant correlation of fragment mass with angle indicating the absence of quasi-fission in the reaction.

6.6 Conclusion

It is thus clear from the present study that, for the ^{19}F + ^{181}Ta and ^{16}O + ^{184}W reactions discussed above, the fusion dynamics pathways are almost identical. There is no indication of any substantial contribution from quasi-fission. Incidentally, in earlier studies of admixture of quasi-fission [109], fission fragment mass distribution was found to be a sensitive tool even in cases where other probes like fragment angular distribution or pre-scission neutron multiplicity were not conclusive. The absence of any deviation from statistical model predicted width [119] of the mass distribution even at the highest excitation energy, where quasi-fission contributions should be more significant if present, leads to infer that quasi-fission is not significantly present in either of the two reactions.

This explanation however, could not account for the suppressed ER yields reported by Shidling *et al.* [115]. If pre-equilibrium fission is the cause for this suppression it is not clear whether the present probe of fission fragment mass distributions is sensitive to it. In other words, whether pre-equilibrium fission is also associated with wider mass distribution or not. In absence of any available theoretical prediction in this regard, this thesis work refrains from making any definite comment at this juncture and lay stress on the need for advanced theoretical models to distinguish between the subtle features of various non-compound fission processes such as fast-fission, quasi-fission and pre-equilibrium fission.

Chapter 7

Summary and Conclusions

The main motivation of this thesis work is to study *nuclear shell effects* and *quasi fission* reaction mechanism using fission fragment mass distribution as an experimental probe. This study particularly emphasizes on understanding the basic fusion-fission reaction mechanism and in general, is relevant to look for the optimum entrance channel condition for the synthesis of super heavy elements (SHE) which is one of the major aspects of today's nuclear physics research. The stability of the SHE is determined by *nuclear shell effects*. However, the production of SHE is hindered by the dynamical process of *quasi fission*.

Using the major accelerator facilities available in India (Kolkata, Mumbai and Delhi), three experiments were carried out in this thesis work. From the measurements of fission fragment mass distributions:

(I) It is identified the excitation energy at which nuclear shell effect is washed out for an actinides nucleus ^{236}U.

(II) The role of shell correction at the saddle point is explored for a neutron shell closed nucleus ^{210}Po.

(III) The role of entrance channel on fusion-fission and quasi-fission dynamics have been studied for ^{200}Pb.

In all the experiments, large area low pressure position sensitive Multi-Wire Proportional Counters (MWPC) were used. These detectors were fabricated at our laboratory at Variable Energy Cyclotron Centre.

The *first experiment* of the thesis work, was carried out at the K130 Cyclotron facility in Kolkata. In this experiment, alpha beam was bombarded on ^{232}Th target for a systematic study of fission fragment mass distribution of the actinides nucleus ^{236}U at an excitation energy range of 21-64 MeV. Measured mass distributions for excitation energies between 43.6 - 64.2 MeV were found to be symmetric in shape. However, the shape of the fission fragment mass distribution was found to change from symmetric to asymmetric at excitation energies $\leq$ 40 MeV which is an indication of washing out of shell effects. This experiment clearly demonstrated for the first time that shell effect is washed at an excitation energy of 40 MeV in ^{236}U.

Theoretically it has been shown that, for the nucleus ^{236}U, there exists two different fission barriers separated by a second minima. The nature of the mass distribution depends on the evolution of this fission barrier. The variation of this barrier with excitation energy is correlated with the nuclear free energy F(=V$-(a-a_{gs})T^2$) that determines the collective dynamics of a hot compound system (V is the potential energy, a is shape-dependent level density parameter with the value a_{gs} at the ground state deformation, T is the temperature). It was shown that the heights of the second barrier decreases rapidly with E^* and at 40 MeV the second barrier merely vanishes (less than 500 KeV), which is correlated with the observed vanishing of asymmetric mass yield.

The *second experiment* of the thesis work, was carried out at the BARC-TIFR pelletron facility in Mumbai to explore another aspect of the nuclear shell effect. The experiment addressed the question of the role of shell correction at the saddle point. The fission of the N=126 shell closed nuclei ^{210}Po was studied for this purpose in this thesis work, as recent experimental data and theoretical calculations indicated dramatic ambiguity regarding the presence or absence of shell correction at saddle point for this nucleus.

Using a direct experimental probe (fragment mass distribution), we clearly showed that there is no shell correction at fission saddle point, contrary to the recent observations [91, 93, 99]. In this thesis, fission fragment mass distribution was measured for both the systems ^{206,210}Po at an excitation energy range of 40 - 60 MeV using ^{12}C beam on ^{194,198}Pt. It was found that there is no anomaly between fragment mass distributions of the two systems and both the distributions were symmetric devoid of any structures. The potential energy surface (PES) using the Finite Range Liquid Drop Model (FRLDM) formula was also calculated and the fission fragment mass distribution were obtained from multi-dimensional Kramers formula. The mass distributions for both systems ^{206,210}Po were also explained theoretically considering only realistic macroscopic potential without any microscopic shell correction. Our experimental finding, is also consistent with the recent dynamical calculation [92]. The results presented in the thesis is likely to have vital impact on the calculation of fission barrier for the next neutron closed shell (N=184) spherical super heavy nuclei.

The *third experiment* of the thesis work was carried out at the Inter University Accelerator Centre pelletron facility in New Delhi, to study the dynamics of fusion fission and quasi-fission reactions. The fission of ^{200}Pb nuclei was studied by populating it though two different entrance channels ^{16}O + ^{184}W and ^{19}F + ^{181}Ta. While the previous measurements [115, 116] of evaporation residue (ER) cross sections for these systems advocated for the presence of pre-equilibrium fission, the two recent theoretical calculations [119, 121] could reproduce the ER data claiming the substantial amount of quasi-fission and fast fission in the above mentioned reactions.

In this thesis work, the mass distributions of ^{16}O + ^{184}W and ^{19}F + ^{181}Ta reactions at an excitation energy range of 50 MeV to 80 MeV were measured. The mass distributions were found to be symmetric and the width of the mass distributions were found to increase monotonically suggesting absence of any quasi-fission and fast fission. The present finding clearly show that the mass distributions data is in contrary to the theoretical findings [119]. The new data calls for the development of advanced theoretical models and new measurements for similar nuclei.

The present string of measurements carried out in this thesis work, aimed at probing deeply into two aspects of nuclear fission (e.g; shell effects and quasi-fission dynamics), throw new light on the enigmatic dynamics of fusion fission process for pre-actinides and actinides nuclei. More studies along this line for nucleus beyond actinides is of interest to chalk out optimum path for synthesis of Super Heavy Elements. Such an experimental program, as a follow up of this thesis work, has recently been initiated by scientists of Variable Energy Cyclotron Centre in collaboration with Joint Institute of Nuclear Research, Dubna, Russia.

Bibliography

[1] O. Hahn and F. Strassmann, Naturwiss. 27, 11 (1939)

[2] L. Meitner and O. R. Frisch, Nature 143, 239 (1939)

[3] N. Bohr, J. A. Wheeler, Phys. Rev 56, 426 (1939)

[4] N. Bohr and F. Kalckar, Kgl. Danske Videnskab. Selskab (1937)

[5] O. Haxel, et al., Phys. Rev. 75, 1766 (1949)

[6] M. G. Mayer, Phys. Rev. 75, 1969 (1949)

[7] B. Mottelson and S. G. Nilsson Phys. Rev. 99, 1615 (1955)

[8] V. M. Strutinsky, Nucl. Phys A 95, 420 (1967)

[9] V.M. Strutinsky, Nucl. Phys. A 122, 1 (1968)

[10] Z. Patyk and A. Sobiczewski, Nucl. Phys. A 491, 267 (1989)

[11] Yu.Ts.Oganessian et al., Radiochimica. Acta 99, 429 (2011)

[12] V. Weisskopf, Phys. Rev. 52, 295 (1937)

[13] M. Beckerman, Phys. Rev. Lett 45, 1472 (1980)

[14] R. G. Stokstad, Z. Phys A 295, 269 (1980)

[15] A. B. Balantekin, S. E. Koonin, et al., Phys. Rev. C 28, 1565 (1983)

[16] C. H. Dasso et al., Nucl. Phys. A 405, 381 (1983)

[17] M. Dasgupta, D. J. Hinde, et al., Ann. Rev. Nucl. Part. Sci 48, 4017 (1998)

[18] S. Kailas, Phys. Rep. 284, 381 (1997)

[19] R. Vandenbosch and J. R. Huizenga, Nuclear Fission (Academic Press, New York, 1973)

[20] B. B. Back, H. G. Glerc et al, Phys. Rev. Lett 46, 1068 (1981)

[21] C. Ngo, Prog. Part. Nucl. Phys.16, 139 (1986)

[22] C. Lebrun, F. Hanappe, et al., Nucl. Phys A 321, 207 (1979)

[23] V. S. Ramamurthy and S. S. Kapoor, Phys. Rev. Lett. 54 , 178 (1985)

[24] B. B. Back, R. R. Betts et al., Phys. Rev. C 32, 195 (1985)

[25] J. Toke, R. Bock et al., Nucl. Phys A 44, 327 (1985)

[26] U. L. Businaro and S. Gallone, Nuovo Cimento 5, 315 (1957)

[27] D. J. Hinde, M. Dasgupta, J. R. Leigh et. al, Phys. Rev. Lett. 74, 1295 (1995)

[28] Reiner Bass, Nuclear Reaction with Heavy Ions, Springer-Verlag, Berlin (1980)

[29] B. Sikora, et al., Phys. Rev. C 21, 614 (1980)

[30] B. Sikora, et al., Phys. Rev. C 25, 885 (1982)

[31] D. L. Hill, J. A. Wheeler, Phys. Rev. 89, 1102 (1953)

[32] C. Y. Wong, Phys. Rev. Lett. 31, 766 (1973)

[33] M. Dasgupta, et al., Ann. Rev. Nucl. Part. Sci 48:1, 401-461 (1998)

[34] A. Bohr and B. R. Mottelson, Nuclear structure Vol. I (Benjamin Press, New York, 1969)

[35] A. V. Ignatyuk, G. M. Smirenkin, and A. S. Tishin, Sov. J. Nucl. Phys. 21, 255 (1975)

[36] L. Meitner and O. R. Frisch, Nature 143, 239 (1939)

[37] S. Cohen and W. J. Swiatecki, Ann. Phys 22, 406 (1963)

[38] S. Cohen, F. Plasil, and W. J. Swiatecki, Ann. Phys 82, 557 (1974)

[39] M. Beckerman, M. Blann, Phys. Rev. Lett. 38, 272 (1977)

[40] F. Plasil, R. L. Ferguson, et al., Phys. Rev. Lett. 45, 333 (1980)

[41] D. J. Hinde, J. R. Leigh, J. O. Newton, W. Galster, and S. Sie, Nucl. Phys. A 385, 109 (1982)

[42] A. J. Sierk, Phys. Rev. C 33, 2039 (1986)

[43] H. J. Krappe, J. R. Nix, and A. J. Sierk, Phys. Rev. Lett 42, 215 (1979)

[44] M. Brack, J. Damgaard, A. S. Jensen, H. C. Pauli, V. M. Strutinsky, and C. Y. Wong, Rev. Mod. Phys.44 , 320 (1972)

[45] H. C. Pauli, T. Ledergerber, and M. Brack, Phys. Lett. B 34, 264 (1971)

[46] P. N. Nadtochy and G. D. Adeev, Phys. Rev. C 72, 054608 (2005)

[47] V. M. Strutinsky, Nucl. Phys A 502, 67C (1989)

[48] Yu. Ts. Oganessian et al., Nature 400 242 (1999)

[49] L C Vaz and J M Alexander,Phys. Rep. 97, 1 (1983)

[50] H. Rossner, D. Hilscher et al, Phys. Rev. C 27, 2666 (1983)

[51] W. J. Swiatecki, Phys. Scr.24, 113 (1981)

[52] R. G. Thomas, D. J. Hinde et. al, Phys. Rev. C 77, 034610 (2008)

[53] T.K. Ghosh et al., Phys. Rev. C 70, 011604 (2004)

[54] B. B. Back, D. J. Blumenthal et al., Phys. Rev C 60, 044602 (1999)

[55] P. Fong, Phys. Rev. 89, 332 (1953)

[56] M. G. Itkis, et. al, Yad. Fiz. 52, 944 (1990)

[57] M. G. Itkis, V. N. Okolovich, A. Ya, Rusanov, and G. N. Smirenkin, Yad. Fiz. 41, 849 (1985)

[58] V. E. Viola, K. Kwiatowski, and M. Walker, Phys. Rev. C 31, 1550 (1985)

[59] H. W. Schmitt, W. E. Kiker and C. W. Williams, Phys. Rev. B 137, 837 (1965)

[60] A. Oed, P. Geltenbort, R. Brissot, F. Gonnenwein, P. Perrin, E. Aker and D. Engelhardt, Nucl. Instr. and Meth. 219, 569 (1984)

[61] G. Charpak, R. Bouclier, T. Bressani, J. Favier and C. Zupancic, Nucl. Instr. and Meth. 62, 262 (1968)

[62] G. Charpak, G. Peterson, A. Policarpo and F. Sauli, Nucl. Instr. and Meth. 148, 471 (1978); A. Breskin, R. Chechik and N. Zwang, Nucl. Instr. and Meth. 165, 125 (1979); A. Breskin, R. Chechik I. Levin and N. Zwang, Nucl. Instr. and Meth. 217, 107 (1983)

[63] T. K. Ghosh, S. Pal, T.Sinha, S. Chattopadhyay and P. Bhattacharya. Nucl. Instrum. Phys. Res. A 540, 285 (2005)

[64] A. Breskin, R. Chechik, Z. Fraenkel, P. Jacobs, I. Tserruya, and N. Zwang, Nucl. Instr. and Meth. A 221, 363 (1984)

[65] http://www.tifr.res.in/ pell/lamps.html

[66] T. K. Ghosh, Ph.D. thesis, Study of heavy ion induced fission fragment angular and mass distribution at near and sub coulomb barrier energies, Jadavpur University, India, arXiv:nucl-ex/0508009 [nucl-ex] (2005)

[67] Nayana Majumdar, PhD thesis, Investigations on Heavy Ion Induced Fission of Heavy Nuclei at Near and Sub-Coulomb Barrier Energies , University of Calcutta, India (1997)

[68] Maria G. Mayer, Phys. Rev. 74, 235 (1948)

[69] R.V. F. Janssens and T. L. Khoo, Annu. Rev. Nucl. Part. Sci. 41, 321 (1991)

[70] R. Kanungo et al., Phys. Rev. Lett. 102, 152501 (2009)

[71] L. J. Colby et al., Phys. Rev. 121, 1415 (1961)

[72] B. B. Back et al., Phys. Rev. C 23, 1105 (1981)

[73] B. B. Back et al., Phys. Rev. C 22, 1927 (1980)

[74] J. Ralarosy et al., Phys. Rev. C 8, 2372 (1973)

[75] J. Fernandez-niello et al., Computer Physics Communications 54, 409, (1989)

[76] N. Majumdar, P. Bhattacharya et al., Phys. Rev. C 51, 3109 (1995)

[77] C. L. Jiang et al., Phys. Rev. Lett. 89, 052701 (2002)

[78] A. Shrivastava et al., Phys. Rev. Lett. 103, 232702 (2009)

[79] T. K. Ghosh et al., Phys. Rev. C 79, 054607 (2009)

[80] B. B. Back et al., Phys. Rev. C 53, 1734 (1996)

[81] T. K. Ghosh et al., Phys. Lett. B 627, 26 (2005)

[82] P. Moller et al., Nature 409, 785 (2001)

[83] P. N. Nadtochy, G. D. Adeev and A. V. Karpov, Phys. Rev. C 65, 064615 (2002)

[84] J. P. Lestone and S. G. McCalla, Phys. Rev. C 79, 044611 (2009)

[85] Bohr A. and Mottelson B. R., Nuclear Structure Vol II: Nuclear Deformations (Benjamin, New York) (1975)

[86] M. Csatlos et al., Phys. Lett. B 615, 175 (2005)

[87] J. Sadhukhan and S. Pal, Phys. Rev. C 78, 011603(R) (2008)

[88] V. S. Ramamurthy et al., Phys. Rev. Lett. 25, 386 (1970)

[89] M. Lunardon et al., Eur. Phys. J. A 13, 419 (2002)

[90] P. C. Rout et al., Phys. Rev. Lett. 110, 062501 (2013)

[91] A. Shrivastava et al., Phys. Rev. Lett. 82, 699 (1999)

[92] C. Schmitt, K. Mazurek and P. N. Nadtochy, Phys. Lett. B 737, 289 (2014)

[93] K. S. Golda et al., Nucl. Phys. A 913, 157 (2013)

[94] R.N. Sagaidak and A. N. Andreyev, Phys. Rev. C 79, 054613 (2009)

[95] A. V. Karpov, A. Kelic and K-H Schmidt, J. Phys. G 35, 035104 (2008)

[96] K. Mahata, S. Kailas and S. S. Kapoor, Phys. Rev. C 92, 034602 (2015)

[97] E. Prasad et al., Phys. Rev. C 91, 064605 (2015)

[98] W. D. Myers and W. J. Swiatecki, Nucl. Phys. A 601, 141 (1996)

[99] K. Mahata, S. Kailas and S. S. Kapoor, Phys. Rev. C 74, 041301 (2006) (R)

[100] A. Gavron, Phys. Rev. C 21, 230 (1980)

[101] M. G. Itkis et al., Yad. Fiz. 53, 1225 (1991) and references therein

[102] M. G. Itkis et al., Yad. Fiz. 52, 23 (1990)

[103] P. Möller, A. J. Sierk et al., Phys. Rev. C 79, 064304 (2009)

[104] H. J. Krappe, J. R. Nix and A. J. Sierk, Phys. Rev. C 20, 992 (1979)

[105] Zhang Jing-Shang and H. A. Weidenmüller, Phys. Rev. C 28, 2190 (1983)

[106] P. Fröbrich and G. R. Tillack, Nucl. Phys. A 540, 353 (1992)

[107] J. Sadhukhan and S. Pal, Phys. Rev. C 84, 044610 (2011)

[108] S.I. Mulgin et al., Nucl. Phys. A 640, 375 (1998)

[109] K. Banerjee, T.K. Ghosh et al., Phys. Rev. C 83, 024605 (2011)

[110] K. Mahata, et al., Phys. Rev. C 65, 034613 (2002)

[111] S. E. Vigdor, H. J. Karwowski et al., Phys. Rev. C 26, 1035 (1982)

[112] W. J. Swiatecki, Phys. Scr. **24**, 113 (1981).

[113] S. Bjornholm and W. J. Swiatecki, Nucl. Phys. A **391**, 471 (1982).

[114] M. Abe, KEK Report No. 86-26, KEK TH-28, (1986).

[115] P.D. Shidling *et al.*, Phys. Lett. B **670**, 99 (2008).

[116] P.D. Shidling *et al.*, Phys. Rev. C **74** 064603 (2006).

[117] V. S. Ramamurthy, S. S. Kapoor, Phys. Rev. Lett. **54**, 178 (1985).

[118] V. S. Ramamurthy *et al.*, Phys. Rev. Lett. **65**, 25 (1990).

[119] A. K. Nasirov *et al.*, Phys. Lett. B **686**, 72 (2010).

[120] G. Fazio *et al.*, Phys. Rev. C **72**, 064614 (2005).

[121] Rajni *et al.*, Phys. Rev. C **90**, 044604 (2014).

[122] A. Chaudhuri, T.K. Ghosh *et al.* Phys. Rev. C **91**, 044620 (2015).

[123] A. Chaudhuri, T.K. Ghosh *et al.* Phys. Rev. C **92**, 041601 (R) (2015).

[124] B. B. Back *et al.*, Phys. Rev. C **53**, 1734 (1996).

[125] G. N. Knyazheva, E. M. Kozulin *et al.*, Phys. Rev. C **75**, 064602 (2007).

[126] M. G. Itkis and A.Ya. Rusanov, Phys. Part. Nucl. **29**, 160 (1998).

[127] K. Hagino, N. Rowley, and A. J. Kruppa, Comput. Phys. Commun. **123**, 143 (1999).

[128] M. G. Itkis *et al.*, Yad. Fiz. **52**, 23 (1990).

[129] T. Wada, Y. Abe, and N. Carjan, Phys. Rev. Lett. **70**, 3538 (1993).

[130] K. T. R. Davies, A. J. Sierk, and J. R. Nix, Phys. Rev. C **13**, 2385 (1976).

[131] A. V. Karpov, P. N. Nadtochy, D. V. Vanin, and G. D. Adeev, Phys. Rev. C **63** 054610 (2001).

[132] K. Nishio *et al.*, AIP Conference Proceedings 1224, 301 (2010).